

FAST PYROLYSIS OF KRAFT BLACK LIQUOR

by

Stuart Alan Gairns

A thesis submitted to the Faculty of Graduate Studies and Research
in partial fulfillment of the requirements of the
degree of Master of Engineering

Department of Chemical Engineering

McGill University

**Montréal, Québec
Canada**

September 1993

Copyright

ABSTRACT

The pyrolysis of kraft black liquor droplets under inert, reducing, and gasifying atmospheres was investigated at temperatures of 500 to 900°C in a well characterized single droplet tube furnace coupled to a fast-response quadrupole mass spectrometer. In addition, the behaviour of sodium during the pyrolysis of black liquor and the presence of adsorbed elemental sodium in pyrolysis char were investigated.

Using the single droplet apparatus and the procedures developed, true gas formation rate data were determined under conditions simulating those in kraft recovery processes. The mass spectrometer allowed the formation rates of several compounds to be determined simultaneously. All major permanent, hydrocarbon, and sulphurous pyrolysis gases, with the exception of H₂, were determined, along with pyrolysis char and tar yields.

The rate data reveal that sulphurous gas formation occurs relatively early as compared to that of the other gases determined. The data also reveal that pyrolysis gases are formed during droplet drying. While CH₃SH and CH₃SCH₃ yields decrease sharply with temperature, and those of H₂S and CH₃SSCH₃ remain quite constant, the CS₂ formation increases to a significant level at 900°C. The yields of ethane and methanol also decrease sharply with temperature, but those for ethylene, methane, CO, and CO₂ correspondingly increase. Acetylene yields become measurable at 900°C. While the influence of gas atmosphere on the sulphur release during pyrolysis is small, the influence on hydrocarbon gas yields is significant. In the presence of 10% CO at 800°C and 15% CO₂ at 900°C the yields of ethylene and methane are reduced substantially, while those of acetylene are much higher. It is suggested that CO and CO₂ act as free radical scavengers to produce this effect.

The presence of adsorbed elemental sodium in black liquor pyrolysis chars was found to be responsible for the pyrophoric nature of some chars. This reduced sodium reacts with water to produce hydrogen. In a recovery boiler, sufficient hydrogen could be formed to produce an explosive mixture above the char bed, which upon detonation could trigger a smelt-water explosion.

RESUME

On a étudié la pyrolyse des gouttelettes de liqueur noire kraft dans une atmosphère inerte et dans des atmosphères qui encouragent la réduction et la gazéification aux températures de 500°C à 900°C. On a utilisé une chaudière aux tubes bien caractérisée pour des gouttelettes individuelles. La chaudière est liée à un spectrographe de masse quadrapole de réponse rapide. En outre, on a étudié le comportement du sodium pendant la pyrolyse de liqueur noire et la présence du sodium élémentaire adsorbé dans le charbon de pyrolyse.

En utilisant l'appareil des gouttelettes individuelles et les procédés qui étaient développés, on a déterminé les vrais taux de formation de gaz sous les conditions semblables aux conditions dans des processus kraft de récupération. Employant le spectrographe de masse, on a pu déterminer simultanément les taux de formation de plusieurs composés. On a déterminé tous les gaz importants permanents, sauf l'H₂, et tous les gaz importants d'hydrocarbure et de soufre. On a déterminé aussi la production de charbon et de goudron de pyrolyse.

Les données du taux révèlent que la formation de gaz sulfureux a lieu relativement tôt comparé à celle d'autres gaz analysés. Les données révèlent aussi que les gaz de pyrolyse sont formés pendant le séchage d'une gouttelette. Pendant que la production de CH₃SH et de CH₃SCH₃ diminue rapidement en augmentation de température et que celle de H₂S et de CH₃SSCH₃ reste assez constante, la production de CS₂ à 900°C accroît à un niveau significatif. La formation d'éthane et de méthanol diminue aussi rapidement en augmentation de température, mais celle d'éthylène, de méthane, de CO et de CO₂ accroît en augmentation de température. La production d'acétylène devient mesurable à 900°C. L'influence de l'atmosphère de gaz sur la dévolatilisation de soufre pendant la pyrolyse est petite, tandis que l'influence sur la production de gaz hydrocarboné est significative. Dans la présence de 10% de CO à 800°C et 15% de CO₂ à 900°C, la production d'éthylène et de méthane est réduite de manière significative, pendant que celle d'acétylène est beaucoup plus haute. On a suggéré que le CO et le CO₂ se comportent comme des charognards des radicaux libres afin de produire cet effet.

On a trouvé que la présence du sodium élémentaire adsorbé dans le charbon de pyrolyse de liqueur noire kraft est la cause pour la nature pyrophorique de quelques charbons. Ce sodium réduit réagit avec de l'eau pour produire de l'hydrogène. Dans une chaudière de récupération, il se pourrait former suffisamment d'hydrogène pour produire un mélange explosif audessus de la couche de charbon, ce qui, par détonation, pourrait déclencher une explosion d'un mélange d'eau et de formation du salin.

ACKNOWLEDGMENTS

I would like to thank first and foremost God and my Lord and Saviour Jesus Christ for blessing me with the opportunity of attending McGill, and the intellectual and spiritual growth it has provided.

I would like to thank my supervisors, Drs. A.R.P. van Heiningen and G.J. Kubes for their support and guidance both during the experimental phase and during the preparation of this thesis.

My friends in the CRISP group, particularly Akilendra, Victor, and François, deserve special thanks for their friendship, encouragement and help.

Thanks go out to the staff of stores, purchasing, and the machine shops of both Paprican and McGill Chemical Engineering for their assistance.

A special word of thanks to Yujing for all her help with chemical analysis.

I would also like to thank NSERC, McGill University, and Paprican for their financial support and for the funds provided for equipment and supplies. Special thanks to the International Energy Agency and its supporting members for providing most of the funding for the equipment.

I would like to thank Bryan and the McGill Christian Fellowship bible study gang for their friendship, support, and prayers which got me through many long nights.

I would like to thank my parents and family for their continuous love and support through all the things I have pursued over the years.

Lastly, I would like to thank my wife Sandra, the best thing that happened to me when I was in Montréal, for her patience, love, and assistance during the preparation of this thesis.

TABLE OF CONTENTS

Abstract	ii
Resumé	iii
Acknowledgments	iv
Table of Contents	v
List of Figures	vii
List of Tables	x
List of Plates	x
CHAPTER 1 INTRODUCTION	1
Basis for Research	3
Description of Thesis	3
CHAPTER 2 PYROLYSIS LITERATURE REVIEW	4
Introduction	4
Ligno-Cellulose Pyrolysis	6
Kraft Black Liquor Composition	6
Pyrolysis of Kraft Black Liquor	8
Swelling of Black Liquor During Pyrolysis	9
Sulphur Volatilization During Black Liquor Pyrolysis	10
Time Scale of Droplet Pyrolysis	12
CHAPTER 3 THERMODYNAMIC PREDICTIONS	13
Introduction	13
Background	13
Model Assumptions and Procedure	13
Conditions Studied	14
Species Considered in Equilibrium Calculations	16
Thermodynamic Data	16
Property Changes Made to the FACT Database	17
Results of Equilibrium Calculations	18
Discussion	24
Conclusions	26
Nomenclature	27
CHAPTER 4 FAST PYROLYSIS EXPERIMENTAL APPARATUS AND METHODS	28
Introduction	28
Design Considerations for Apparatus	28
Description of Final Version of Apparatus	29
Measurement of Drop and Furnace Temperatures and Computer Control	35
Background Information on Mass Spectrometry	38
Mass Spectrometer Statistical Data Reduction Method	42
Method Used to Analyse Mass Spectrographic Response Data and Typical Results	43
Calibration of Mass Spectrometer	49
System Impulse Responses	50
Fast Fourier Transform Deconvolution of Data	53

CHAPTER 5 FAST PYROLYSIS EXPERIMENTAL RESULTS	57
Introduction	57
Experimental	57
Experimental Procedures	57
Analysis of Black Liquor and Black Liquor Char	60
Experimental Strategy	65
Results and Discussion	65
Mass Balances	67
Tar, Char, and Gas Yields	69
Possible CS ₂ Formation Routes	80
Effects of CO and CO ₂ on Pyrolysis	83
Droplet and Furnace Experimental Temperature-Time Histories	85
Pyrolysis Gas and Volatile Formation Rates	87
Formation Rate and Conversion Data Corrected by FFT Deconvolution	96
Summary of Black Liquor Droplet Pyrolysis	96
Conclusions	99
 CHAPTER 6 BEHAVIOUR OF SODIUM AND FORMATION OF ELEMENTAL SODIUM DURING FAST PYROLYSIS OF KRAFT BLACK LIQUOR	 100
Introduction	100
Sodium Loss During Black Liquor Pyrolysis	100
Smelt Water Explosions: History and Mechanism	103
Experimental	104
Experimental Procedures	105
Results and Discussion	108
Behaviour of Sodium During Single Droplet Fast Pyrolysis	108
Presence of Reduced Sodium in Black Liquor Chars	113
Conclusions	118
 CHAPTER 7 GENERAL CONCLUSIONS	 119
Contributions to Knowledge	119
Suggestions for Future Work	120
 References	 122
 APPENDIX A Analysis For Back Dispersion In Shielding Tube	 125

LIST OF FIGURES

Figure 1.1	Combined fluidized bed pyrolysis and partial gasification	2
Figure 2.1	Pyrolysis of organic matter	4
Figure 3.1	Experimental phase diagram for $\text{Na}_2\text{CO}_3\text{-Na}_2\text{S}$ system	15
Figure 3.2	Ideal phase diagram for $\text{Na}_2\text{CO}_3\text{-Na}_2\text{S}$ system	15
Figure 3.3	65% black liquor solids. (a) gas phase (b) condensed phases	19
Figure 3.4	Pyrolysis yields for condensed phases. (a) 65% solids liquor (b) 93% solids liquor	20
Figure 3.5	Pyrolysis yields for condensed phases. (a) 100% solids liquor (b) 100% solids liquor with gas phase dilution by helium	21
Figure 3.6	Pyrolysis gas yields. (a) 65% solids liquor (b) 93% solids liquor	22
Figure 3.7	Pyrolysis gas yields. (a) 100% solids liquor (b) 100% solids liquor with gas phase dilution by helium	23
Figure 3.8	Sodium vapour yield	23
Figure 4.1	Schematic flow and instrumentation diagram for the fast pyrolysis apparatus	29
Figure 4.2	Fast pyrolysis tube furnace, sample insertion assembly, and condensables trapping apparatus	31
Figure 4.3	Detail of removable drop thermocouple probe showing pin connection in the unheated zone and the shape of the droplet thermocouple	34
Figure 4.4	Results of digitally filtering furnace temperature data using a fourth order Butterworth filter with a cutoff frequency of 0.025 (a) Drop data (b) Furnace	36
Figure 4.5	Distribution of sample insertion times for 22 fast pyrolysis experiments	38
Figure 4.6	Temperature profile along the centre-line of tube furnace with helium flow rate of about 2.0 slm and a set point of 650°C	38
Figure 4.7	Typical time-temperature history for pyrolysis experiment at 700°C. (a) Full history (b) initial 10 seconds showing drying and devolatilization stages	39
Figure 4.8	Comparison of heating history of liquor drops between using probes made from 1/4" and 1/8" alumina rod	39
Figure 4.9	Overlapping cracking patterns for CO , C_2H_4 , and C_2H_6	41
Figure 4.10	Gas concentration calculated using statistical method for the overlapping gases. (a) With 5 overlapping gases (b) With 6 overlapping gases	46
Figure 4.11	Ion response data from mass spectrometer for a typical experiment	47

Figure 4.12	Gas concentrations calculated from mass spectrometer data for a typical experiment. Relatively high concentration (a) and low concentration (b) compounds	48
Figure 4.13	Total flow rate of carrier gas through apparatus calculated on the basis of concentrations of produced gases.	48
Figure 4.14	Calibration data for dimethyl disulphide showing linear response and variation in sensitivity over the range of m/z ratios	50
Figure 4.15	Normalized system impulse responses to CO injected at the midpoint of the tube furnace. Furnace temperature of 700°C with helium carrier gas flow rates as noted	53
Figure 4.16	Normalized system impulse responses for dimethyl sulphide showing the effect of condenser cooling. Furnace at 700°C with a carrier gas flow of 2.0 slm helium	53
Figure 4.17	Example of deconvolution results showing how the deconvolved data is shifted to the left and more abrupt	56
Figure 4.18	Normalized discrete response of fast pyrolysis apparatus for H ₂ S. Non-adsorbing gases are quite similar	56
Figure 5.1	Typical mass flow rate curve from which water production was determined	59
Figure 5.2	Char gasification apparatus	63
Figure 5.3	Fixed carbon gasification - typical result	64
Figure 5.4	Tar yield for fast pyrolysis with 20 mg 70% solids droplets	70
Figure 5.5	Char yield for fast pyrolysis with 20 mg 70% solids droplets	70
Figure 5.6	Total gas yield for fast pyrolysis with 20 mg 70% solids droplets. (a) as calculated (b) with CO reduced 50%	71
Figure 5.7	Pyrolysis yield of sulphur in char for 20 mg 70% solids droplets	73
Figure 5.8	Pyrolysis yield of sulphur in gases for 20 mg 70% solids droplets	73
Figure 5.9	Pyrolysis yield of sulphur in tar for 20 mg 70% solids droplets	73
Figure 5.10	Pyrolysis yield of fixed carbon in char for 20 mg 70% solids drops	75
Figure 5.11	Pyrolysis yield of ethane for 20 mg 70% solids droplets	75
Figure 5.12	Pyrolysis yield of ethylene for 20 mg 70% solid droplets	75
Figure 5.13	Pyrolysis yield of methane for 20 mg 70% solids droplets	77
Figure 5.14	Pyrolysis yield of methanol for 20 mg 70% solids droplets	77
Figure 5.15	Pyrolysis yield of carbon monoxide for 20 mg 70% solids droplets	77
Figure 5.16	Pyrolysis yield of carbon dioxide for 20 mg 70% solids droplets	78
Figure 5.17	Pyrolysis yield of hydrogen sulphide for 20 mg 60% solids droplets	78
Figure 5.18	Pyrolysis yield of methyl mercaptan for 20 mg 70% solids droplets	78
Figure 5.19	Pyrolysis yield of dimethyl sulphide for 20 mg 70% solids droplets	81
Figure 5.20	Pyrolysis yield of carbon disulphide for 20 mg 70% solids droplets	81
Figure 5.21	Pyrolysis yield of dimethyl disulphide for 20 mg 70% solids drops	81

Figure 5.22	Pyrolysis yield of produced water for 20 mg 70% solids droplets	82
Figure 5.23	Pyrolysis yields of acetylene (a) and acetone (b) for 20 mg drops	82
Figure 5.24	Typical drop temperature histories for fast pyrolysis experiments in helium. (a) 90 seconds (b) initial 10 seconds	86
Figure 5.25	Replicate drop temperature histories for drop pyrolysis at 800°C showing temperature decrease due to rapid sulphate reduction	88
Figure 5.26	Effect of gas environment on drop and furnace temperature histories for liquor pyrolysis at 900°C	88
Figure 5.27	Methanol formation rate measured at MS for droplet pyrolysis	91
Figure 5.28	Methane formation rate measured at MS for droplet pyrolysis	91
Figure 5.29	Ethylene formation rate measured at MS for droplet pyrolysis	91
Figure 5.30	Ethane formation rate measured at MS for droplet pyrolysis	92
Figure 5.31	Carbon dioxide formation rate measured at MS for droplet pyrolysis	92
Figure 5.32	Carbon monoxide formation rate measured at MS for drop pyrolysis	92
Figure 5.33	Hydrogen sulphide formation rate measured at MS for drop pyrolysis	94
Figure 5.34	Methyl mercaptan formation rate measured at MS for drop pyrolysis	94
Figure 5.35	Dimethyl sulphide formation rate measured at MS for drop pyrolysis	94
Figure 5.36	Carbon disulphide formation rate measured at MS for drop pyrolysis	95
Figure 5.37	Dimethyl disulphide formation rate measured at MS for drop pyrolysis	95
Figure 5.38	Initial water vapour flow measured at MS	95
Figure 5.39	Methane formation rate at droplet calculated using deconvolution	97
Figure 5.40	Methane conversions calculated from deconvolved formation rates	97
Figure 5.41	Methane conversions calculated from non-deconvolved formation rates	97
Figure 5.42	H ₂ S formation rate at droplet calculated using deconvolution	98
Figure 5.43	H ₂ S conversions calculated from deconvolved formation rates	98
Figure 5.44	H ₂ S conversions calculated from non-deconvolved formation rates	98
Figure 6.1	Sodium detection apparatus	106
Figure 6.2	(a) Effect of ultrasonic agitation on hydrogen diffusion to gas phase (b) Typical gas chromatogram for hydrogen analysis	109
Figure 6.3	Char yields for fast pyrolysis experiments. Pure He unless noted (a) Sodium yield (b) CO ₃ and total S yields as fractions of sodium in BLS required to form Na ₂ CO ₃ and Na ₂ SO _x (x = 0, 3, 4) salts	110
Figure 6.4	Reduced sodium - calculated from measured hydrogen	115
Figure 6.5	Reduced sodium as a function of sodium yield during pyrolysis	116
Figure 6.6	Reduced sodium as a function of pyrolysis time	117

LIST OF TABLES

Table 2.1	Typical Mill Black Liquor Elemental Composition	7
Table 2.2	Black Liquor Solids composition	8
Table 3.1	Molar Composition of Systems Studied	16
Table 3.2	Species Included in Initial Calculations	16
Table 3.3	Species Included in Final Calculations	16
Table 3.4	Thermodynamic Properties of Selected Mercaptans and Thioalkanes	17
Table 3.5	Thermodynamic Data Used for Sodium Sulphide	18
Table 4.1	System Impulse Response Parameters Furnace at 700°C	52
Table 5.1	Approximate Chip Composition of Cook from which the Studied Kraft Black Liquor was Obtained	60
Table 5.2	Kraft Black Liquor Ultimate Chemical Composition	60
Table 5.3	Kraft Black Liquor Composition of Inorganic Ions and Distribution of Organic and Inorganic Sulphur	61
Table 5.4	List of Fast Pyrolysis Experiments and Conditions	66
Table 5.5	Carbon Mass Balance	67
Table 5.6	Sulphur Mass Balance	68
Table 5.7	Comparison of IR and MS CO and CO ₂ Determination	68
Table 5.8	Equilibrium Constants K _p for Reactions [5.15] and [5.16] (calculated with data from (69))	83
Table 5.9	Times for Onset of Formation and Peak Formation Rate During Black Liquor Droplet Pyrolysis	89
Table 6.1	Reduced Sodium Formation Experiments	114

LIST OF PLATES

Plate 4.1	Experimental fast pyrolysis apparatus showing swaged quartz tube, tube furnace, condenser, sample cooler, push rod, and bottom limit switch	32
Plate 4.2	Drop thermocouple probe constructed of 1/8" diameter alumina. Type K pin connectors are at left. Break in thermocouple wire has been repaired adjacent to junction	32
Plate 4.3	Drop thermocouple shown bare (a), with 20 mg black liquor droplet (b), and with the resulting swollen char (c)	33
Plate 6.1	Char after 10 minutes of pyrolysis at 800°C in argon. Smelt nodules which have migrated to the surface are evident	114

CHAPTER 1 INTRODUCTION

The kraft process is the dominant process used for the production of chemical pulp in North America. Pulp, a random mat of cellulose fibres, is produced in this process by digesting wood chips in an aqueous solution called white liquor, which has sodium hydroxide and sodium sulphide as active cooking chemicals. The kraft process has several advantages over competing processes but the three primary advantages are high pulp strength, well established chemical recovery, and high energy self sufficiency.

In the conventional kraft recovery process the spent cooking liquor - black liquor - is separated from the pulp, concentrated to 58-75% dry solids content, and used to fuel a so-called recovery boiler. The recovery boiler is an ingenious piece of equipment in that several "unit operations" are performed in one compartment. By controlling the introduction of air, three zones are created in the furnace. The black liquor is sprayed into the furnace and either dries and pyrolyses as it falls to the char bed of the furnace or it dries and pyrolyses on the walls of the furnace before falling to the bed (1). In the reducing atmosphere maintained in the lower zone of the furnace, pyrolysis is completed, carbon is gasified, and the inorganic chemicals are converted to a liquid smelt of primarily sodium sulphide and sodium carbonate. The smelt is removed and dissolved in water to produce "green liquor" which is further processed to produce fresh white liquor. The reducing gases produced at the char bed and the volatiles produced during pyrolysis are combusted with an excess of air in the upper furnace. Thus, there are three zones which necessarily overlap somewhat: a drying and pyrolysis zone; a reduction and gasification zone; and a combustion zone. The overall heat of combustion is substantial and the heat generated is used to produce steam, some of which is commonly used to generate electric power.

Although recovery furnaces generally function well, they are extremely expensive pieces of equipment and have inherent dangers due to the presence of the liquid smelt. Explosions, believed to be caused by water coming into contact with the smelt (2), have occurred with substantial loss of life and considerable expense (3,4). Due to these factors there has been considerable interest in alternative recovery processes whereby drying, pyrolysis, gasification and reduction, and combustion occur in separate units - perhaps fluidized beds - without the formation of a molten phase (5). These processes offer the advantage of eliminating the hazard of smelt-water explosions and also present methods of adding incremental capacity to existing mills.

One alternative process proposes combined pyrolysis and partial gasification of the black liquor at 700-800°C in a fluidized bed reactor during which much of the Na_2S produced will be volatilized through reaction with the gaseous pyrolysis products (6). The

residue from gasification would then be leached with water to a Na_2CO_3 solution with some Na_2S . The volatilized sulphur subsequently would be absorbed into this solution from the gas stream to produce green liquor. The clean gases could then be used as fuel for combined cycle power and steam generation, or burned with the residual char in a fluidized bed with heat recovered in a boiler bank. Figure 1.1 shows a possible configuration for a fluidized bed combined pyrolysis and gasification unit.

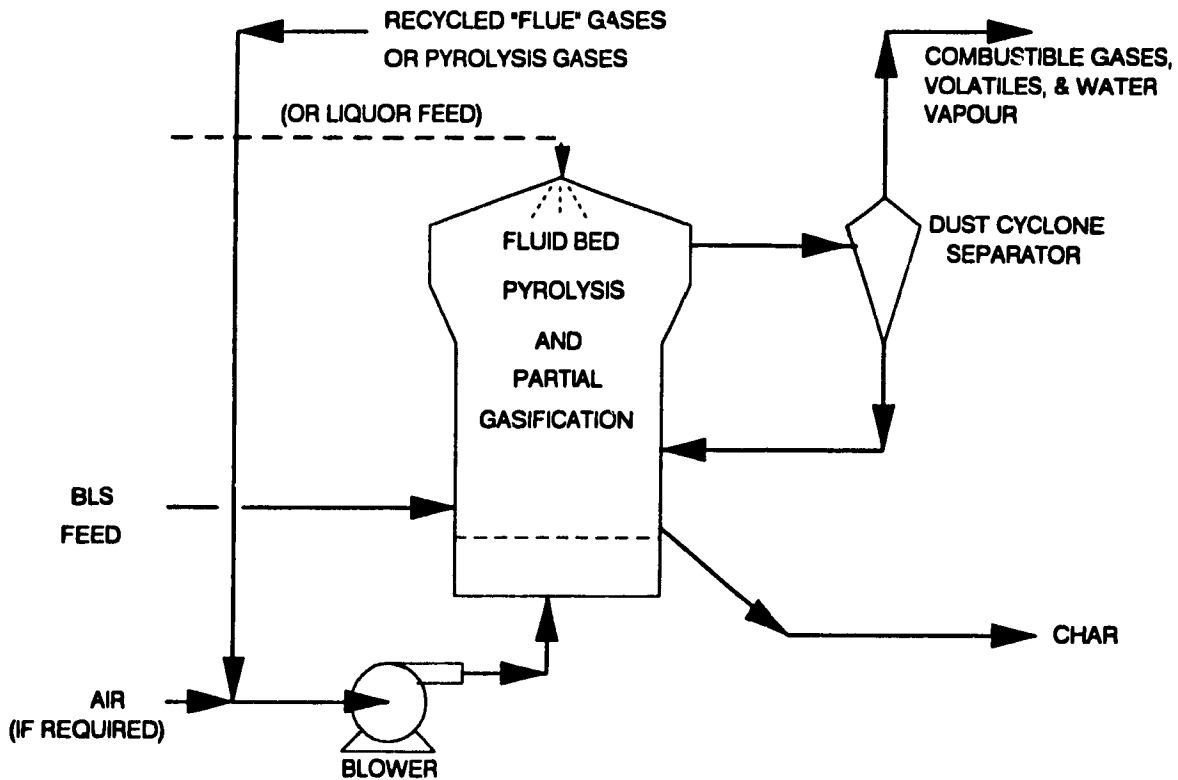


Figure 1.1 Combined fluidized bed pyrolysis and partial gasification

Another process describes pyrolysis of black liquor or black liquor solids at 600°C in a fluidized bed where flue gases are used to fluidize the bed (7). At these conditions it is believed that only a portion of the sulphur will be volatilized which can subsequently be recovered in a fluidized bed combustor. The solid pyrolysis product, char, would be reduced in the solid state in a separate reactor and then leached in water to produce green liquor. The char residue would be subsequently burned in the fluidized bed combustor.

These processes in which gasification and/or combustion are carried out in fluidized beds offer the additional possibility of high pressure operation. Higher pressures would in

turn make it possible to achieve much greater ratios of electrical power generated to steam produced (8).

Basis for Research

Although there have been several studies of black liquor pyrolysis reported in the literature (9-27) there still exists a need for more fundamental data regarding black liquor pyrolysis before new processes such as those described above can be successfully developed at a commercial scale. Data which are noticeably absent are kinetic and yield data for the release of individual pyrolysis gases during single droplet pyrolysis and data on the effect of gasification atmospheres on pyrolysis processes. The effect black liquor solids concentration on droplet pyrolysis yields has also never been reported in the literature. The parameters which have been investigated in some detail under inert conditions, such as sulphur and sodium loss and drying times, are also unknown when gasification atmospheres are present. An additional area which does not appear to have been studied for droplet pyrolysis is the yield of tars and other condensable products.

Thus the basis for the present research is the gathering, assembling, and interpreting of data to fill in the gaps mentioned above. The execution of these objectives required the development of new experimental techniques and the design and construction of new experimental equipment. This development and design process formed a major part of this thesis and as a result is explained in detail in subsequent chapters.

Description of Thesis

Briefly this thesis is organized as described below. Chapter 2 provides a general literature review of pyrolysis processes and the pyrolysis of black liquor and related compounds. A thermodynamic study of combined pyrolysis and gasification is presented in Chapter 3 along with a review of the relevant literature. A detailed description of the fast pyrolysis equipment and the mass spectrographic methods developed comprise Chapter 4. Chapter 5 presents the results of the fast pyrolysis experiments and a discussion of such. The behaviour of sodium during black liquor pyrolysis is reviewed and experimental results pertaining to this topic are presented in Chapter 6. Chapter 7 presents general conclusions, contributions to knowledge, and suggestions for future work.

CHAPTER 2 PYROLYSIS LITERATURE REVIEW

Introduction

Tromp and Moulijn (28) define pyrolysis as chemical "decomposition due to exposure to high temperature". Others (1) label pyrolysis thermal decomposition under inert atmospheres and use the term devolatilization when oxidizing or reducing conditions exist. In this thesis the broader definition of pyrolysis is generally employed with non-inert atmospheres identified. Pyrolysis is an important phenomena as it occurs in all processes for the combustion, gasification, liquefaction, or carbonization of organic matter (28). Pyrolysis of organics generally produces hydrogen rich non-condensable gases, hydrogen rich condensables (tars), and carbon rich char as depicted in Figure 2.1.

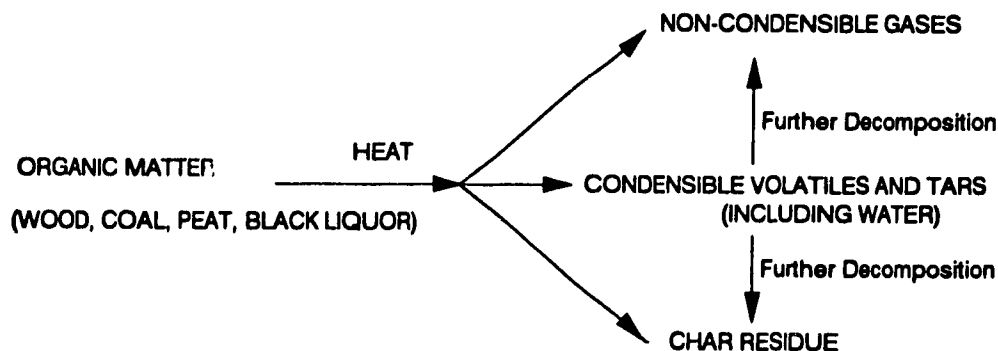


Figure 2.1 Pyrolysis of organic matter

Pyrolysis of different types of organics is similar and the mechanisms discussed below are taken from a review of coal pyrolysis literature by Tromp and Moulijn (28). The least stable bonds in organics such as coal and lignin are the functional group bridges between the aromatic building blocks and these bonds are the first to break during pyrolysis. Radicals are formed as these bonds break and some materials such as bituminous coal and black liquor solids soften. Volatile radicals may either react to form "stable" volatiles or, along with non-volatile radicals, react through polymerization and condensation reactions to form a more aromatic - compared to the original material - carbon rich char. "Stable" volatiles may further crack to produce lighter hydrocarbons as they diffuse to regions of higher temperature. Subsequent to this active phase of bond breaking, higher temperatures cause dehydration reactions which produce hydrogen and carbon monoxide.

Bhattacharya *et al* (17) state a similar but slightly different route based on Wen and Dutta (29). They believe the formation of pyrolysis gases is mainly due to decarbonylation, decarboxylation, dealkylation, and aromatic ring rupture, and that in black liquor the carbonyl and mercaptan bonds are the weakest, and rupture at lower temperatures producing CO₂ and H₂S. As the temperature is increased dealkylation becomes predominant, and in the final stages CO is produced by the breaking of ether linkages and H₂ by aromatic ring rupture. In a pyrolysis apparatus where the produced gases and tars are exposed to high temperature conditions, further pyrolysis reactions will occur, thereby obscuring the pattern of pyrolysis of the parent material.

Pyrolysis experiments have traditionally been classified as either slow or rapid (11,28). Heating rates of 1.0°C/s and less define slow pyrolysis, while rates of 1000°C/s and greater define rapid pyrolysis. Rapid pyrolysis is also known as flash pyrolysis (28). In fluidized beds with particle sizes under 100 microns, rapid pyrolysis can be achieved and slow pyrolysis occurs in moving bed reactors (28), but the majority of real processes appear to fall between these limits.

Slow pyrolysis is characterized by high char yields since the production of radicals is slower and allows sufficient residence time for many volatile radicals to undergo polymerization and condensation reactions. Mass and heat transfer are typically not limiting and constant heating rate kinetic models have been developed (28,30). These models typically employ three parallel first order independent equations, one each for the formation of char, tar, and gases from the parent material.

In rapid pyrolysis, secondary condensation and polymerization reactions are minimized since the rapid production of radicals reduces residence times in the parent material by displacing the produced gases (28). Rapid pyrolysis tends to be heat and mass transfer limited by the diffusion of gases and tars to the particle surface and the evaporation of the tars.

While it is commonly believed that higher heating rates lead to higher gas yields, Howard in his review (31) agrees with this conclusion and states that the yield is a function of final temperature. He believes that since most high heating rate studies also have high final temperatures, the incorrect conclusion has been drawn.

A simple heat transfer limiting model has been presented for the devolatilization of black liquor drops (1), but at the heating rates expected in an industrial process of 200-300°C/s (1) it is likely that kinetics, mass transfer, and heat transfer will all be important. Harper (9) has developed a combined heat transfer and sulphur release model which takes into account the swelling of kraft black liquor drops during pyrolysis.

Further background information and literature relevant to black liquor pyrolysis are

discussed below, with the exception that thermodynamic considerations and the behaviour of sodium are discussed in Chapters 3 and 6 respectively.

Ligno-Cellulose Pyrolysis

Castillo *et al* (32) used carbon 14 labelling in ligno-cellulosic materials to study mechanisms of flash pyrolysis of such materials. They determined that the gas produced by lignin degradation is primarily CO with CH₄, CO₂, and C₂ hydrocarbons in smaller quantities. Most of the CH₄, CO₂, and C₂ hydrocarbons were found to be due cellulose and hemicellulose degradation. The methoxy (-OCH₃) group degrades equally to CO and CH₄ and shows that CH₄ in lignin pyrolysis comes from the methoxy group. They also concluded that the CO₂ in lignin pyrolysis comes from the α -carbon of the guaiacyl or syringyl lignin monomer.

In their apparatus, in which secondary pyrolysis of products was suppressed by rapid removal from the high temperature zone, they measure very low gas yields of 6% for lignin - based on carbon containing gases - and a high tar yield of 50%, with the balance being solids (char). Of the carbon containing gases produced from the lignin, 41% of the carbon was α -carbon, 34% methoxy carbon, and 15% ring carbon.

Degraded cellulose and hemicellulose form sugar acids in black liquor. Pyrolysis of sugar acids results in lower char yields and higher gas yields as compared to lignin (11).

Miller (11) has summarized the results of several studies on the influence of inorganic impurities in carbonaceous material during pyrolysis. Very small amounts of salts of alkali and transition metals strongly catalyse some reactions during pyrolysis. The effect appears to be catalysed decarboxylation, dehydration, and condensation at low temperatures which leads to substantial increases in char yields due to stabilization of carbon in the aromatic char. The effects for lignin pyrolysis are similar but far less pronounced. Considerable work in the field of alkali catalysed carbon gasification (33) and the work of Li (10,34) have shown that sodium is an effective catalyst in the gasification of carbon from black liquor, and thus sodium will promote rapid gasification during combined pyrolysis and gasification.

Kraft Black Liquor Composition

Kraft black liquor is a dark brown fluid which is extracted and washed from the wood pulp after the digestion stage of the kraft pulping process. At high solids contents it is a very viscous material. Below 50% solids its behaviour is approximately Newtonian while at higher solids fractions it exhibits shear thinning at high shear rates (1). A typical solids analysis of a black liquor, as extracted from pulp, is shown in Table 2.1 (1). Potassium, chlorine, and inerts enter the system with makeup chemicals and the wood.

The chemical composition of kraft black liquor is very complex as it contains inorganic chemicals, both residual and spent, from the parent white liquor and dissolved organic compounds from the wood chips. In addition, both the inorganic and organic fractions of black liquor are dependent on the species of wood being pulped. The chemical makeup of deciduous trees - hardwoods - is substantially different from that of conifers - softwoods - and large variations exist within these two subgroups. These variations result in different requirements for cooking chemicals and can also substantially affect the behaviour of black liquor during pyrolysis and combustion (1,11,12).

Table 2.1
Typical Mill Black Liquor Elemental Composition (1)

	wt %
Carbon	39.0
Hydrogen	3.8
Oxygen	33.0
Sodium	18.6
Potassium	1.2
Sulphur	3.6
Chlorine	0.6
Inerts (Si, Al, Fe, Ca, etc.)	0.2

Softwoods differ from hardwoods in that they contain more lignin and less hemicellulose, and in that these substances are chemically different. The monomer for softwood lignin is predominantly guaiacyl, whereas the more methoxy rich syringyl monomer is equally abundant in hardwoods. The hemicelluloses differ in that those of softwoods are rich in glucomanans and poor in xylans, while for hardwoods the converse is true (35,36). Within the softwoods, the level of extractives can be as low as 1% for spruce and as high as 5% for pine. Since methoxyl groups react with OH^- and HS^- to produce methanol and methyl mercaptan respectively (35), the greater number of methoxyl groups in hardwoods causes increased amounts of these compounds in hardwood black liquors.

The inorganic portion of black liquor is somewhat difficult to define (11) as much of the sodium is associated with dissolved organics. The major inorganic species are Na_2S , NaOH , Na_2CO_3 , Na_2SO_4 , NaCl , polysulphides (Na_2S_x , $x = 2, 3, \dots$) and possibly elemental sulphur (10). There is considerable disagreement in the literature on the division of sulphur between the organic and inorganic fractions. Miller (11) and Harper (9) in their reviews claim 10% is organic sulphur and Harper's own data shows 85-90% inorganic (on basis of sulphate, sulphide, thiosulphate, and sulphite) supporting his claim. Li (10) in his work found evidence to support that 44% of the sulphur was organically bound but his liquor was strongly oxidized with oxygen under pressure, and this may have altered the sulphur distribution. Blackwell and King (37) estimate that 35% is organically

bound.

A proximate analysis of black liquor solids in Table 2.2 below indicates the major components of the organic fraction (35). The solubilized, or alkali, lignin makes up the largest fraction and is present as large colloidal molecules which are made soluble by hydrophilic functional groups (35). Hydroxy and carboxylic acids are formed from the hemicellulose and partial degradation of the cellulose. The extractives consist mainly of resin and fatty acids and are present as sodium salts. The amount of extractives strongly affects the swelling behaviour of black liquor during pyrolysis (11,12) by altering the viscosity, as explained below.

Table 2.2
Black Liquor Solids Composition (35)

	wt %
Alkali Lignin	30-45
Hydroxy Acids	25-35
Extractives	3-5
Acetic Acid	5
Formic Acid	3
Methanol	1

Pyrolysis of Kraft Black Liquor

Studies on the pyrolysis of black liquor solids indicate that pyrolysis begins between 200 and 250°C (10,11,14). Feuerstein *et al* (14) pyrolysed batches of unoxidized black liquor in an initially evacuated system at temperatures from 398-970°C. Carrier gas was not used and black liquor of 65% solids content was brought to 100% solids during initial heating. The heating rate used is unclear but they claim the experiments were carried out at essentially constant temperature (16). Char yields of 60-70% decreased with increasing temperature, pyrolysis water was constant at 20%, while pyrolysis liquids and gases increased from 4 to 10% and 5 to 15% respectively with increasing temperature. The main gases produced were CO, CO₂, CH₄, C₂H₆, and C₂H₂. The main sulphur gases detected were CH₃SH, (CH₃)₂S, (CH₃)₂S₂, and H₂S. In all, 60-80% of the sulphur was volatilized. Over 60 compounds were detected in the pyrolysis liquid (15) and, despite the use of dual condensers and an inter-condenser aerosol breaker, 32 of these were detected in small quantities in the pyrolysis gas.

Brink *et al.* (16) reported on continuous pyrolysis experiments performed by the same group at U.C. Berkeley. Because of the large amount of water entering the steady state reactor with the liquor, much carbon was gasified and gas yields were substantially higher than during batch pyrolysis. They found that steady state gas yield was over 55% at 1025°C. In the continuous reactor sulphur volatilization was greatest at about 750°C and lowest at 1025°C, when it was comparable to batch pyrolysis.

Bhattacharya et al. (17) pyrolysed black liquor solids under nitrogen in a tube furnace between 590 and 740°C. Their main objectives were to determine gas yields and kinetics at isothermal conditions so they used a large samples (2000 mg) which took about 15 minutes to pyrolyse. The samples were sieved into three different size fractions and pyrolysed in a ceramic boat. With increasing temperature char yield decreased from 55 to 47% while gas yield increased from 13 to 20 % and tar yield remained relatively constant at 32-35%. Gas yield increased slightly with smaller sieve sizes, but it is likely that confinement of the boat would have lead to agglomeration of particles during swelling of the black liquor solids, thereby obscuring the effect of initial differences. The kinetics were modelled with three parallel independent first order reactions, one for each of the gas, tar, and char fractions. The calculated frequency factors and activation energies were strongly dependent on particle size indicating mass and heat transfer were important. For the five gases analysed, H₂ and CO formation were greater at higher temperatures while CO₂, CH₄, and H₂S formation were greater at lower temperatures.

Li (10) pyrolysed black liquor solids with a heating rate of 20°C/min in a thermogravimetric analyzer (TGA). Li reported that during pyrolysis to temperatures above 610°C, Na₂SO₄ was reduced by CO to Na₂S and 90% reduction was achieved. Later work (34,38) demonstrated that carbon is actually the main reducing agent for sulphate. Gasification of char with CO₂ and steam showed that essentially all the Na₂S in the pyrolysis char is volatilized during gasification (34). Li's findings on sulphur release (10) suggest that the organic sulphur gases produced during pyrolysis (thioalkanes and mercaptans) result from the decomposition of thiolignin.

Harper (9) studied the total sulphur release from black liquor drops during rapid pyrolysis in a nitrogen atmosphere. Yields of individual gases were not determined. He concluded that sulphur release is greatest for pyrolysis at 490°C and that it increases with increasing solids content and drop size. Others (39) have found that during devolatilization under oxidizing conditions sulphur release decreases with increasing drop size. The temperature of 490°C correlates strongly with the maximum swelling temperature of 500°C found by Miller (11), but both these temperatures are much lower than those found in industrial processes.

Swelling of Black Liquor During Pyrolysis

Miller (11) studied the swelling of black liquor droplets in a single particle reactor under a nitrogen gas atmosphere. He found that a typical kraft black liquor swelled to 20-30 times its original volume (2.7:1 to 3.1:1 diameter ratio). Earlier work by Milanova *et al* (12) showed that liquor composition, and in particular increased extractives, content can

reduce swelling (and combustibility) dramatically. Hupa *et al* (40) studied single droplet combustion in air, and, in addition to the observations made above, found that sulphite liquors swell to only 3-4 times their original volumes.

The degree of swelling is dependent on the rheological properties of the liquor (1,11,12). Very viscous liquors swell little as the matrix prevents the volatile bubbles from expanding and low viscosity liquors swell little as volatiles simply escape from the droplet. Liquors of moderate viscosity, or mixtures of high and low viscosity liquors, are fluid enough to allow bubbles to expand but viscous enough to prevent all the bubbles from escaping (11,12).

Miller found that the swollen volume was maximum for a pyrolysis temperature of 500°C. He reasoned that at lower temperatures volatilization is less and at higher temperatures the outer surface of a drop becomes carbonized and hard, thus restricting swelling (11).

A recently-reported study by Frederick *et al* (25) investigated swelling of sulphite, kraft softwood, and kraft hardwood black liquors. They found that the swelling which occurs during drying is independent of liquor type, droplet size, and furnace temperature over the temperature range of 600-900°C. For devolatilization in air, the maximum swollen volume was found to decrease with increasing temperature. They suspect that this may be due in part to lower char yields at higher temperatures. They found that the atmosphere in which devolatilization takes place dramatically affects the swollen volume. The average swollen volumes they found at 800°C were: 133 cm³/g in N₂, 234 cm³/g in 4-12% O₂, 66 cm³/g in air, 43 cm³/g in CO₂, and 61 cm³/g in 20% H₂O. The much lower swollen volumes in CO₂, H₂O, and air are likely due to substantial gasification of carbon during the devolatilization stage. When they investigated the effect of solids concentration on swelling, they found that for hardwood and sulphite liquors there was no effect, while for softwood liquors there was a substantial increase in swollen volume with increasing solids concentration.

Swelling properties of liquors are important as they affect both the combustibility (12) and the carry-over of black liquor in a recovery furnace (1,25). Swollen volume can also affect the reactivity of chars to subsequent gasification (41) or reduction stages in low temperature fluidized bed recovery systems. Another concern in a fluidized bed would be the durability of the char under the turbulent action of the bed. Generation of excessively small particles could make solids handling difficult. Swelling also affects the pyrolysis rate of droplets, since heat and mass transfer are functions of transport properties and size (1).

Sulphur Volatilization During Black Liquor Pyrolysis

Much of the release of sulphur to the gas phase in a recovery furnace occurs during pyrolysis and since loss of sulphur is problematic both economically and environmentally, it has been the subject of several studies. The sources of sulphur in kraft black liquor are residual Na_2S , $\text{Na}_2\text{S}_2\text{O}_3$, Na_2SO_3 , Na_2SO_4 , polysulphides, and organically bound sulphur. Na_2SO_4 and Na_2SO_3 are present in the white liquor and are also formed by oxidation of Na_2S , as are $\text{Na}_2\text{S}_2\text{O}_3$ and polysulphides.

Strohbeen (13) and Harper (9) pyrolysed model compounds and concluded that thiosulphate, sulphide, and organic sulphur are the major contributors to volatilized sulphur during pyrolysis, while very little sulphur is volatilized from sulphate and sulphite. During slow pyrolysis, Li and van Heiningen (26) found that the peak emission rates for H_2S , COS , CH_3SH , $(\text{CH}_3)_2\text{S}$, and $(\text{CH}_3)_2\text{S}_2$ occurred at approximately 415, 410, 350, and 370°C respectively. The sulphur emission was 22% of the total sulphur and was not significant above 460°C. They proposed that H_2S was formed by the following mechanism.



Bhattacharya *et al* (17) found H_2S to be the major sulphur gas produced during pyrolysis at temperatures of 570 to 740°C, but the yields of other sulphurous gases were not determined. Feuerstein *et al* (14) report that for batch pyrolysis of liquor, CH_3SH peaked at 480°C, $(\text{CH}_3)_2\text{S}$ at 610°C, and $(\text{CH}_3)_2\text{S}_2$ at 770°C, while H_2S increased monotonically from 400 to 1000°C. During steady state pyrolysis of liquor, Brink *et al* (16) found H_2S rose from 470°C to a peak at about 800°C and then decreased steeply. CH_3SH appeared to peak at 580°C and $(\text{CH}_3)_2\text{S}$ at 630°C. Harper (9) studied the kinetics of sulphur release from black liquor droplets during pyrolysis but did not identify individual sulphur gases.

Frederick *et al* (19,20) recently concluded that at temperatures below 600°C sulphur release during pyrolysis is controlled by both kinetics and heat and mass transfer. However, above 750°C it appears that the process is heat and mass transfer limited. They also concluded that sulphur release is associated with pyrolysis reactions and that it does not occur until droplet drying is complete. This conclusion was based on drying times calculated by a model and times to onset of sulphur release estimated from the difference in time between sample insertion and detection of sulphur. However, the residence time distribution for their apparatus indicates that a significant time lag is present due to transport of the gases generated at the droplet to the location of sulphur detection.

Therefore this conclusion is suspect based on the error caused by the time lag and possible errors in the calculated drying times.

Time Scale of Droplet Pyrolysis

Hupa *et al.* (40) while studying the combustion of black liquor droplets (0.5-2.5mm) at 700-800°C in an oxidizing environment measured times for devolatilization. They identified four stages for droplet combustion: drying, volatile formation and burning, char burning, and inorganic reactions. Using 60% solids black liquor they found that drying times ranged from 1-2 seconds and devolatilization times from 0.5-1.0 seconds. However, this devolatilization time was very insensitive to furnace temperature as the volatiles were burning on the outside of the drop, heating it very quickly.

Miller conducted swelling experiments in an inert gas and found that the time to reach maximum volume was a strong function of temperature and particle size (11). For the pyrolysis of 65% solids liquor at 700°C swelling times increased from 2.5 to 14.5 seconds as droplet size went from 1.36 to 3.93 mm. For 4 mm drops at 80% solids the relevant times were 9, 14, and 27 seconds at 900, 700, and 500°C respectively. Harper (9) measured the heating rates of black liquor droplets in a single particle reactor. He found that the temperature of the centre of the droplet was the same as the surroundings after 20 seconds, but most of the temperature rise occurred in the first 10 seconds. The results did not appear to differ much between 6.4 and 10.3 mm drops. It should be noted that both Miller (11) and Harper (9) heated their drops by directing a hot gas stream into a cold furnace. Thus heating of the furnace walls would have been occurring simultaneously and a net radiative loss from the particle to the walls could be expected.

Verrill and Nichols (22,23) report drying and swelling - devolatilization - times as a function of droplet mass (1 to 9 mg of solids) at 500°C in 5% O₂, 600°C in 5% CO, and 900°C in 5% CO. Drying times range from less than one second to seven seconds, are strongly dependent on temperature, and weakly dependent on droplet size. Swelling times range from one to four seconds, with trends similar to those of drying times.

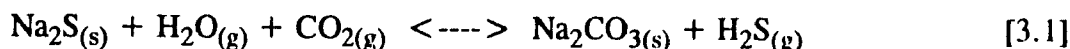
CHAPTER 3 THERMODYNAMIC PREDICTIONS

Introduction

This chapter describes the methods and results of thermodynamic equilibrium calculations which were performed to model combined black liquor pyrolysis and gasification in a fluidized reactor, assuming the fluidization atmosphere to be that of the produced gases. Although black liquor pyrolysis processes are generally known to be limited by heat transfer, mass transfer, and kinetics, one can still gain insight and understanding of what is achievable by examining predictions made on the basis of equilibrium thermodynamics. Often these predictions are useful as they indicate what the best possible yield of a particular compound is, or they may make evident that conditions of slow kinetics are required to prevent a particular undesirable product from forming.

Background

Equilibrium thermodynamics have been used by many researchers to predict black liquor conversion processes, with most of the work concentrating on recovery boilers (42,43) and also evaluation of alternative recovery processes (44,34,45). Strohbeen (13) used thermodynamic calculations to predict sulphur volatilization during black liquor pyrolysis and concluded that the sulphur loss was kinetically controlled below 750°C, but that at temperatures over 1000°C thermodynamic equilibria is approached for the reaction



Strohbeen's analysis was through the use of classical equilibrium constant methods, while the calculations for the more recent studies have all been performed using the equilibrium solver computer program SOLGASMIX by Eriksson (46), or a modified version of this program (47). The program solves multiphase, multicomponent equilibrium problems by constrained minimization of the Gibbs free energy.

The literature does not appear to contain any detailed studies of the thermodynamics of black liquor pyrolysis. This is understandable as pyrolysis of black liquor is a very complicated process producing a multitude of components (15), is kinetically controlled, and in a kraft recovery furnace probably never approaches equilibrium. However, the conditions of high heat and mass transfer, plus the fluidizing medium of product gases, during pyrolysis in a fluidized bed reactor, may produce conditions in which equilibrium is approached. For these reasons thermodynamic modelling was performed and is presented below.

Model Assumptions and Procedure

Chemical equilibrium calculations were made with a module of the FACT computer program by Thompson *et al* (47). The module, called EQUILIB, solves multiphase,

multicomponent equilibrium systems by constrained minimization of the total Gibbs free energy. It is a modified version of the SOLGASMIX program developed by Eriksson (46) which uses Lagrange multipliers in the solution algorithm.

The model used by the program is as follows. The molar Gibbs free energy for each component of each phase consists of two terms, as shown in equation [3.2] below.

$$g_i^\alpha = g_i^{\circ\alpha}_T + RT \ln(x_i^\alpha \tau_i) \text{ for solutions (phase } \alpha) \quad [3.2a]$$

$$g_i^\beta = g_i^{\circ\beta}_T + RT \ln(x_i^\beta \phi_i P) \text{ for gases (phase } \beta) \quad [3.2b]$$

$$g_i^{\circ\alpha}_T = h_i^{\circ\alpha}_{f,298} + \int_{298}^T C_{pi}^{\alpha} dT - T(s_i^{\alpha\circ}_{298} + \int_{298}^T \frac{C_{pi}^{\alpha}}{T} dT) \quad [3.2c]$$

The first term is the Gibbs free energy for the pure compound at standard state conditions, which is calculated using standard state properties at 298 K and an expression for the specific heat as a function of temperature. Thus, the specific heat equations employed must be valid from 298 K to the temperature of the system. For phases which are not stable at 298 K, pseudo properties at 298 K must be back calculated from the phase transition temperature. The second term is the activity correction term for compounds in solution. Unless specified otherwise, all solutions are treated ideally in the Lewis sense and the gas phase is treated as an ideal gas.

At the low pressure (1 atm) and relatively high temperatures (550-800 °C) considered in this study, assuming the gas phase behaves ideally introduces little error. As is a common and necessary simplification in heterogeneous systems, the solids are considered to be pure compounds with unit activity.

Although the liquid phase is known to be non-ideal (42,45,48,49,83), the lack of an appropriate method to characterize these non-idealities, and the limitations of the program to accept excess Gibbs energy functions of a suitable form, the smelt was also considered ideal. The effects of this assumption are that the melting temperature of the liquid phase is underestimated, the eutectic composition is incorrect, and - to some unknown degree - chemical potentials are incorrect. Figure 3.1 shows the experimental phase diagram for the Na₂CO₃/Na₂S system (83), while Figure 3.2 is the phase diagram for the same system calculated from the freezing point equation (50), appropriate thermodynamic properties (51,53), and assuming ideal solutions. Comparison of these figures demonstrates the magnitude of the first two effects.

Conditions Studied

An ideal liquor of the same composition as that of Pejryd and Hupa (42) was used and is shown in Table 3.1. The composition is very similar to those in standard references (1,37). Three different black liquor solids (BLS) contents were considered, 100, 93, and

65 percent solids, the balance being water. A fourth case with 100% BLS and a large quantity of helium was run to determine the effect of typical conditions of the present experimental study on equilibrium. Experimental techniques in gasification, reduction, and pyrolysis typically use an inert purge stream to dilute and carry away the products for analysis. The the four systems studied are presented in Table 3.1.

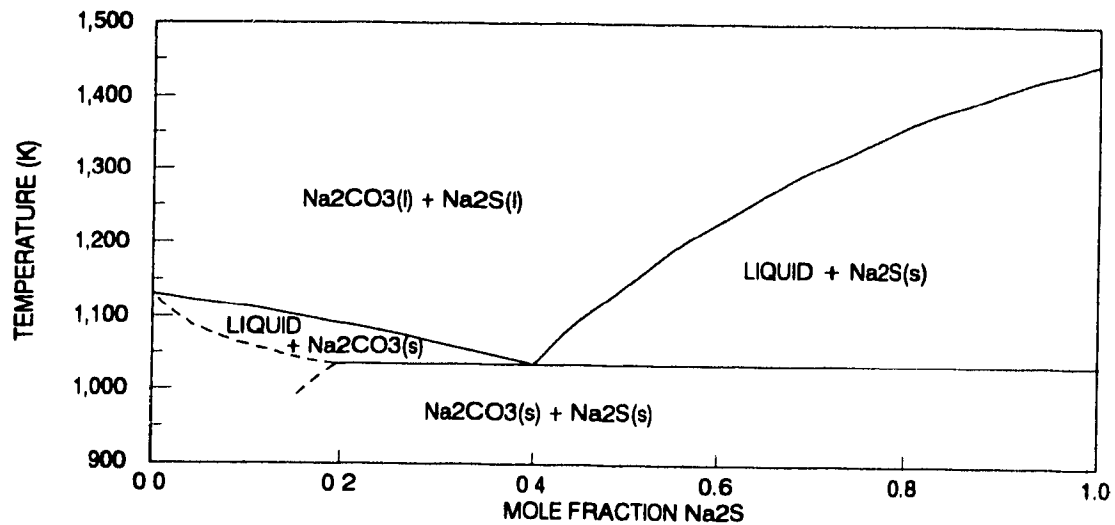


Figure 3.1 Experimental phase diagram for $\text{Na}_2\text{CO}_3\text{-Na}_2\text{S}$ system (ref. 83)

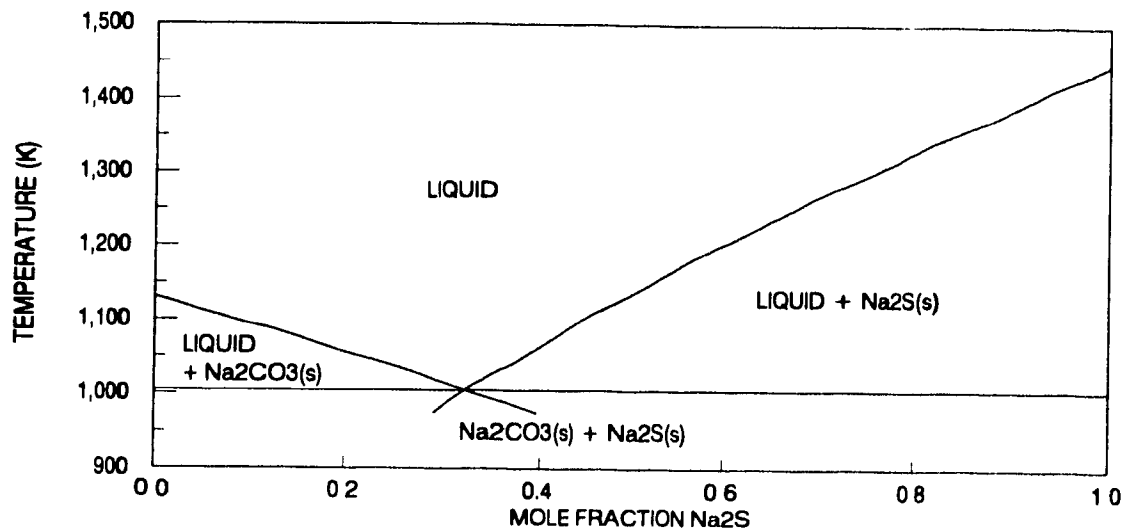


Figure 3.2 Ideal phase diagram for $\text{Na}_2\text{CO}_3\text{-Na}_2\text{S}$ system

The primary range of temperatures investigated was 450-800°C (723-1073 K). The 100% BLS, case (i), was also investigated over the range 350-450°C to determine if favourable conditions for sulphur gas formation exist during droplet heating. Calculations were performed by specifying the temperature, pressure, and system composition - a

closed system analysis - holding the pressure constant at one atmosphere and using temperature increments of 50°C.

Table 3.1
Molar Composition of Systems Studied

System	Descript.	Carbon	Hydrogen(H)	Oxygen(O)	Sodium	Sulphur	Water	Helium
(i)	100% BLS	10.0	12.5	7.0	2.4	0.36	----	----
(ii)	93% BLS	10.0	12.5	7.0	2.4	0.36	1.301	----
(iii)	65% BLS	10.0	12.5	7.0	2.4	0.36	9.309	----
(iv)	100% BLS	10.0	12.5	7.0	2.4	0.36	----	100.0

Species Considered in Equilibrium Calculations

Several simulations were initially made with the large number of species listed in Table 3.2 below, in order to determine the most important equilibrium species. These initial calculation runs were chosen to cover the extremes of both temperature and composition. Thus, runs were made at 550, 650, and 800°C with both 65% and 100% solids black liquor. In order to improve computational efficiency, only those species which were calculated to be present in mole fractions greater than one ppm were included in subsequent calculations. These species are shown in Table 3.3. The additional sulphurous gas species, mercaptans and thioalkanes, shown in Table 3.4 were also included in the final calculations as several are known to be produced during black liquor pyrolysis (15).

Table 3.2
Species Included in Initial Calculations

<i>Gaseous</i>	CH ₃ CSOH, COS, H ₂ SO ₄ , S ₂ O SO ₃ , SO ₂ , SO, CS ₂ , CS, H ₂ S ₂ , H ₂ S, SH, S ₈ , S ₇ , S ₆ , S ₅ , S ₄ , S ₃ , S ₂ , S, Na ₂ O ₂ H ₂ , NaO, NaH, Na ₂ , Na, HCOOH, CH ₃ CH ₂ OH, CH ₃ CHO, CH ₃ OH, CH ₂ O, HCO, C ₃ O ₂ , CO ₂ , CO, H ₂ O ₂ , HO ₂ , H ₂ O, OH, O ₃ , O ₂ , O, C ₂ H ₄ , C ₂ H ₃ , C ₂ H ₂ , C ₂ H, CH ₄ , CH ₃ , CH ₂ , CH, C ₅ , C ₄ , C ₃ , C ₂ , C, H ₂ , H
<i>Liquid</i>	Na ₂ S, Na ₂ SO ₄ , Na ₂ SO ₃ , Na ₂ S ₃ , NaS ₂ , NaS, Na ₂ CO ₃ , NaOH, Na ₂ O, C ₂ Na ₂ , Na
<i>Solid</i>	Na ₂ S, Na ₂ SO ₄ , Na ₂ SO ₃ , Na ₂ CO ₃ , Na ₂ O, C

Table 3.3
Species Included In Final Calculations

<i>Gaseous</i>	H ₂ , CO, H ₂ O, CO ₂ , CH ₄ , H ₂ S, COS, CH ₂ O, Na, CH ₃ SH, CH ₃ CH ₂ SH, CH ₃ CH ₂ CH ₂ SH, CH ₃ CH(SH side)CH ₃ , CH ₃ SCH ₃ , CH ₃ CH ₂ SHCH ₃ , CH ₃ SSCH ₃
<i>Liquid</i>	Na ₂ CO ₃ , Na ₂ S, NaOH, NaS, Na
<i>Solid</i>	C, Na ₂ CO ₃ , Na ₂ S

Thermodynamic Data

The thermodynamic data used by the FACT program must be either present in the large permanent data base or added to the user's personal data base. The properties in the data base were used for all compounds except for the sulphur gases and sodium sulphide,

which are discussed below. The information in the data base has been taken from Barin *et al* (51). The data shown for the sulphur gases in Table 3.3 below are typical of the information necessary. In addition, for phase changes, heats and temperatures of vaporization and fusion must be included.

Property Changes Made to the FACT Database

High temperature thermodynamic data are not present in the FACT database for several sulphur gases which are known to be products of black liquor pyrolysis (15). Data for these species (see Table 3.4) were obtained from the TRC Thermodynamic Tables (52). Equations for specific heats were calculated by linear regression of the ideal gas specific heats. The form of the equation used to fit the specific heats was determined by the standard input format of FACT. As indicated below, the curves for most of the species were only fit over the range of 298-1000 K, as this is the range for which the data are available, and probably the range for which the compounds are stable. Each equation was checked to ensure that it was well behaved for the range 1000-1100 K which covers the highest temperatures considered in this study.

Table 3.4
Thermodynamic Properties of Selected Mercaptans and Thioalkanes (52)

Species	formula	h°_{f298} (kJ/mol)	s°_{298} (J/mol-K)	g°_{f298} (kJ/mol)
Methyl Mercaptan	CH ₃ SH	-22.59	255.03	-9.50
Ethyl Mercaptan	C ₂ H ₅ SH	-46.02	296.14	-2.14
n-propyl Mercaptan	C ₃ H ₇ SH	-67.53	336.44	2.57
isopropyl Mercaptan	CH ₃ CHSHCH ₃	-75.90	324.30	-2.18
Dimethyl Sulphide	CH ₃ SCH ₃	-37.29	285.85	7.34
Methyl-Ethyl Sulphide	CH ₃ SC ₂ H ₅	-59.40	333.09	11.82
Dimethyl Disulphide	CH ₃ SSCH ₃	-23.61	35.46	15.37

Specific Heat Coefficients (T in K)

$$C_p = A + B \cdot 10^{-3} \cdot T + C \cdot 10^{-5} / T^2 + D \cdot 10^{-6} \cdot T^2 \quad (\text{J/mol-K})$$

	A	B	C	D	Temp (K)
Methyl Mercaptan	28.577	91.344	-2.91143	-25.588	298-1500
Ethyl Mercaptan	42.878	146.217	-8.89405	-41.581	298-1500
n-propyl Mercaptan	26.139	268.290	-2.72107	-92.806	298-1000
isopropyl Mercaptan	31.899	262.799	-5.39497	-91.197	298-1000
Dimethyl Sulphide	28.915	174.076	-1.592114	-56.064	298-1000
Methyl-Ethyl Sulphide	30.350	258.474	-3.83301	-91.139	298-1000
Dimethyl Disulphide	42.817	199.812	-1.80537	-69.539	298-1000

Until relatively recently there has been considerable disagreement and confusion in the literature regarding thermodynamic properties for pure Na₂S. Warnqvist (53) states that the standard references for inorganic compounds (51,54) report erroneous properties based on outdated experimental work. The difficulty in obtaining accurate data stems from having impure Na₂S, which dramatically lowers the melting temperature (53,48).

While Warnqvist reports the melting temperature to be 1443 ± 10 K Barin *et al* (51) list a value of 1251 K. There has also been some confusion as to the correct value of the heat of fusion of Na_2S . Early work (55) calculated a value of 2.00 kcal/mol from a crude $\text{Na}_2\text{S}/\text{Na}_2\text{CO}_3$ phase diagram considering the solution to be simple regular. Tegman and Warnqvist (48) report a value of 7.3 kcal determined calorimetrically. Warnqvist (53) updates this value to 30.1 kJ/mole (7.2 kcal/mol), but Perjyd and Hupa (42) and Backman (49) use 32.1 kJ/mol as it results in superior prediction of the phase diagram.

The thermodynamic data used for Na_2S can be found in Table 3.5. Specific heats were calculated for both liquid and solid Na_2S in the temperature ranges indicated, using the data of Warnqvist (53). The other data is also from Warnqvist, with the exception that the slightly different value of 32.1 kJ/mol was used as the heat of fusion (42,49). The effect of using this different value should be small, and only play a role when both a solid and a liquid are present, by affecting the mole fractions, melting temperature, and distribution of species between the two phases.

Table 3.5
Thermodynamic Data Used for Sodium Sulphide

h°_{f298}	-386.6 kJ/mol	
s°_{298}	90.3 J/mol-K	
heat of fusion	32.1 kJ/mol	
melting point	1443 K	
C_p _solid	= -31.268 + 0.0927T kJ/mol-K	1000-1400 K
C_p _liquid	= 3.4 + 0.0905T kJ/mol-K	1000-1400 K

Results of Equilibrium Calculations

The results of the equilibrium calculations are presented graphically in Figures 3.3 to 3.7 below. Figure 3.3(a) shows the composition of the gaseous phase and 3.3(b) the combined condensed phases for the case with 65% BLS. As can be observed in Figure 3.3(b), melting of the inorganic salts begins at about 700°C and is complete by 750°C . This is typical for all four cases studied. The quantities of COS gas and Na vapour predicted for the gas phase in Figure 3.3(a) are typical of the 93% and 100% solids cases as well. Formation of mercaptans and thioalkanes, which are typically found in black liquor pyrolysis gases, is not predicted by the thermodynamic analysis.

While the form of presentation used in Figure 3.3 facilitates presenting mole fractions which vary by several orders of magnitude, it does not allow one to determine the distribution of the products as a percentage of the input, i.e. as yields, as is typically desired in an engineering application and measured experimentally. For this reason the results were replotted to show the predicted yields of the products and the distribution of the sulphur. In this form, Figures 3.4 and 3.5 depict the calculated pyrolysis yields, of

the chemical compounds, as well as their combined total yield, for the condensed phases. The yields of the gaseous species are presented in Figures 3.6 and 3.7. Since the water introduced into the system with the black liquor solids becomes part of the gas phase, the total yields do not sum up to 1.0, as they are based on the weight of black liquor solids. This basis was employed to allow direct comparison with the experimental results presented in Chapter 5.

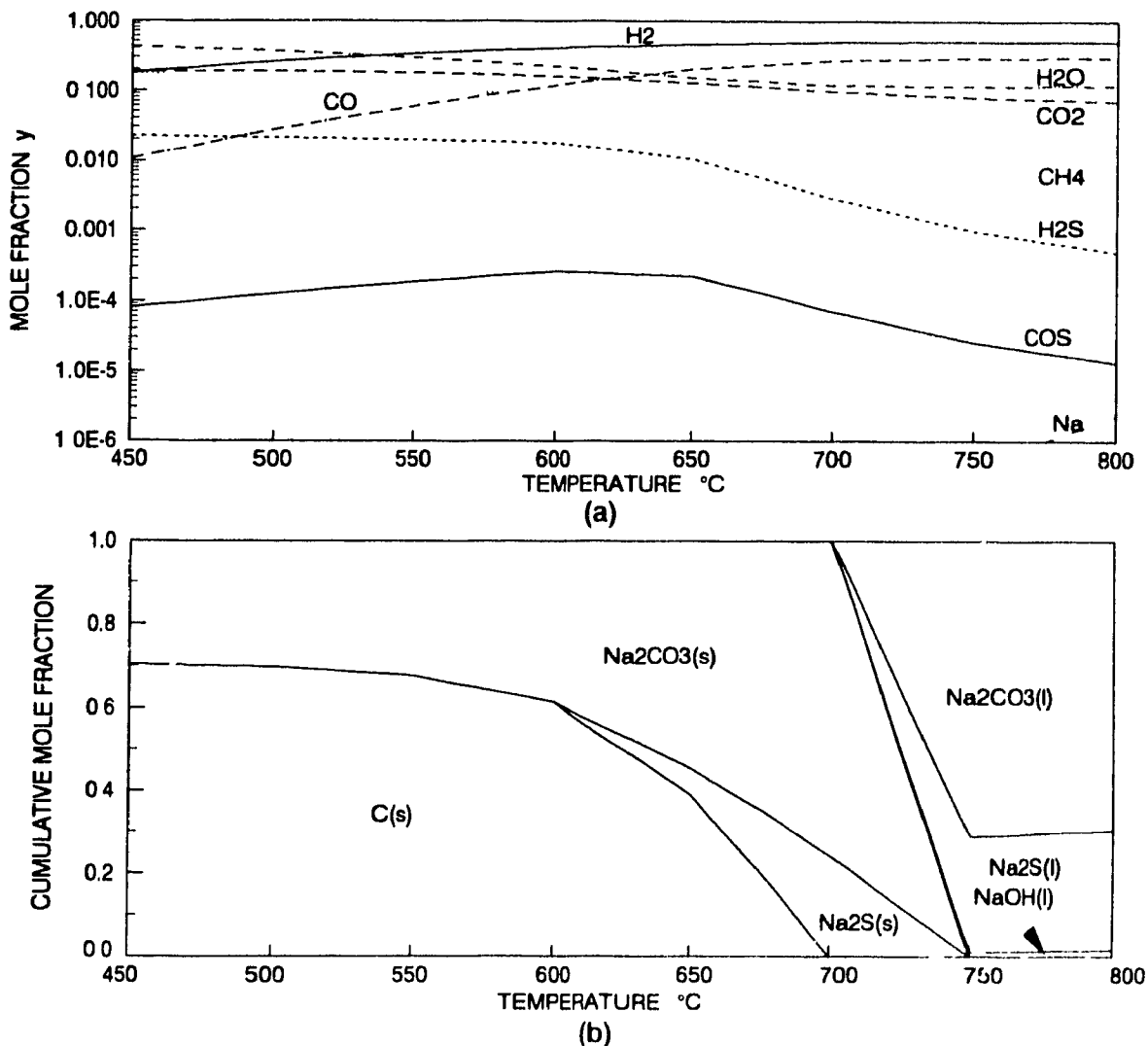


Figure 3.3 65% black liquor solids. (a) gas phase (b) condensed phases

The figures clearly indicate that lower char yields are thermodynamically favoured at higher temperatures. A characteristic common to all four cases is that at higher temperatures, essentially all of the sulphur is retained in the char. In addition, all the

sodium is present as Na_2CO_3 at low temperatures, and the yield of Na_2CO_3 remains constant until sulphur is retained in the char. At this point some of the sodium becomes associated with Na_2S . System (i), with 65% solids, shows some yield of NaOH above 750°C . Over the range of 550 to 750°C , the retention of sulphur in the char as Na_2S is predicted to increase as the solids content of the liquor increases.

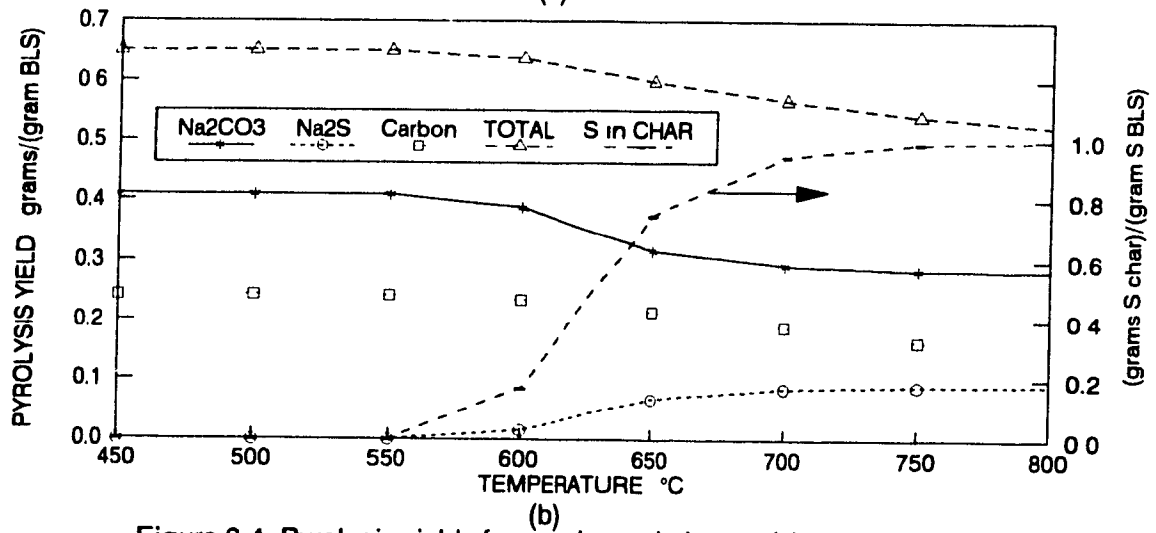
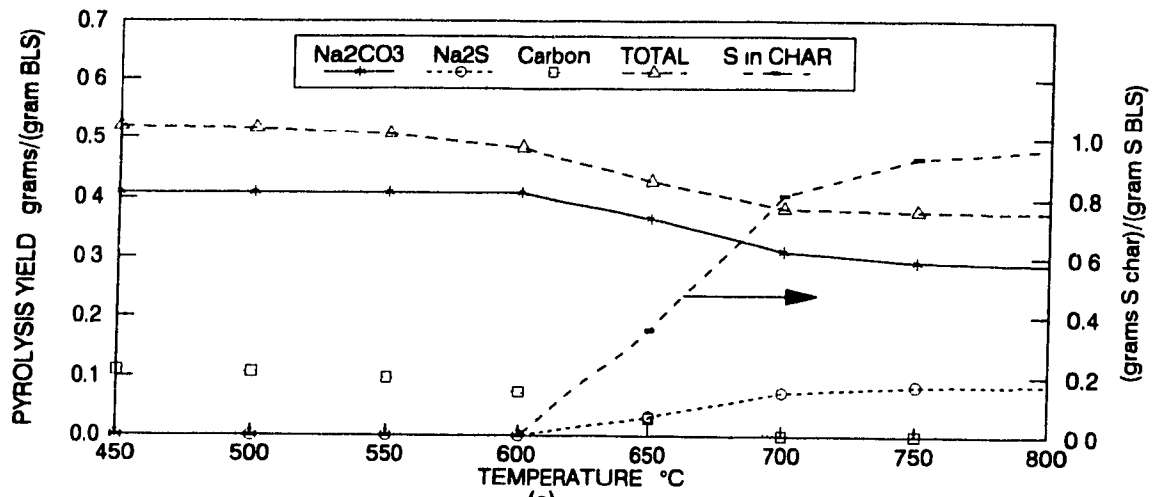


Figure 3.4 Pyrolysis yields for condensed phases (a) 65% solids liquor
(b) 93% solids liquor

The total yield of char increases as the solids content is increased, almost entirely due to an increase in the yield of fixed carbon in the char. At 65% solids content, complete gasification of the fixed carbon is predicted above 700°C .

The dilution of the gas phase with a large quantity of inert gas is predicted to have a

marked effect on the yields of the products. As can be seen by comparison of Figures 3.5(a) and 3.5(b), the retention of sulphur in the char as Na_2S at low temperatures is much higher with helium, as compared to the same temperatures without helium dilution. This correspondingly decreases the yield of Na_2CO_3 due to the Na balance. As compared to system (i), the total char yield for system (iv) is predicted to be slightly higher at 450°C , but somewhat lower from 500 to 800°C due to moderately greater gasification of fixed carbon.

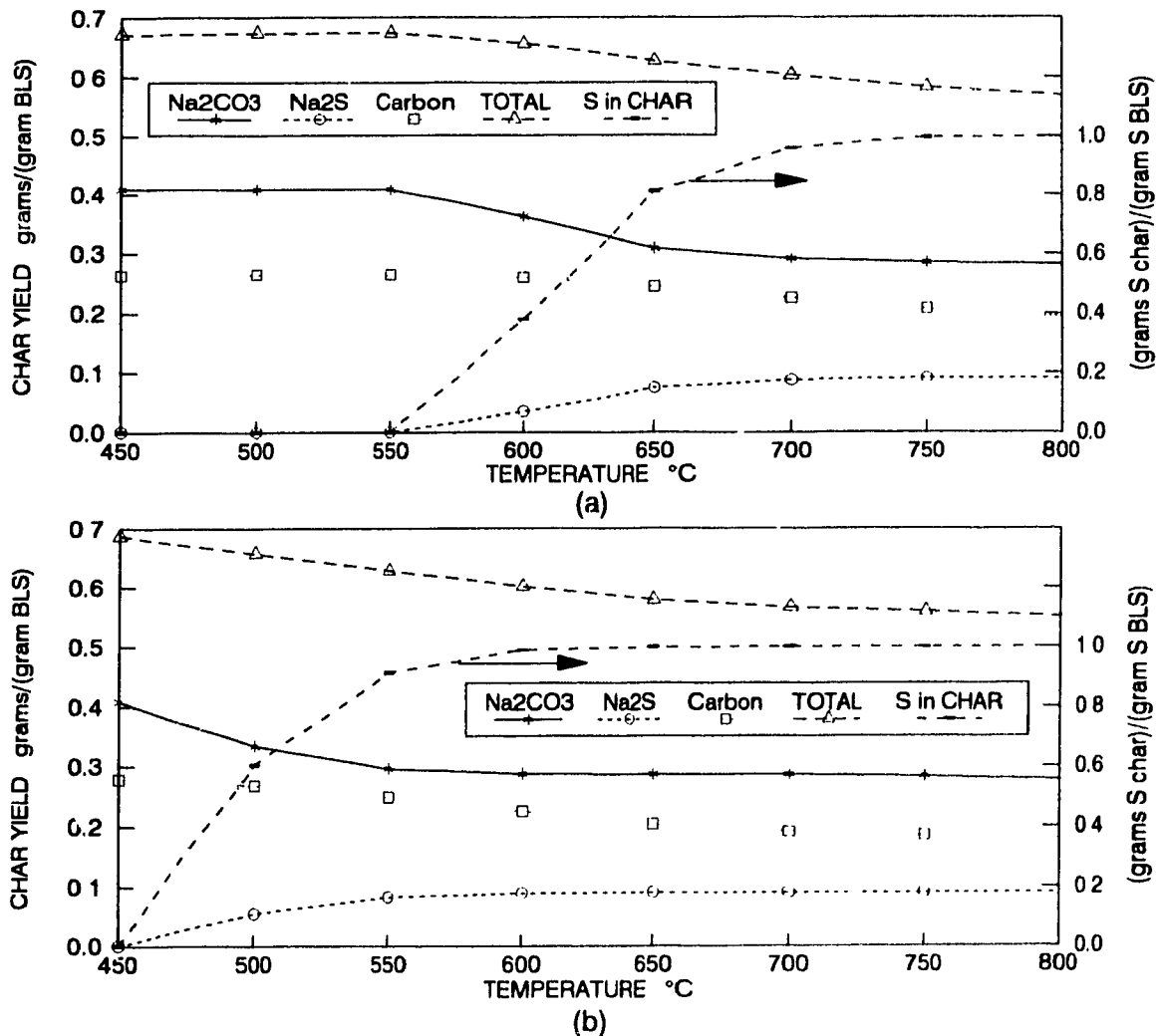


Figure 3.5 Pyrolysis yields for condensed phases. (a) 100% solids liquor
(b) 100% solids liquor with gas phase dilution by helium

The calculated gas phase pyrolysis yields are presented in Figures 3.6 and 3.7. General trends to observe for the gas yields, with increasing temperature, are: increasing

total gas yields; strongly increasing yields of CO; moderately increasing then decreasing yields of CO₂; decreasing yields of H₂O; decreasing yields of CH₄; increasing yields of H₂; and decreasing yields of H₂S. Not visible on the scale of these plots are decreasing yields of COS with temperature. As a verification of the sulphur balance, the yield of sulphur in the gas phase is the difference between 1.0 and the sulphur yield in the char.

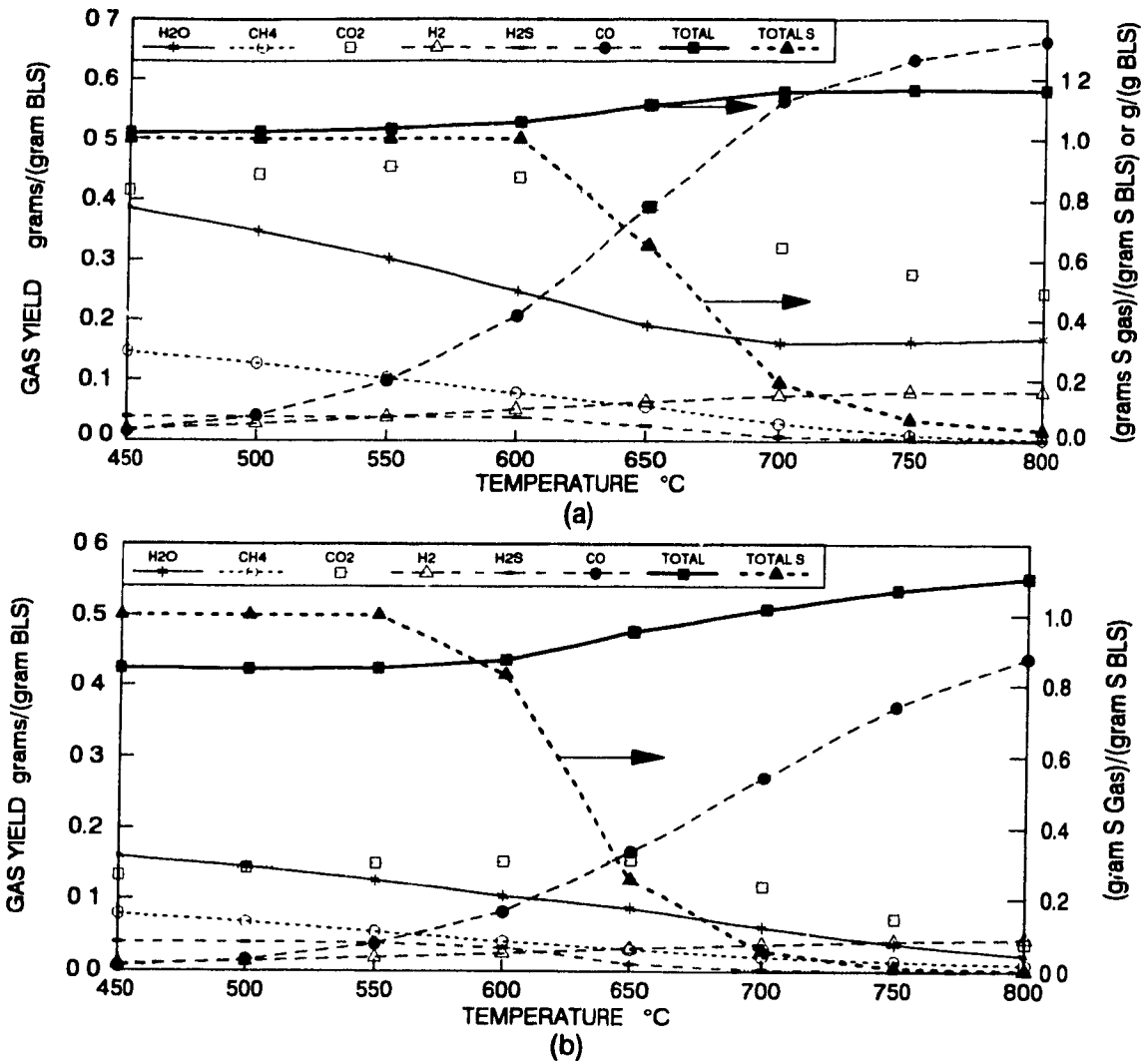


Figure 3.6 Pyrolysis gas yields. (a) 65% solids liquor (b) 93% solids liquor

Figure 3.8 shows the predicted sodium vapour yield for the gas phase. While the yield increases steadily with temperature, it remains below 0.01% in all systems except that with helium dilution. In the diluted case the sodium vapour yield is about two orders of magnitude higher, and reaches 1% at 800°C.

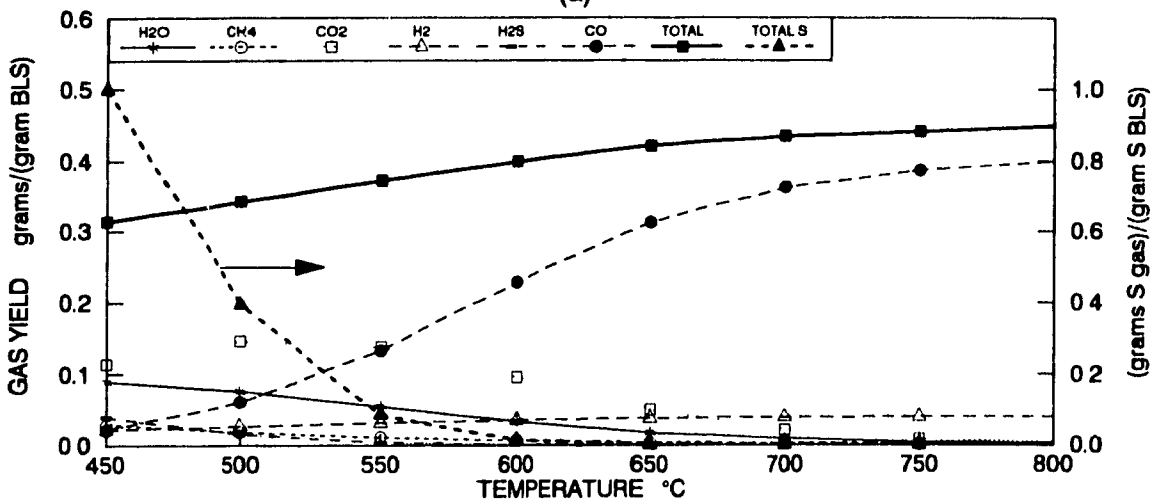
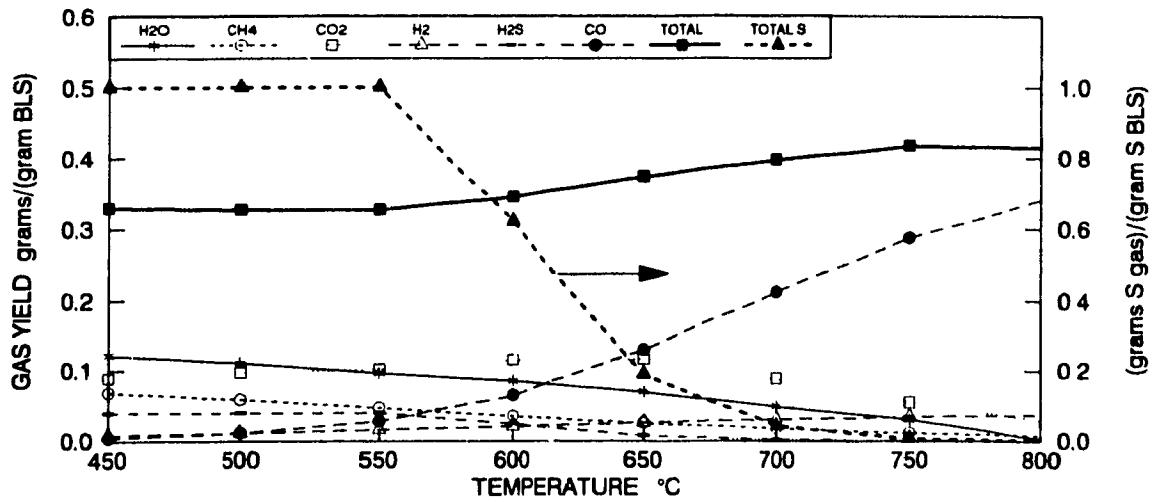


Figure 3.7 Pyrolysis gas yields (a) 100% solids liquor (b) 100% solids liquor with gas phase dilution by helium

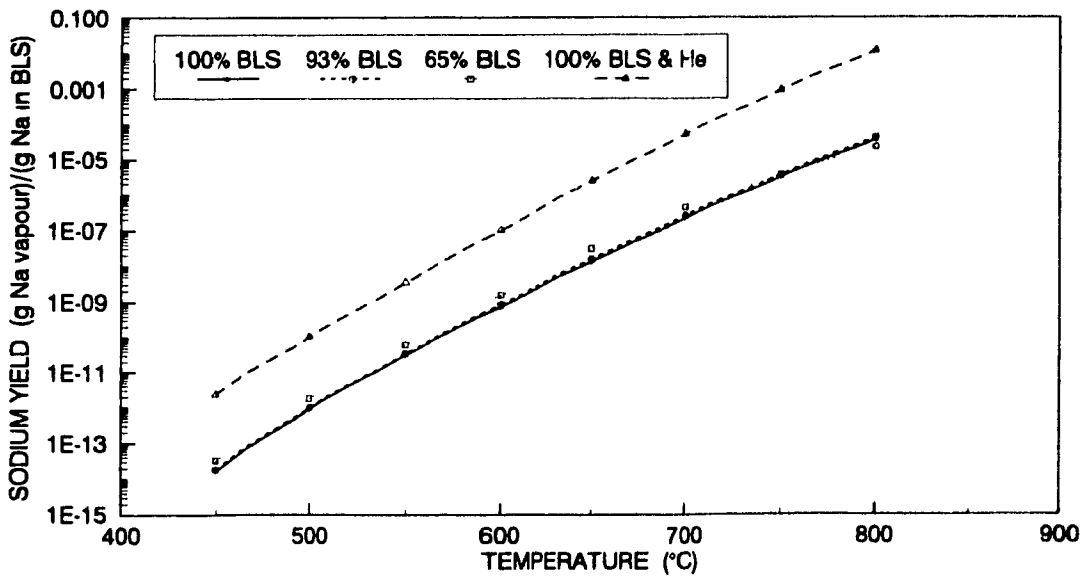


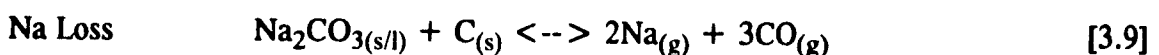
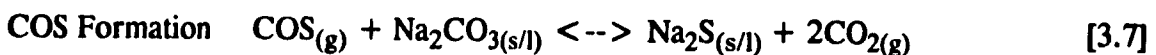
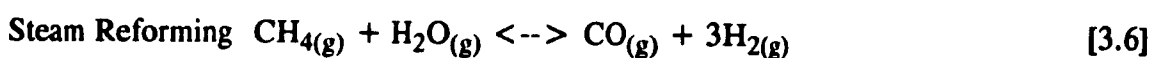
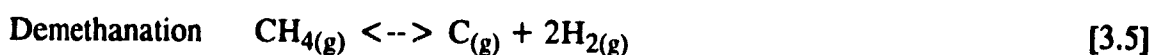
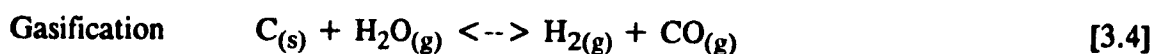
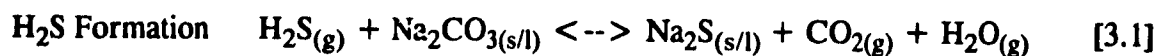
Figure 3.8 Sodium vapour yield

Comparison of Figures 3.6(a), 3.6(b), and 3.7(a) demonstrates the predicted effect of increased solids content on the gas yields. The readily observable trends with increasing solids content are decreased total gas yield and decreased gas yields of all important gaseous species. H₂S yield falls off the most strongly with increased solids content while CH₄ falls off more slowly than the other gases.

The effect of the helium dilution is also large on the gas phase yields, particularly at low temperatures, as can be observed in Figure 3.7(b). Yields of CO and H₂ are increased over the entire temperature range, while the peak in the CO₂ yield is increased moderately and shifted substantially from 650°C to 500°C. The dilution also causes suppression of H₂S formation at temperatures 100°C lower than the 100% solids case without helium.

Discussion

Most of the results described above can be explained in terms of the several competing reactions below which are known to occur in black liquor conversion processes (10,13,14,16,18,34,37). The reactions are written with the products favoured by high temperatures on the right-hand side of the equation.



In all four cases studied, lower char yields with increasing temperature can be explained by increased gasification of carbon as reactions [3.2] and [3.4] shift to the right at higher temperatures. The increase in Na₂S yield, and thus sulphur yield, in the char is due to the shifting of [3.1] to the right with temperature. The increase in sulphur retained in the char can also be explained by [3.1], as H₂O from the low solids content liquor shifts [3.1] to the left. The decrease in char yield with decreasing solids content is due to shifting [3.4] to the right with the addition of H₂O. The dramatic increase in retention of

sulphur in the char as Na_2S with the dilution of the gas phase with helium is best explained by considering equation [3.1]. The forward equilibrium constant for this equation, assuming the pressure is one atmosphere, is

$$K_p = y_{\text{H}_2\text{O}} \cdot y_{\text{CO}_2} / y_{\text{H}_2\text{S}} \quad [3.10a]$$

If System (i), 100% solids black liquor, is used as the starting point for the analysis, the equilibrium can be expressed as

$$K_p = (n_{\text{H}_2\text{O}} + \epsilon) \cdot (n_{\text{CO}_2} + \epsilon) / [(n_{\text{H}_2\text{S}} - \epsilon) \cdot (n_{\text{O}_2} + \epsilon)] \quad [3.10b]$$

where ϵ is the reaction extent. In the present case the reaction is limited by H_2S and thus ϵ is substantially less than n_{O_2} , $n_{\text{H}_2\text{O}}$, and n_{CO_2} . Therefore [3.10b] can be approximated by

$$K_p = n_{\text{H}_2\text{O}} \cdot n_{\text{CO}_2} / [(n_{\text{H}_2\text{S}} - \epsilon) \cdot n_{\text{O}_2}] \quad [3.10c]$$

Which upon rearrangement gives

$$\epsilon = n_{\text{H}_2\text{S}} - n_{\text{H}_2\text{O}} \cdot n_{\text{CO}_2} / (K_p \cdot n_{\text{O}_2}) \quad [3.10d]$$

Thus the dilution of the gas phase increases the extent of the reaction by reducing the second term on the right-hand side of equation [3.10d]. For large n_{O_2} the second term becomes insignificant and all the H_2S is converted to Na_2S . This dilution effect also increases the reaction extent for any reaction at atmospheric pressure in which the number of moles of gaseous products is greater than that of the reactants.

This dilution effect also explains the reduction in COS as there is a net increase in the number of moles of gas for reaction [3.7]. Similarly, the right hand sides of reactions [3.2], [3.4], [3.5], [3.6], [3.8], and [3.9] are favoured by dilution. The first four of these reactions explain the increased yields of CO and H_2 , since they are products, and also the reductions in H_2O , C, and CH_4 , which are consumed in these reactions. Equations [3.8] and [3.9] explain the large increase in sodium vapour yield caused by dilution, however the predicted extents of these reactions are relatively small.

Insight into the predicted changes in gas yields with temperature can also be obtained from examination of equations [3.1] through [3.9]. The strongly increasing yields of CO result from shifting to the right of equations [3.2], [3.3], [3.4], and [3.6]. While [3.8] and [3.9] also involve CO, the low extents of these reactions make their effects on CO minimal.

The pattern of increasing and then decreasing CO_2 yield must be explained in terms of equations [3.2], [3.3], [3.4] and [3.6]. As the temperature increases reactions [3.2], [3.4], and [3.6] will shift to the right producing CO and H_2 . At relatively low temperatures the shift reaction [3.3] will favour CO_2 and H_2 and thus H_2O will combine with CO to produce CO_2 . As the temperature increases, the tendency of CO to react to form CO_2 becomes weaker than the temperature shift of equation [3.3] to the right, thus

the CO₂ yield decreases.

Equations [3.4] and [3.6] explain the decrease in H₂O with temperature while [3.3] moderates this decrease. The decrease in CH₄ with temperature is predicted by equations [3.5] and [3.6]. The many routes of H₂ formation explain its increase with temperature while the shift reaction [3.3] again moderates the temperature effect. As discussed above, equation [3.1] explains the decrease in H₂S yield at higher temperatures.

Increasing solids content tends to decrease the gas yields because less H₂O is available to gasify carbon and form CO and H₂. Reduced concentrations of these species, and H₂O, strongly effect CO₂ primarily through reactions [3.2] and [3.3]. Since H₂ is still present in the system, and CH₄ is formed by combination of H₂ and carbon (reverse of reaction [3.5]), methane yield does not drop off as dramatically as the other fixed gases. The lower H₂S yield predicted is expected as lower H₂O and CO₂ concentrations result in [3.1] being shifted to the right.

Conclusions

Thermodynamic equilibrium modelling of combined black liquor pyrolysis and gasification, for conditions in which the gas phase is composed of pyrolysis/gasification products and possibly inerts, predicts the following:

- i) complete gasification above 700°C of all carbon not associated with Na₂CO₃ for 65% solids liquor
- ii) inorganic species, Na₂S and Na₂CO₃, being in a fully molten state above 750°C
- iii) high fixed carbon yields for high solids liquors
- iv) high sulphur loss to the gas phase at temperatures below 700°C
- v) enhanced retention of sulphur in the char and increased carbon gasification with dilution by inerts, but much higher sodium vaporization
- vi) an absence of mercaptans and thioalkanes in the gas phase
- vii) greater retention of sulphur in the char at higher solids contents
- viii) produced gases rich in CO and H₂ at temperatures above 700°C
- ix) produced gases relatively high in CO₂, H₂O, CH₄, and H₂S at temperatures below 700°C

Nomenclature

C_p	specific heat at constant pressure, kJ/mol/K
g	molar Gibbs free energy (chemical potential), kJ/mol
h	molar enthalpy, kJ/mol
K_p	gas phase equilibrium constant in terms of partial pressures
n	number of moles, mol
P	absolute pressure, atm
s	molar entropy, kJ/mol/K
T	absolute temperature, K
x	phase mole fraction (usually liquids)
y	gas phase mole fraction
τ	activity coefficient
ϕ	fugacity coefficient
ϵ	reaction extent, mol

Subscripts

f	indicates formation property
i	indicates species i
o	indicates initial quantity
T	indicates variable evaluated at the system temperature
T	indicates total quantity (in equations [3.10])
298	indicates property evaluated at 298 K

Superscripts

$^{\circ}$	indicates pure compound property - as an ideal gas at 1 atmosphere for gases and as pure liquid at its saturation pressure for liquids
α	indicates phase α
β	indicates phase β

CHAPTER 4 FAST PYROLYSIS EXPERIMENTAL APPARATUS AND METHODS

Introduction

A new experimental apparatus was designed and constructed in order to meet the objective of the present investigation of characterizing the transient production of gases evolved during the pyrolysis of kraft black liquor. The additional objective of achieving a complete mass balance for pyrolysis was also a major consideration in the design and the development of the experimental procedures. Since the design, construction, and development of the experimental procedures and equipment form a major part of this thesis, they are described in detail in this chapter.

Design Considerations for Apparatus

Previous workers in the field of black liquor pyrolysis have used many different types of experimental equipment to obtain their data. Feuerstein *et al* (14) conducted batch pyrolysis experiments by heating large quantities of liquor in evacuated carbuoys. Brink *et al* (16) sprayed liquor into a continuous pyrolysis reactor. Bhattacharya *et al* (17) pyrolysed relatively large quantities of solids in a preheated tube furnace. Many recent studies (9,11,39,40,19,20,21) have employed single droplet reactors, as they closely mimic the conditions of a droplet sprayed into a recovery furnace and they also allow the characterization of the phenomena during pyrolysis, as well as the analysis of the products of single droplets. While studies involving low heating rates (10,18,26) and large samples (14,16) have reported the yields of gaseous pyrolysis products, none of the single-droplet fast-pyrolysis-rate studies supply such information. Also, although some studies (9,11,19,20) have measured total production rates of sulphurous gases, or of CO and CO₂, the instruments used were usually too slow to measure the true production rates of these gases.

Thus, the primary requirement of the apparatus used in this study was that it be able to measure the production rates of the important gases produced during single droplet pyrolysis of kraft black liquor. For this reason, a fast response quadrapole mass spectrometer (MS) was chosen as the method of gas detection. Another desired characteristic of the apparatus and procedures was that they allow the establishment of mass balances, particularly those of carbon and sulphur. The ability to continuously measure the temperature of the black liquor droplets during pyrolysis was another requirement, so that kinetic analyses would be possible. A final objective was that the experimental apparatus allow accurate control of the pyrolysis atmosphere.

Description of Final Version of Apparatus

The fast pyrolysis apparatus in its final form is depicted schematically in Figure 4.1. The equipment can be split functionally into five units. The first functional unit is the gas preparation and flow control system. The second is the pyrolysis furnace complete with the sample insertion apparatus. The system immediately downstream of the furnace, which traps condensable products and aerosols produced during pyrolysis, forms the third unit. The fourth unit is the on-line gas analysis and data acquisition system, of which the quadrupole mass spectrometer and its controlling PC form the major part. The fifth functional unit comprises the tasks controlled by the personal computer, such as temperature data acquisition and synchronization.

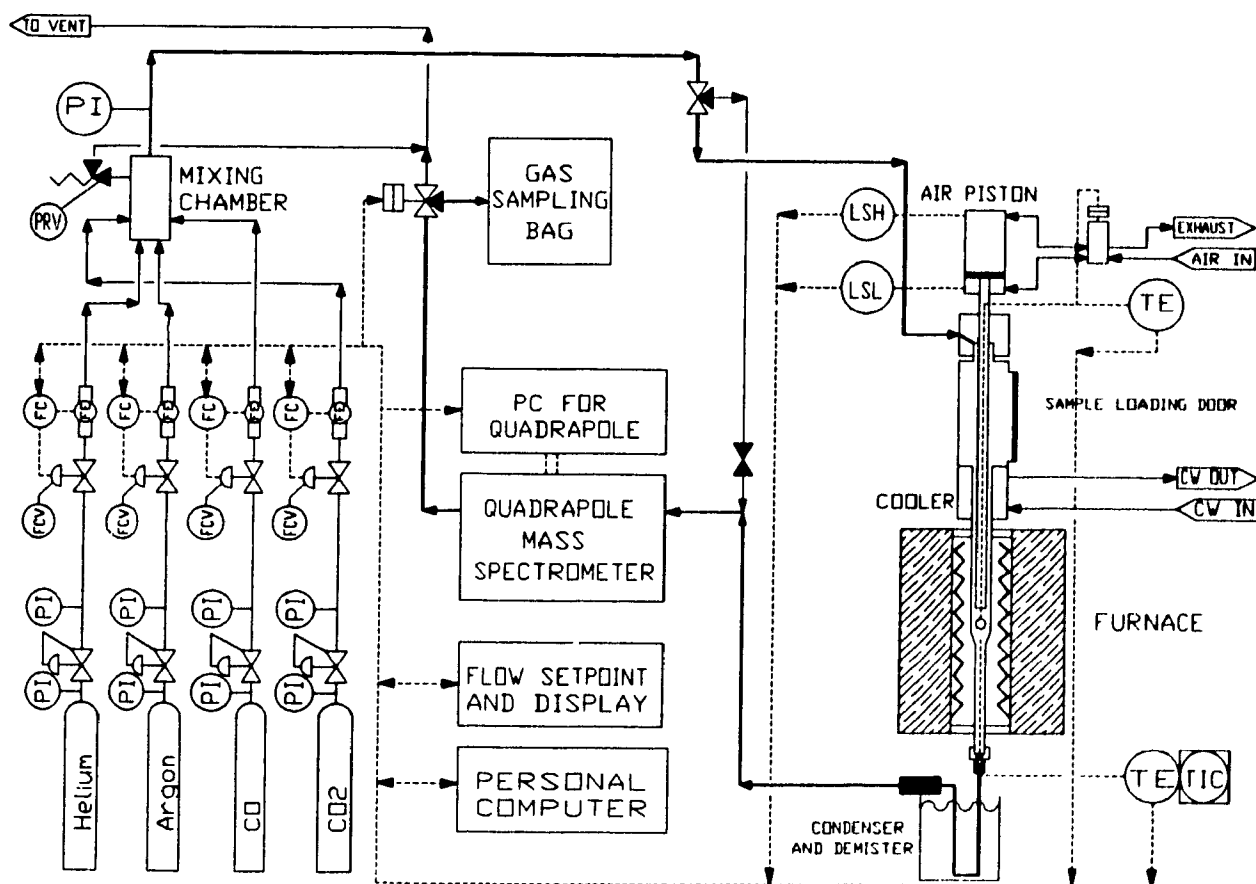


Figure 4.1 Schematic flow and instrumentation diagram for the fast pyrolysis apparatus

The gas preparation and control system is designed to produce inert, reducing, and gasification atmospheres of well defined compositions. All the gas flows are controlled by fast response mass flow controllers (Tylan Model 280-SAV) with the following ranges: He, 0-4.5 slm; Ar, CO, and CO₂, 0.300 slm (litres per minute at 1 atm and 0°C). Each gas is regulated to about 30 psig, passed through a combined moisture and hydrocarbon

trap, and then through an oxygen trap. The gas streams are combined in a small chamber, in which the flow is turbulent to promote mixing, and then fed to the furnace through inert PTFE tubing. A relief valve (PRV) protects the system from over-pressurization.

Pure helium is used to establish inert atmospheres and CO and CO₂ are added to establish reducing and gasification atmospheres respectively. Argon was considered as a tracer in the gas stream to measure the total gas flow rate, which varies as a result of dilution by product gases, following the method used by Cerfontain *et al* (56). However, it was found that the ion pump of the quadrupole MS was unstable when pumping argon, and a pumpable, non-reactive tracer gas was not identified. An alternative method to estimate the total gas flow rate is presented in a section below.

The pyrolysis furnace and sample insertion apparatus are designed to closely reproduce the heating history of a droplet sprayed into a recovery boiler or a fluidized bed unit. The furnace used is a commercially available tube furnace modified to mount in a vertical position. The temperature is controlled by a PID controller using a type K thermocouple as the temperature sensor, which is located in the centre of the tube about 20 mm below the sample. In order to reduce the response time of the apparatus, the quartz tube is reduced from 25 mm to 9.5 mm outside diameter immediately below the sample position, as shown in Plate 4.1 and Figure 4.2. This reduction greatly lowers the residence time of the produced gases in the furnace, thereby reducing the extent of secondary pyrolysis reactions and the mixing caused by axial dispersion in the tube.

The sample insertion apparatus is based on the much simpler arrangement of Deur-Siftar *et al* (57). When the furnace is hot or being heated, the sample is kept cool by the continuous flow of purge gas and indirectly by cooling water. Liquor can be applied to the thermocouple through the access door when the push-rod is retracted, or by removing the thermocouple probe (Figure 4.3 and Plate 4.2) after disassembling the furnace. The sliding seal on the push rod is attained with a double stuffing box using 1/8" x 1/8" asbestos packing. The seals between the stuffing box and the cooler and the cooler and the quartz tube are made with Viton O-rings. The lower joint between the quartz tube and the cooler is cooled by an external copper cooling-water coil as seen in Plate 4.1.

A pneumatic cylinder is used to rapidly move the sample from the cooler to the centre of the furnace and also to retract the sample from the furnace. The cylinder is controlled by an electric solenoid valve via a switch.

The thermocouple probe is designed to be removable so that the amount of liquor applied and the char yield can be determined accurately with an analytical balance. Initially a probe short enough to fit through the access door was used. However, the pin connections required were exposed to the high furnace temperatures and surface corrosion

occurred rapidly, making it impossible to maintain reliable electrical contacts. In addition, some weight loss of the probe occurred due to build-up and loss of the oxide film on the pins and this introduced additional error into the char yield measurements. To solve these problems, a long probe, see Figure 4.3, is used such that the pin connections are located in the core of the push rod outside of the furnace, where they remain cool. Unfortunately this long probe makes it necessary to cool and disassemble the furnace prior to loading and unloading the samples.

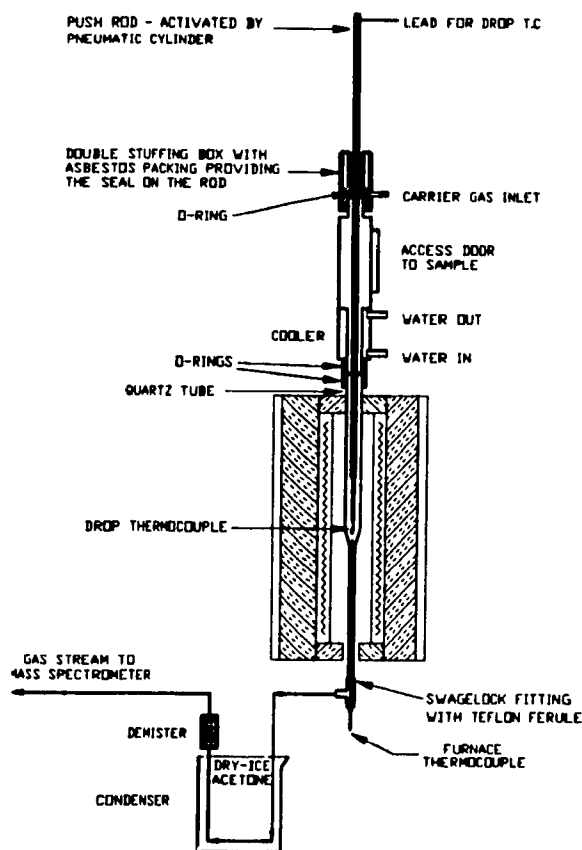


Figure 4.2 Fast pyrolysis tube furnace, sample insertion assembly, and condensables trapping apparatus.

The 0.010" diameter bare-wire type-K thermocouple at the end of the probe is formed such that the junction points up with a loop of wire below it, as shown in Figure 4.3. Plate 4.3a, b, and c show respectively the thermocouple bare, with a 20 mg liquor sample, and with the resulting char. As a liquor drop is heated, it first becomes less viscous before rapidly swelling and hardening. During the fluid stage, a drop will fall off unless the thermocouple is shaped as shown in Figure 4.3 to provide sufficient support.

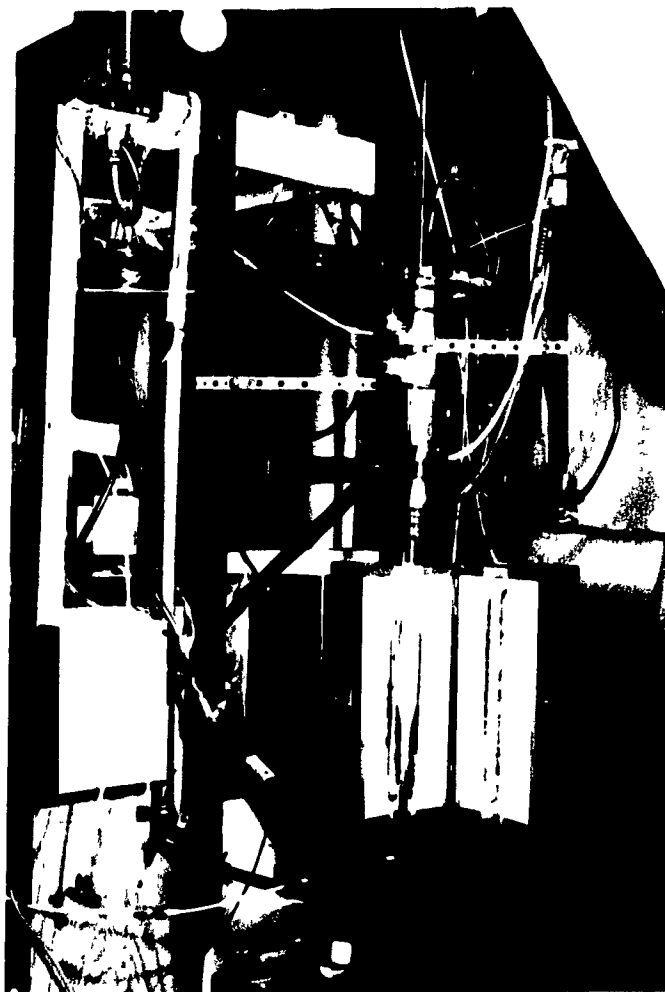
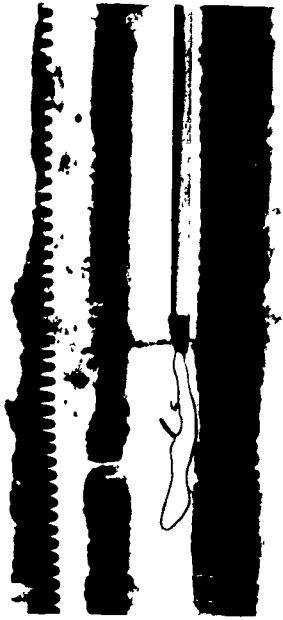


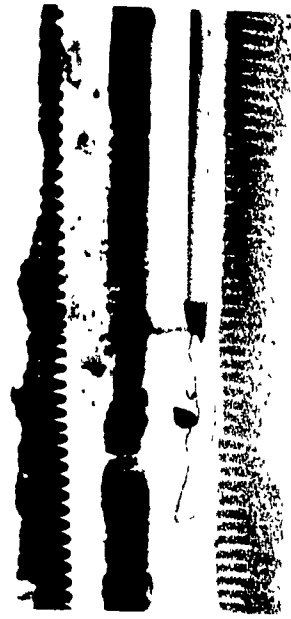
Plate 4.1 Experimental fast pyrolysis apparatus showing swaged quartz tube, tube furnace, condenser, sample cooler, push rod, and bottom limit switch.



Plate 4.2 Drop thermocouple probe constructed of 1/8" diameter alumina. Type K pin connectors are at left. Break in thermocouple wire has been repaired adjacent to junction.



(a)



(b)



(c)

Plate 4.3 Drop thermocouple shown bare (a), with 20 mg black liquor droplet (b), and with the resulting swollen char (c).

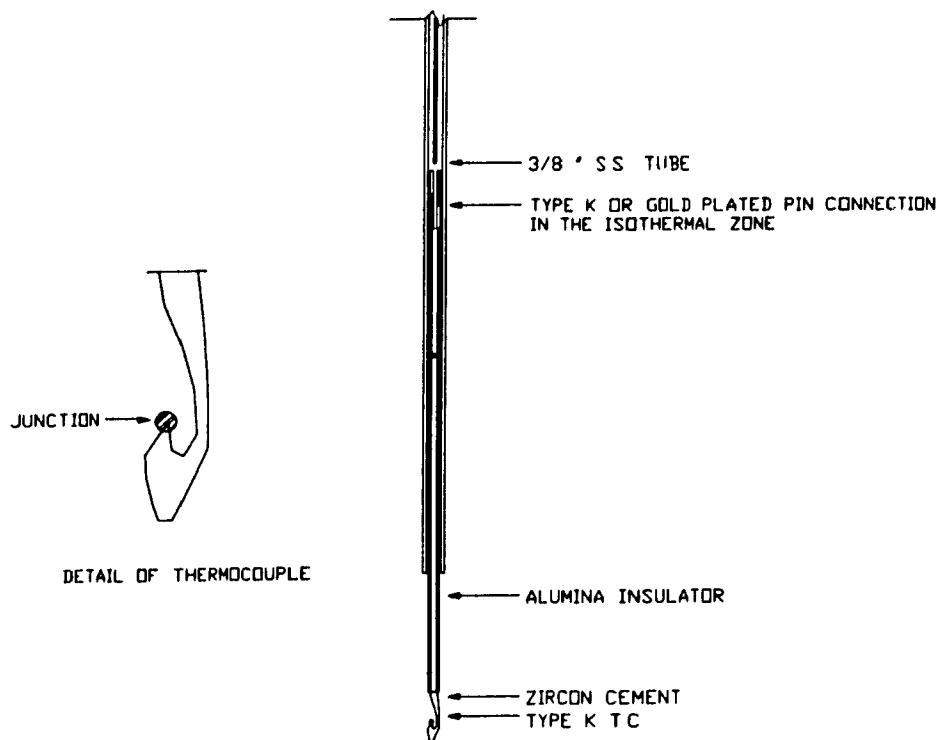


Figure 4.3 Detail of removable drop thermocouple probe showing pin connection in the unheated zone and the shape of the droplet thermocouple

Immediately downstream of the furnace the carrier gases and the volatile pyrolysis products enter the condenser followed by the combined demister and aerosol trap. The condenser is simply a 1/4" glass tube bent into the shape shown in Figure 4.2. The U-shaped tube is immersed in a coolant which is normally a mixture of dry-ice and acetone at -78 to -75°C . In some cases an ice and water slurry is used, but it is not nearly as effective as the dry-ice mixture. Fine GC grade glass wool is inserted into the downstream end of the glass tube to act as a demister and aerosol trap. New glass wool is normally used for each experiment.

Initially a more elaborate two piece U-shaped condenser was used, with both inlet and outlet valves, so that all the condensables could be trapped in the condenser and its weight gain determined both before and after the evaporation of condensed water and other volatile products. Unfortunately the weighing errors associated with this method were greater than the yields of condensables and thus the simpler condenser was employed. An alternative arrangement was also tested using ice-water coolant, followed by a glass wool demister, and then by an additional moisture trap containing glass wool saturated in fuming H_2SO_4 . However, tar condensation was not efficient with this method

and some tar was trapped in the H_2SO_4 , rendering tar analysis impossible. In addition, H_2SO_4 appeared to interfere with some of the produced sulphur gases, notably CS_2 .

From the condenser and the demister the gas flows through PTFE tubing to the inlet of the mass spectrometer (MS). The inlet of the MS is constructed of PTFE and stainless steel which is heated to 60°C to minimize the effects of adsorption. The MS, a VG Instruments Petra Survey, has a membrane inlet system which is designed to provide superior sensitivity to organic molecules, but as a result the sensitivity to some important gases, such as CO, is relatively poor. The gas stream flows past this membrane allowing a tiny fraction to diffuse across into the high vacuum chamber of the MS. The gas flow then exits the MS and is either discharged to a fume hood or collected in a previously evacuated sample bag. The form of data collected by the MS and its analysis are presented in a latter section. The gas collected in the sample bag can be analysed by gas chromatography to identify compounds and to determine gas yields as a check on the MS results.

The personal computer is equipped with an analog to digital (A/D) input-output (I/O) communications board and was used to both control and synchronize the experiments, and also to acquire data from the drop and furnace thermocouples. These functions are described in the following section.

Measurement of Drop and Furnace Temperatures and Computer Control

The temperatures of both the tube furnace and the liquor sample are recorded continuously during experiments. The millivolt signals from both the furnace and droplet thermocouples are conditioned using electronic ice-point compensators and then amplified 50 times using low noise battery powered amplifiers. The amplified signals are digitized and recorded at a sampling rate of 60 Hz per channel via the A/D board and a program written specifically to acquire the data and to perform experimental control functions. After gathering the data from an experimental run, the program also converts this data to temperatures using the NBS type-K eighth order polynomial correlations (58).

The calculated temperature series is then digitally filtered by either a non-recursive (FIR) or recursive (IIR) filter provided in a separate data file. Filtering is performed first in the forward direction and then the once filtered data is filtered again in the reverse direction to eliminate the phase shift caused by the first filtering. This method has been commonly used and has the additional benefit of doubling the order of the filter (59). In order to reduce filter transients, the first measured value is used to initialize the filter in the forward direction and the final filtered output value from the forward filtering is used to initialize the reverse filtering.

After investigating the effects of various filters on the temperature data, a fourth order Butterworth (IIR) filter with a cutoff frequency of 2.5% of the sampling frequency was selected. The filter was designed using MATLAB (59). A 2.5% cutoff corresponds to 1.5 Hz in the time domain and, as shown in Figure 4.4, is effective in reducing the noise level in the furnace temperature data, and yields smooth, differentiable curves for the drop temperature as a function of time, without significantly distorting the initial data.

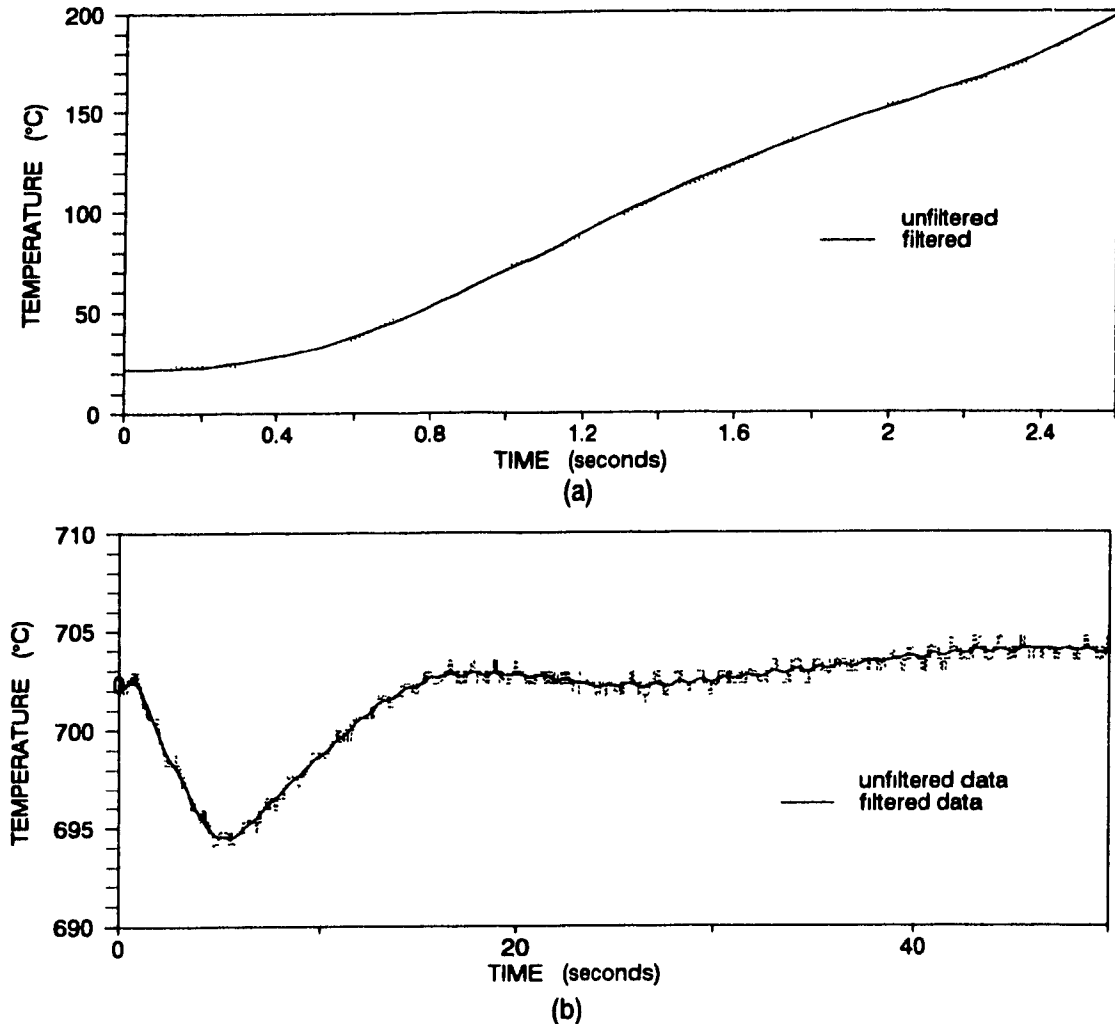


Figure 4.4 Results of digitally filtering furnace temperature data using a fourth order Butterworth filter with a cutoff frequency of 0.025
 (a) Drop data (b) Furnace data

The computer program also monitors the digital inputs and controls the digital outputs on the communications board. Limit switches at the top and bottom of the sample-insertion piston-stroke are connected as digital inputs. The bottom limit switch is

visible in Plate 4.1, immediately above the stuffing box. The signal from the top limit switch is used to trigger the temperature acquisition and its activation marks the beginning of a run. Upon this activation, the program sets a digital output high which is connected as an input to the MS computer, and is used to synchronize the two sets of data. In addition, a digital output is also used to control the sampling bag solenoid valve on the exhaust. This is opened at the beginning of the data acquisition and closed at the end, but can be kept closed by overriding the control with a switch.

The limit switch at the bottom of the piston stroke was used to measure the time required to move the sample from the cooler to the centre of the furnace. This sample insertion time was recorded for most of the experiments. Figure 4.5 shows that the distribution of insertion times is quite narrow with an average of 0.700 seconds and a standard deviation of 0.045 seconds.

As is evident in Figure 4.6, the temperature along the centre-line of the tube furnace rises rapidly to the set point, and axial gradients midway through the tube furnace are not significant in the pure helium atmosphere used in most of the present experiments. In addition, the radial temperature gradients midway through the furnace were found to be very small in pure helium, with a temperature difference of less than 5°C between the tube wall and centre-line. The relatively rapid temperature rise along the tube centre-line and the small radial temperature gradients are due to the high thermal conductivity and low heat capacity of helium. When the same tests were repeated with pure CO₂ the results were much different. The length of the tube required to heat the gas was increased and large radial temperature gradients were evident, with the temperature near the tube wall being about 30°C hotter than that at the centre-line. Due to the low thermal diffusivity of CO₂, bulk mixing is much more important and thus temperature fluctuations are large and random, reflecting the underlying turbulence of the flow.

A typical time-temperature history for a pyrolysis experiment in helium at 800°C is shown in Figure 4.7. It is evident that both heating and cooling are rapid in the apparatus. The changes in slope of the drop time-temperature curve shown in Figure 4.7(b) clearly show the insertion period, the relatively low heating rate period during drying, the rapid heating rate period above 200°C during which most of the devolatilization and swelling occurs, and then finally a phase of secondary devolatilization during which CO is also produced due to reduction of sulphate to sulphide by carbon. The final temperature rises above that of the furnace thermocouple due to the superior ability of the black liquor char to absorb radiant heat from the tube furnace. When both sample and drop thermocouples were bare, their temperature readings were in close agreement.

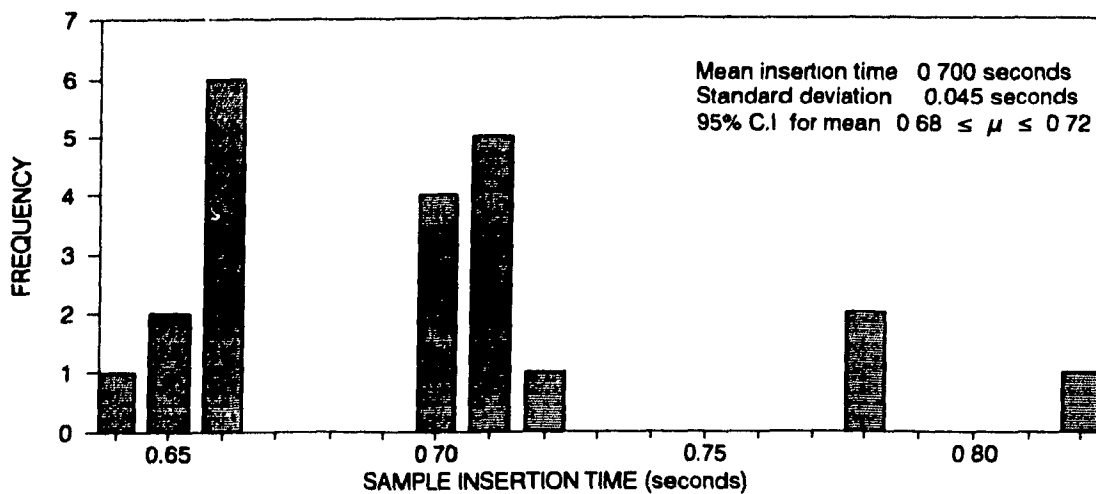


Figure 4.5 Distribution of sample insertion times for 22 fast pyrolysis experiments

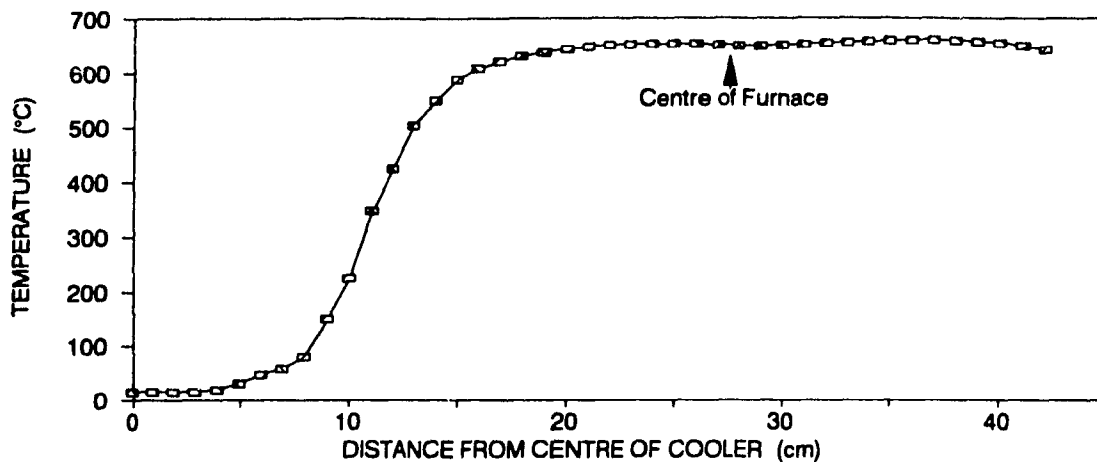


Figure 4.6 Temperature profile along the centre-line of tube furnace with helium flow rate of about 2.0 slm and a set point of 650°C.

Originally a 1/4" diameter drop thermocouple probe with a shorter length of bare thermocouple wire was used. Figure 4.8 shows the large improvement in heating rate obtained when the 1/8" diameter probe was used.

Background Information on Mass Spectrometry

Mass spectrometry is used to both separate and quantify species in a mixture, or to identify pure compounds. Mass spectrometers separate particles on the basis of mass to charge ratio m/z , where m is the particle mass in amu and z is the particle's positive charge expressed in fundamental charge units e . Magnetic field mass spectrometers

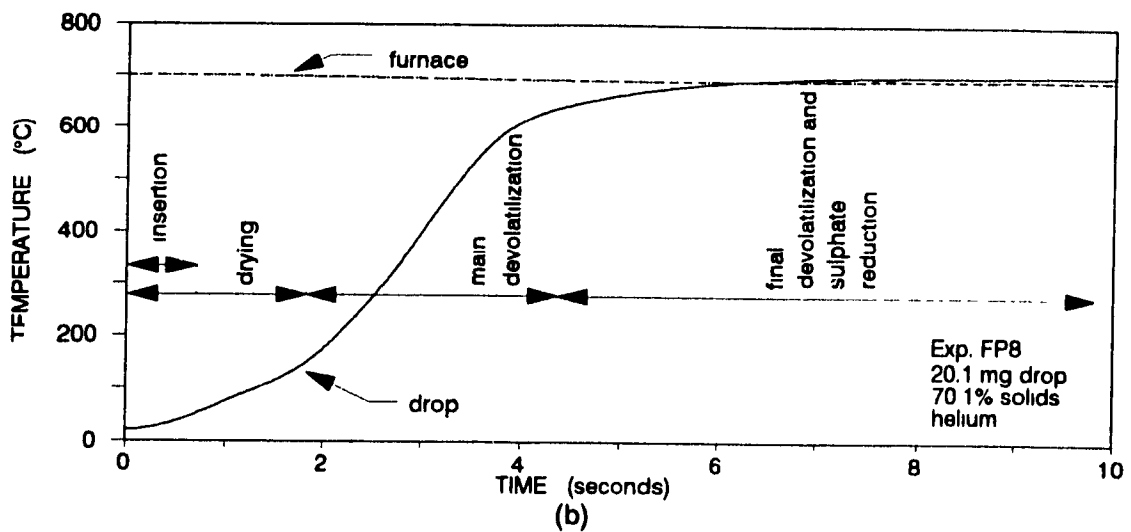
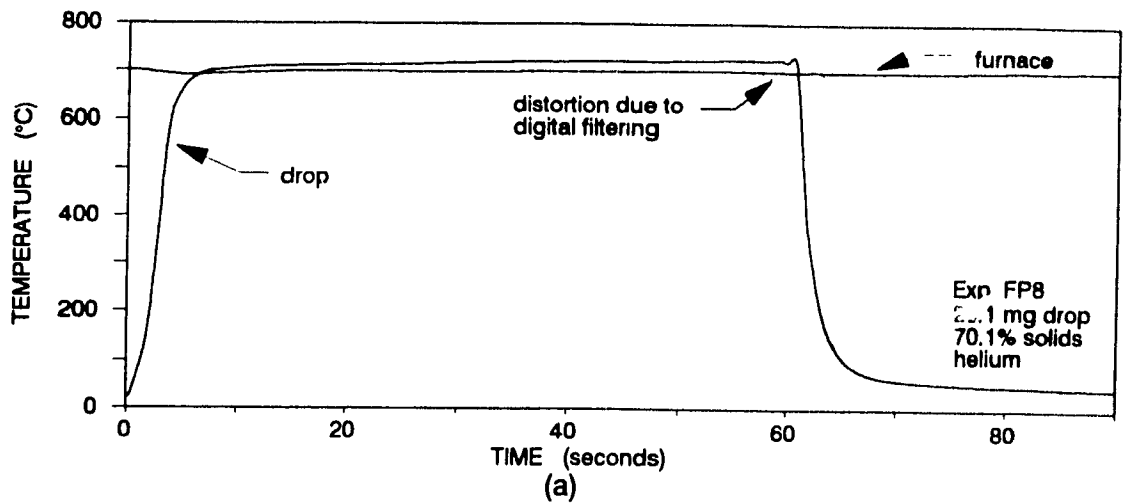


Figure 4.7 Typical time-temperature history for pyrolysis experiment at 700°C.
 (a) Full history
 (b) Initial 10 seconds showing drying and devolatilization stages

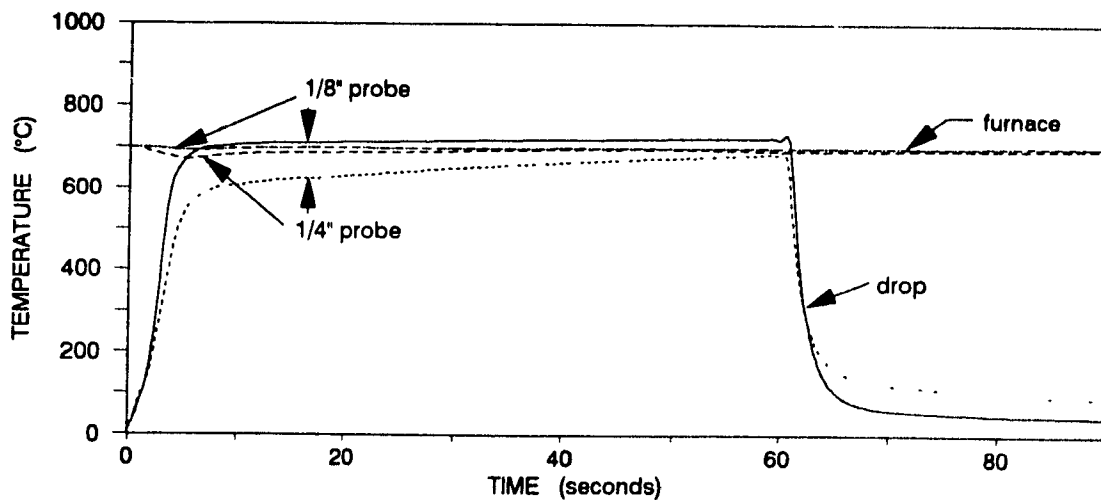


Figure 4.8 Comparison of heating histories for liquor drops and the furnace when using probes made from 1/4" and 1/8" diameter alumina rod.

separate on the basis of the curvature of a particle's path through a magnetic field. Quadrupole mass spectrometers separate on the basis of path stability in an oscillating electric field. Quadrupoles are generally only able to resolve particles to the nearest integer valued m/z while magnetic field instruments can have much greater resolution.

The material to be analysed in a MS must be first be vaporized and then ionized. Vaporization is normally achieved by heating and with reduced pressures of 10^{-6} Torr or lower. The gaseous molecules are ionized by impact with an electron beam which is typically of an energy level of 70 eV. Although this energy level is generally much higher than that required to ionize an average molecule (60), it is necessary to produce enough ionized particles to have sufficient response. Since the energy level of the electron beam (ca. 1600 kcal/mol) is much greater than that typically required to break covalent bonds (50-100 kcal/mol) (60), molecules also fragment. A fragmentation pattern is distinct for a particular compound on a given apparatus and may be used to identify pure species, for example those eluting from a column in a GC-MS system. Fragmentation produces both free radical and radical cations but only the radical cations are detected by the MS. Hydrocarbon fragmentation will always produce a greater abundance of carbocations with secondary carbons rather than primary carbons because of the greater stability of the secondary carbocations due to charge delocalization (60). Similarly C-C bonds next to carbonyl groups break easily because resonance stabilized ions are produced. This is also true for any C-C bond adjacent to an atom with unshared electron pairs (60). Small neutral molecules are sometimes mass eliminated from the parent molecule in this process, such as H_2O from an alcohol radical, or CO_2 from a carboxyl radical (60). These fragmentations in the ion beam are generally similar to decompositions that occur during pyrolysis.

The response of a MS at a particular m/z ratio is indicative of the abundance of cations with that charge ratio and the relationship is generally linear, provided that the response of the inlet system is also linear. Thus, when monitoring a single gaseous compound a carrier gas, for example CO_2 in helium, which have primary response peaks at m/z ratios of 44 and 4 respectively, the response at the m/z ratio of 44 is a function of the CO_2 concentration. However, when a higher molecular weight compound such as CS_2 is also present, and this compound also produces a cation with a m/z ratio of 44, the response at this ratio is now due to both gases. In this case the solution to determining the amount of CO_2 is relatively simple as the amount of CS_2 can be determined from the response at the m/z ratio of 76 and the contribution of CS_2 to the response at the m/z ratio of 44 can be calculated knowing its fragmentation pattern. After subtracting the contribution of CS_2 to the m/z ratio of 44, the CO_2 concentration can be directly

calculated. This strategy can be repeatedly applied to quantify a mixture of several known gases, provided that each compound with successively higher atomic weights has a response in its fragmentation pattern at a m/z ratio which is distinct from those of compounds with lower atomic weights. For such a mixture, the contribution of the heavier compounds to responses at lower m/z ratios can be accounted for one by one by beginning with the heaviest compound and then proceeding with each progressively lighter species. The only information necessary is the fragmentation pattern for each compound, the response of the mass spectrometer to each compound (i.e. calibration), and which gases are in the mixture. The latter of these can be determined by gas chromatographic analysis, although in practice it may be difficult to identify all the compounds.

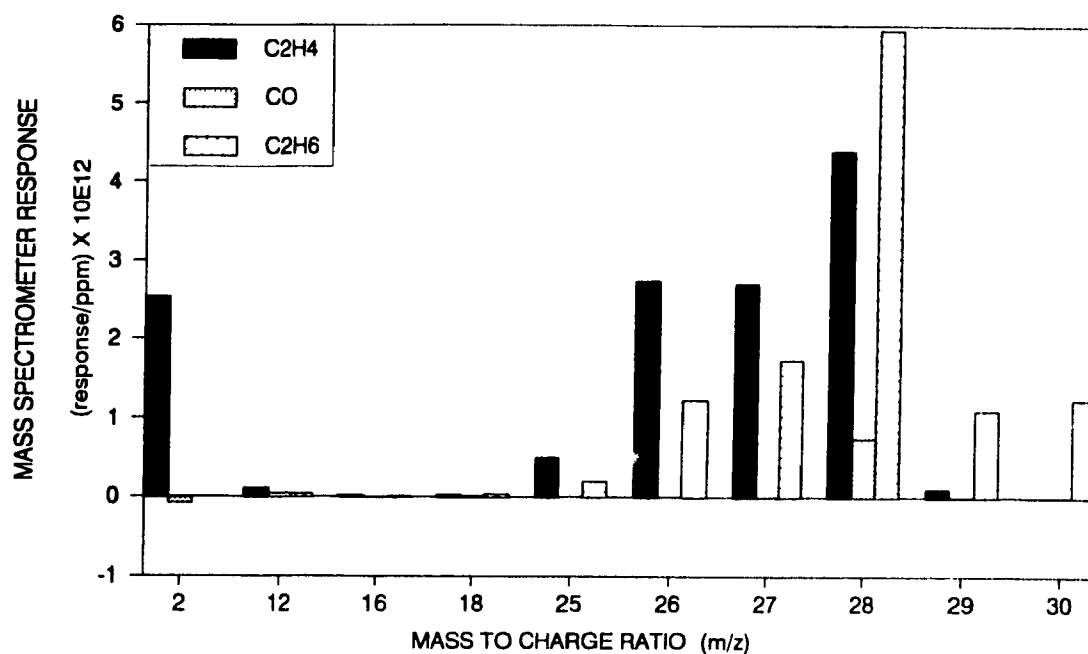


Figure 4.9 Overlapping cracking patterns for CO, C₂H₄, and C₂H₆

Difficulties arise when there are several compounds in the mixture which share a single m/z ratio as their strongest or primary response peak. This is true, for example, for mixtures of CO, N₂, C₂H₄, and C₂H₆ which share a m/z ratio of 28 as their primary peak, as can be seen in Figure 4.9. In this case it is usually necessary to use a statistical method to estimate how much each compound is contributing to each m/z ratio. The objective of such a method is to determine which combination of gas concentrations provides the best fit to the measured response. The success of this procedure is dependent on the accurate knowledge of the fragmentation patterns and the response calibrations of all the gases in the mixture.

Mass Spectrometer Statistical Data Reduction Method

The statistical data reduction method proceeds as follows:

- Let
- peak-j = a unique m/z ratio of value not normally equal to j
 - s_j = measured response at peak-j (a particular m/z)
 - n = total number of peaks (different values of m/z)
 - p = total number of gases
 - M_{jk} = linear response factor at peak-j due to gas k
 - s = response vector ($s_1, s_2, s_3, \dots, s_n$)
 - c_k = estimated concentration of gas k
 - c = estimated concentration vector ($c_1, c_2, c_3, \dots, c_n$)
 - S_j = estimated response at peak-j
 - S = estimated response vector

The estimated response is then

$$S_j = c_1 M_{j1} + c_2 M_{j2} + \dots + c_p M_{jp} \quad [4.1]$$

This is analogous to a linear regression in which the response s_j is the measured dependent variable, S_j is the estimate of the dependent variable, M_{jk} is the j th measurement of the k th independent variable, and the c_k are the linear coefficients determined by the regression. Continuing the analogy, the number of data sets is equal to n , the number of m/z responses measured. The objective function minimized, ϕ , is the sum of squares error between the measured dependent variable and its estimate:

$$\phi = \sum_j w_j (S_j - s_j)^2 \quad [4.2]$$

Here w_j is a weighting parameter which can be used to make peak j more or less important than other peaks, depending on the expected variance of peak j . For example, higher values of w_j can be used for peaks which are deemed to be more reliable than others due to such effects as the instrument being more stable at higher gains (61), and lower values of w_j for peaks which are considered unreliable due to effects such as background noise. ϕ is minimized by taking derivatives with respect to the coefficients c_k in the usual manner. The resulting set of p equations in p unknowns, expressed in matrix form, is:

$$N \cdot c = r \quad [4.3]$$

$$\text{where } N_{ab} = \sum_j w_j M_{ja} M_{jb} \quad \text{for } j = 1 \text{ to } n \quad [4.4]$$

$$r_k = \sum_j w_j M_{jk} s_j \quad \text{for } j = 1 \text{ to } n \quad [4.5]$$

The solution for c can be easily determined by a number of methods for solving sets of linear equations, for example LU decomposition (62). Only the vectors c and r change for a new set of data. The matrix N is invariant for a particular set of conditions as it only depends on the cracking patterns and the weighting factors. The shortcoming of this method is that it does not guaranty that the values of c_k calculated will be positive. When

negative values of c_k are calculated, which is impossible in reality, one strategy is to discard that gas from the procedure and repeat the calculations (61). Another is to adjust the weighting factors. When it is not reasonable to discard any of the gases from the calculations, for example when they are known to exist in the mixture, and negative concentrations are calculated, it could be due to the presence of an unidentified compound in the mixture.

Since this method is actually a statistical best fit, it is necessary to maintain several degrees of freedom for analysis of error if confidence intervals for the parameter estimates are to be kept small. The applicable number of degrees of freedom is equal to $(n - p)$, the difference between the number of peaks and the number of gases. Thus as p approaches n the results will become progressively more uncertain.

Method Used to Analyse Mass Spectrographic Response Data and Typical Results

The mass spectrometer was used in a Multiple Ion Monitoring (MIM) mode to gather the experimental response data since this provides the fastest scanning rate. The instrument employed is only able to monitor 16 selected inputs or m/z ratios in this mode. Since one input was used to synchronize the MS data to the sample insertion and temperature data, only 15 channels were available to monitor m/z ratios. The m/z ratios chosen were 12, 16, 18, 25, 26, 27, 28, 29, 30, 34, 44, 48, 62, 76, and 79. The latter six were chosen as they are either primary or strong peaks for H_2S , CO_2 , CH_3SH , CH_3SCH_3 (DMS), CS_2 , and CH_3SSCH_3 (DMDS) respectively, and these peaks are not influenced by lighter compounds. The lower nine mass peaks, i.e. m/z ratios of 30 and less, were used to calculate the concentrations of CH_4 , H_2O , C_2H_2 , C_2H_4 , C_2H_6 , CH_3OH , and in some cases CH_3COCH_3 . The cracking patterns of this latter group of compounds have many common peaks, and for this reason many peaks in the mass range 12 to 30 were sampled so that the statistical fit method presented above could be employed to estimate the concentrations. It is interesting to note that none of the earlier papers in this field reports both C_2H_2 and C_2H_4 , but many report either one or the other. Acetylene and ethylene are difficult to separate, so it is probable that what many authors have classified as either C_2H_2 or C_2H_4 may in fact be a mixture of the two gases (14,16,63,68).

Since all the experiments were performed in carrier gas which was predominantly helium, it was not possible to use the MS to determine with any accuracy the amount of hydrogen produced. This limitation results from helium having a relatively large secondary peak at the m/z ratio of 2, the same ratio which would be used for hydrogen detection. The relatively small contribution of H_2 to the response at this m/z ratio did not

allow meaningful determination of hydrogen concentrations. Experiments performed in N_2 would allow H_2 to be determined, but since nitrogen would interfere with many other gases at the m/z ratio of 28, these experiments would have to be performed in addition to those in helium. Other inert gases, such as argon, cannot be used since they are not effectively pumped by the ion pump of the MS.

The method of analysis used to calculate the concentrations of the sulphurous gases and CO_2 was to use the major peaks listed for them above, and the response factors determined by calibration with standards. The contribution of the heavier compounds to the lower peaks was accounted for by successive analysis of compounds of decreasing molecular weight, from CH_3SSCH_3 to H_2S . Since H_2O was the dominant contributor to the response at the m/z ratio of 18, the next step was to use this peak to calculate the H_2O concentration and to subsequently account for the contribution of H_2O to the response at the m/z ratio of 16.

The method used to calculate the remainder of the gas concentrations to use the response at the m/z value of 30 for ethane, 29 for methanol, 28 for carbon monoxide, 27 for ethylene, 26 for acetylene, and 16 for methane. The concentrations were calculated from ethane to methane in the order given above, subtracting the contributions of heavier compounds to responses at lower m/z values for each subsequently lighter compound. Since ethane and methane each contribute substantially to the responses at both the m/z ratios of 29 and 30, their concentrations are overestimated by this calculation procedure, and therefore so are those reported in this thesis. In order to prevent this overestimation from severely distorting the calculated values for CO, only 50% of each calculated contribution to the m/z ratio 28 was subtracted for these compounds. This procedure was determined by a trial and error process, such that no negative response values were obtained as a result of subtractions to lower peaks. At $500^\circ C$, when it appeared that acetone was more significant than ethylene, the response at the m/z ratio of 27 was used to estimate the acetone concentration.

The concentrations of the compounds calculated in this manner are believed to be of reasonable accuracy, except for perhaps that of CO. The much lower sensitivity of the MS to CO compared to those of other gases led to large errors, due to small errors in accounting for the contributions of other gases to the m/z ratio of 28, which was used to calculate CO concentrations. C_2H_4 was determined using the m/z ratio of 27, but it also contributes substantially to m/z 28. Although C_2H_4 is produced in molar quantities at least an order of magnitude less than those of CO (63), the contribution of C_2H_4 still can produce appreciable errors because the relative response of the MS to C_2H_4 at m/z 28 is 6 to 7 times that of CO at this peak. Other substances which also contribute to the m/z ratio

of 28, but which are not taken into account, compound the errors.

A program was written which can perform the data analysis following the statistical or the more pragmatic method which was used for the actual data, or a combination of the two methods. Depending on the arrangement and value of the linear response factors M_{jk} , and of the parameters which select the number of gases to be considered and the method of analysis, either data reduction method can be employed. The program also includes options for performing digital filtering and deconvolution computations (explained below).

The data from some experiments were also analysed using the statistical method. However, large negative concentrations were calculated for compounds which were certainly present in the mixture, as can be seen in Figure 4.10(a). Adjustment of the weight factors had little effect on the results. Since the raw mass spectrometer data suggested that methanol and acetone were probably present in the pyrolysis gases, these compounds were added to the data reduction procedure. Although some improvement was obtained (see Figure 4.10b), the results were still unacceptable and therefore the statistical data reduction method was not used for the final analysis of the present data. Probable explanations for these results are threefold. Firstly, the presence of unidentified compounds in the mixture may produce a magnified response at one or more m/z ratios and therefore cause a peak pattern which cannot be produced by addition of the cracking patterns used. Secondly, small errors in the determination of cracking patterns during calibration could also produce the observed results since it would not be possible for a linear combination of the cracking patterns to be equal to the response. Finally, the latter problem may have been aggravated by the small number of degrees of freedom available for the estimation techniques, due to the large number of gases and the limitation of 15 different m/z ratios.

Each m/z ratio response measured by the mass spectrometer was sampled at a rate of approximately 2 Hz, the maximum attainable with the present apparatus when using all of the available 16 channels. The recorded ion responses were slightly distorted due to random instrument error (noise). Sixteen 16 times oversampling was used on the m/z ratio of 28 in order to reduce this noise to an acceptable level. This extra noise at the m/z ratio of 28 was due to slight background levels of nitrogen in the system, despite efforts to eliminate it. Digital filtering was tested on the response data, but since the time scales of the pyrolysis events and of the sampling period were similar, filtering caused excessive attenuation of high frequency events, and was therefore not used.

Figure 4.11 shows the unfiltered ion responses of the MS for a pyrolysis experiment at 800°C performed in helium. The step in the synchronization in Figure 4.11(b) marks the insertion of the drop into the furnace. The negative starting values shown were caused

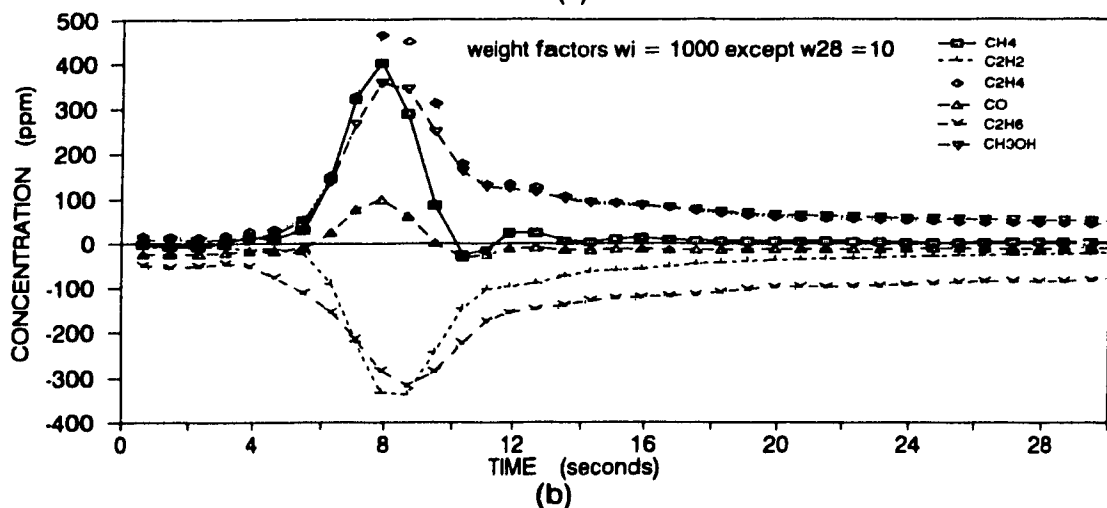
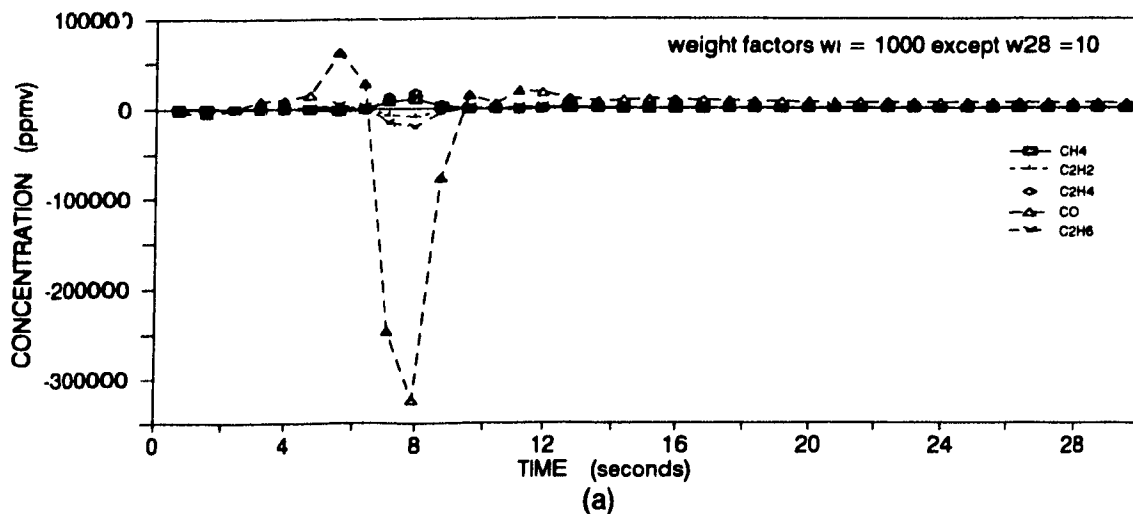


Figure 4.10 Gas concentrations calculated using statistical method for the overlapping gases
 (a) With 5 overlapping gases (b) With 6 overlapping gases

by drift of the instrument and changes in background levels. Before calculating the gas concentrations shown in Figure 4.12, each ion response curve was zeroed by subtracting the average of its first five response values from each of its response values, in order to compensate for instrument drift and changes in background levels, and by synchronizing time zero with the temperature data. The gas concentrations were used to calculate the total flow rate shown in Figure 4.13, and subsequently the concentrations and total flow were used to calculate the mass flow rates. Any negative concentrations calculated by the data reduction procedure were set to zero when calculating the mass flow rates. The mass flow rates were numerically integrated by the trapezoidal method to obtain the total gas

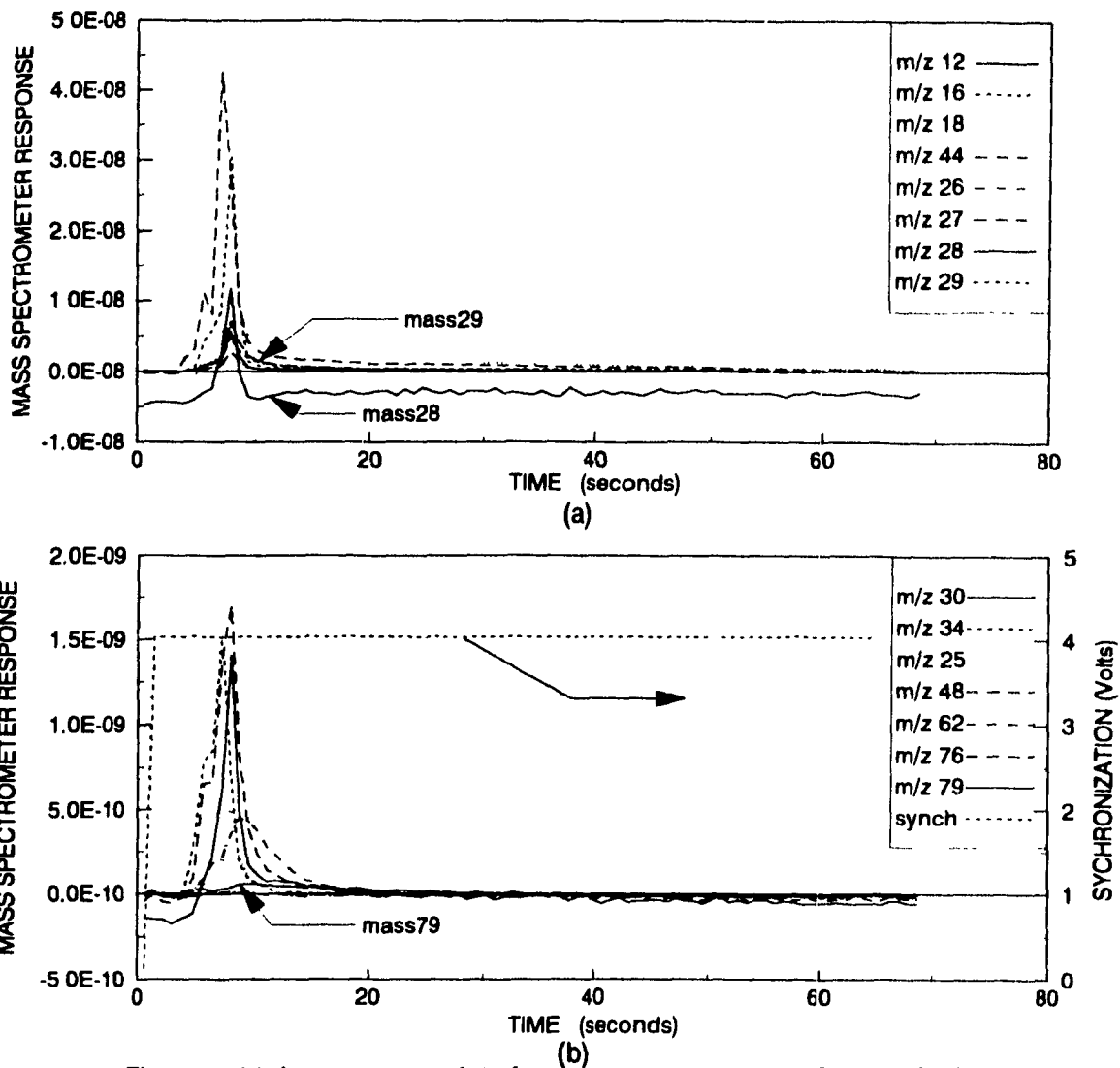


Figure 4.11 Ion response data from mass spectrometer for a typical experiment

production. In cases where the response curve was very noisy, the integration was terminated shortly after the mass flow rate approached zero.

The total gas flow $Q_{v,total}$ was calculated using

$$Q_{v,total} = Q_{v,carrier} / (1 - \sum_i y_i) \quad [4.6]$$

which assumes that the stream is composed of the controlled carrier gas flow rate $Q_{v,carrier}$ plus the calculated mole fractions y_i . It was assumed that the hydrogen concentration was 10% of that of CO based on the results of Bhattacharya *et al* (17). Figure 4.13 shows that the increase in flow rate due to the produced gases is only a few percent, and thus the error in the gas production rate data resulting from the above assumption is negligible.

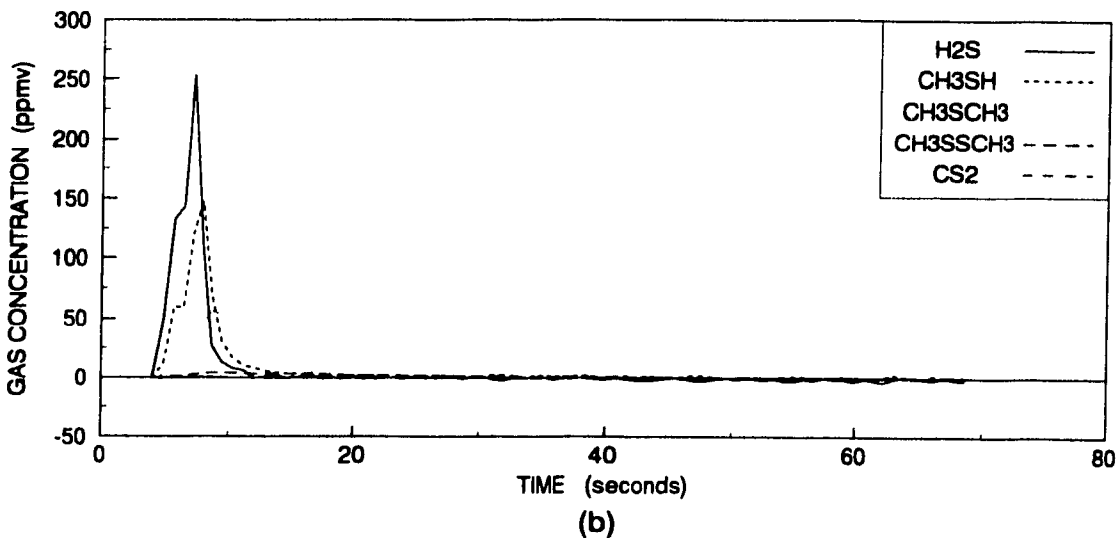
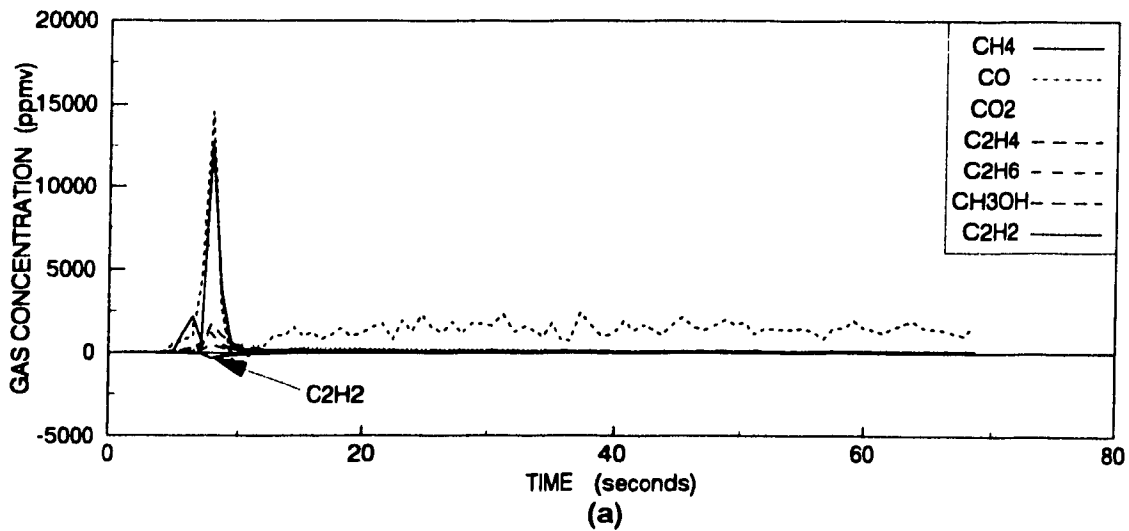


Figure 4.12 Gas concentrations calculated from mass spectrometer data for FP8. Relatively high concentration (a) and low concentration (b) compounds

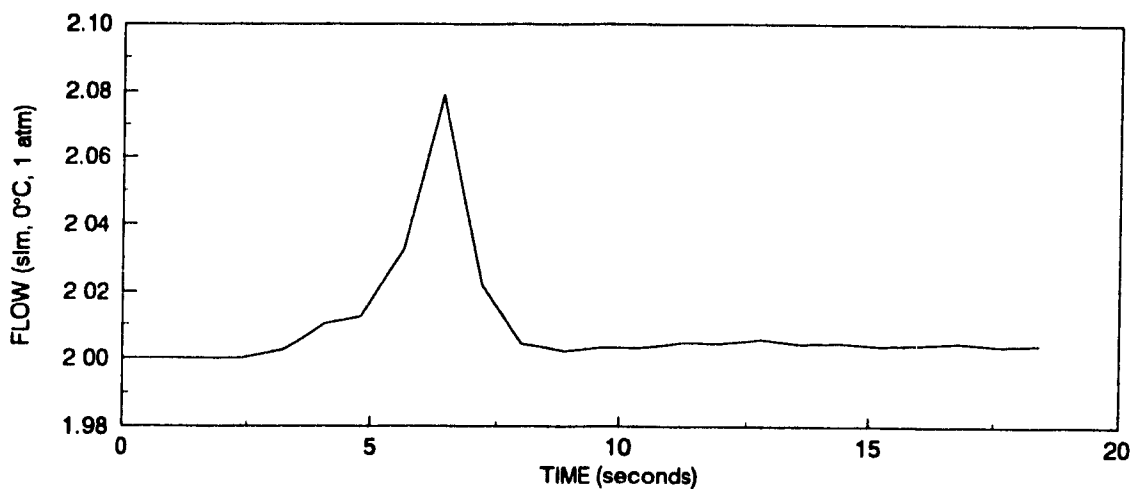


Figure 4.13 Total flow rate of carrier gas through apparatus calculated on the basis of concentrations of produced gases

Calibration of the Mass Spectrometer

The first step in the calibration procedure for the Petra Survey MS was the determination of which gases were produced during black liquor pyrolysis. Based on the black liquor pyrolysis and related literature, the possible fixed gases, hydrocarbons, and sulphur gases were identified. In addition, full scan mass spectrographs of a black liquor pyrolysis test run were also used to estimate the gas composition. It was from this test that the presence of CS_2 was first noticed. The presence of H_2S , CH_3SH , CH_3SCH_3 , CS_2 , and $\text{CH}_3\text{S}\text{SCH}_3$ were all verified by GC analysis using flame photometric detection. From this analysis it was found that COS and SO_2 were non-detectable in gases produced during pyrolysis in helium.

Since methanol and acetone had not previously been reported as black liquor pyrolysis products, they were not initially included in the mass spectrometer calibration. However, it became evident that methanol was produced at lower pyrolysis temperatures and that acetone was produced at the lowest temperature used of 500°C . These findings are consistent with lignin pyrolysis results (63). Therefore, in hindsight the detection of these two components may have been improved if the m/z ratios of 32 and 46 had been included amongst the selected m/z ratios used for the MS analysis.

The mass spectrometer was calibrated by injecting known volumes of pure gases or calibration standards into the calibration loop, which was also of known volume. This loop is an integral component of the MS which consists of a pump, valves, and an injection septum, such that the gas in the loop can be continuously recirculated. Calibration responses were determined at the 15 pre-selected m/z ratios which were discussed in detail above. Prior to gas injection the loop was purged with UHP helium until the background levels detected were low. At this point the calibration loop was isolated and the MS was "zeroed" by using background subtraction. The gas for which the instrument was being calibrated was then injected and, after allowing sufficient time for mixing, the response levels were logged with the MS PC with the internal instrument averaging set at 256 for about 20 cycles (total of $20 \times 256 = 5120$ readings per m/z ratio). This procedure was repeated for a minimum of three or four concentration levels.

For the higher boiling sulphur compounds DMS, CS_2 , and DMDS, as well as CH_3OH and CH_3COCH_3 , standards were prepared by injecting pure liquids into gas sampling tubes which had precisely determined volumes. These standards were then employed in the same manner as that described above for the pure gases. Initially permeation tubes were used to calibrate the MS for the sulphur compounds, but they were not effective as much time was required for the concentrations to stabilize, allowing the instrument to drift and greatly lengthening the time required for calibration.

Calibration of the MS for H₂O proved especially challenging, and a completely satisfactory calibration method was not devised. The method used was to inject known quantities of water into the calibration loop using a micro-syringe. The difficulty with this method was that it took substantial time for the water to evaporate, and after this time the MS zero may have drifted and it was difficult to determine exactly when all the water had evaporated. Furthermore, water may have adsorbed onto the surfaces in the calibration loop, causing the calculated sensitivities to be too low.

Once the MS calibration response data had been collected, the response for each gas at each of the pre-selected m/z ratios was least-squares fitted to a straight line. The instrument response was linear for all concentrations encountered. The slopes of these lines are the response factors M_{jk} , used in equation [4.1]. For those m/z ratios at which responses were not statistically significant, the value of M_{jk} was set to zero. In some cases the response at certain m/z ratios were ignored when they were obviously caused by the presence of impurities in the gases. For example, the responses at m/z ratios of 16 and 18 for DMS and DMDS, which were due to water, were ignored. Figure 4.14 shows a typical set of calibration curves for DMDS.

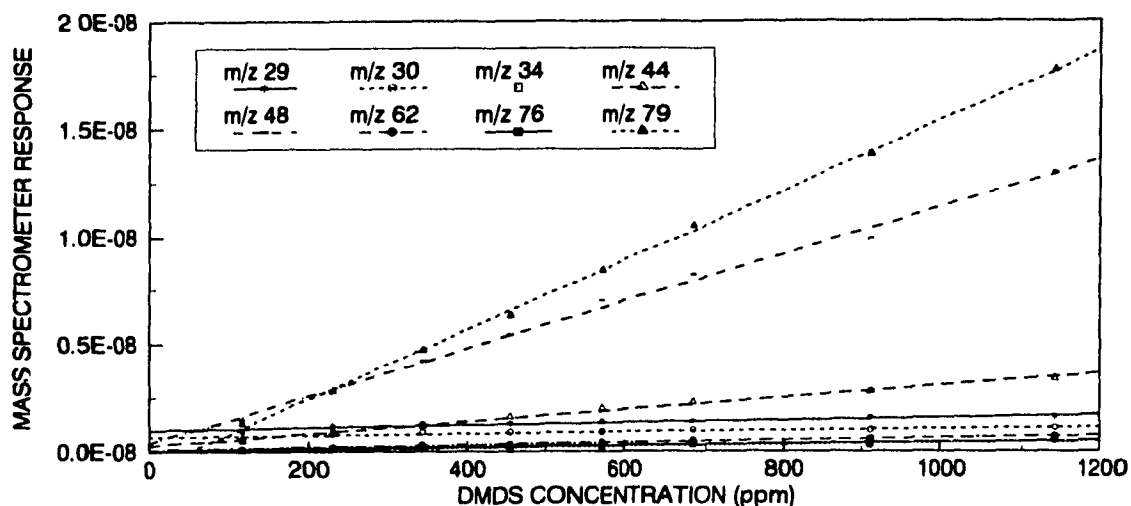


Figure 4.14 Calibration data for dimethyl disulphide showing linear response and variation in sensitivity over the range of m/z ratios

System Impulse Responses

Gas samples were injected into the furnace at its midpoint in order to obtain impulse responses for most of the gases of interest. This was achieved by removing the sample

cooler and push-rod from the furnace assembly and directly coupling the stuffing box assembly, which was equipped with a septum port, to the quartz tube. The syringe inserted through the septum was equipped with a long needle such that the end of the needle was at the midpoint of the furnace. The limit switches normally used to monitor the push-rod position were modified to detect the moment the syringe was emptied into the furnace, so that the MS response was accurately synchronized with this event. Gas volumes of 1.0 ml were injected rapidly, with the duration of the event estimated to be 1 to 2 tenths of a second. Very low noise mass spectrometer responses were obtained by using a sampling rate of 10 Hz with each sample the average of 16 instrument readings. The program used to calculate the experimental flow rates was modified to process the response data. The responses were normalized in the usual manner so that the integral of the response curve was equal to one.

The mean μ and variance σ^2 of the impulse response curves were calculated for each species using equations [4.7] and [4.8] below. The mean is the first moment of the concentration-time curve about $t = 0$ and is a measure of the average time to detection. It differs from the residence time of the apparatus due to the response of the instrument. The variance is the second moment about the mean and is a measure of the dispersion of the data about the mean, and here is a measure of the dispersion caused by the apparatus (64,65) and by the mass spectrometer inlet and detection. μ and σ^2 were evaluated by numerically integrating [4.7] and [4.8] using the trapezoidal rule.

$$\mu = \frac{\int_0^{\infty} t \cdot c \, dt}{\int_0^{\infty} c \, dt} \quad [4.7]$$

$$\sigma^2 = \frac{\int_0^{\infty} (t - \mu)^2 \cdot c \, dt}{\int_0^{\infty} c \, dt} \quad [4.8]$$

Since most experiments were performed with the condenser cooled with a mixture of dry-ice and acetone, the responses were determined using this method of cooling. For those gases which were delayed due to substantial adsorption or condensation effects resulting from the cooling, responses with air cooling of the condenser were also determined for comparison. Consistent with experimental conditions, a helium carrier-gas flow rate of 2.0 slm was normally used. However, the effect of flow rate was also investigated for CO and CO₂. The furnace temperature was kept at 700°C during all response tests.

The calculated means and variances are presented in Table 4.1. C₂H₄ was used to characterize the C₁ and C₂ hydrocarbons and shows essentially the same response as Ar, as do CO and CO₂. H₂S has a moderately greater μ and substantially greater variance due to dispersion caused primarily by adsorption. The effect of the dry-ice bath as opposed to

air cooling is moderate for H₂S, suggesting that adsorption, or reaction and adsorption, occur on other surfaces downstream of the furnace besides in the condenser. CS₂ behaves similarly, but dry-ice cooling has a larger effect. Although CH₃SH has μ and σ^2 values which are greater than those of the non-adsorbing gases, they are not significantly affected by the dry-ice cooling. Responses and dispersion for CH₃SCH₃ and CH₃SSCH₃ appear to be significantly improved with air cooling, although the extended tailing of the data for these compounds produced large confidence intervals. The boiling points of these compounds, which are also included in Table 4.1, generally correlate strongly with the μ and σ^2 values.

Table 4.1
System Impulse Response Parameters Furnace at 700°C

Gas & B.P. °C	Condenser Cooling	Flow rate slm	mean time μ (seconds)	variance σ^2 (seconds) ²
CO ₂ (-78.5)	dry-ice	1.00	2.529 ± 0.246**	0.418 ± 0.007
		2.00	1.588 ± 0.236	0.35 ± 0.38
		3.00	1.256 ± 0.168	0.45 ± 1.04
CO (-191.5)	dry-ice	1.00	2.404 ± 0.133	0.370 ± 0.124
		2.00	1.397 ± 0.071	0.187 ± 0.232
		3.00	1.142 ± 0.178	0.82 ± 0.61
C ₂ H ₄ (-84.0)	dry-ice	2.00	1.524 ± 0.152	0.463 ± 0.378
Ar (-185.7)	dry-ice	2.00	1.510 ± 0.343	0.84 ± 0.93
H ₂ S (-60.7)	dry-ice	2.00	1.866 ± 1.1	1.81 ± 3.0
	air	2.00	1.81	1.50
CH ₃ SH (6.2)	dry-ice	2.00	2.511 ± 0.340	5.62 ± 2.54
	air	2.00	2.30 ± 0.40	4.84 ± 3.77
CH ₃ SCH ₃ (37.3)	dry-ice	2.00	4.08 ± 1.05	12.68 ± 13.6
	air	2.00	2.37 ± 0.15	2.02 ± 0.45
CS ₂ (46.3)	dry-ice	2.00	2.304 ± 0.183	1.64 ± 0.28
	air	2.00	1.87 ± 0.22	0.904 ± 0.29
CH ₃ SSCH ₃ (109.7)	dry-ice	2.00	5.47 ± 6.2	19.8 ± 37.0 - m/z 79
	dry-ice	2.00	3.53 ± 0.54	16.10 ± 0.87 - m/z 48
	air	2.00	2.95 ± 1.18	11.2 ± 36.1

** - 95% confidence interval n = 3

It was discovered during the impulse response testing that DMDS decomposed in the 700°C furnace and that the response at the m/z ratio of 79 was very weak, but the response was strong at the m/z ratio of 48 which is only a secondary peak for DMDS. Thus, the measured response at the m/z ratio of 48 is not the response of DMDS, but that of its decomposition products, and the true response of DMDS reaching the MS is better represented by that measured at the m/z ratio of 79. This finding also implies that at

furnace temperatures of 700°C and higher, and perhaps lower, substantial decomposition of any DMDS produced during pyrolysis will occur and that the decomposition products (i.e. CH₃SH) will be detected by the MS.

Figure 4.15 presents the normalized CO response curves which are representative of the non-strongly adsorbing gases. The DMS response curves in Figure 4.16 are typical of the strongly adsorbing compounds and shows how the response peak broadens as a result of the dry-ice and acetone bath cooling.

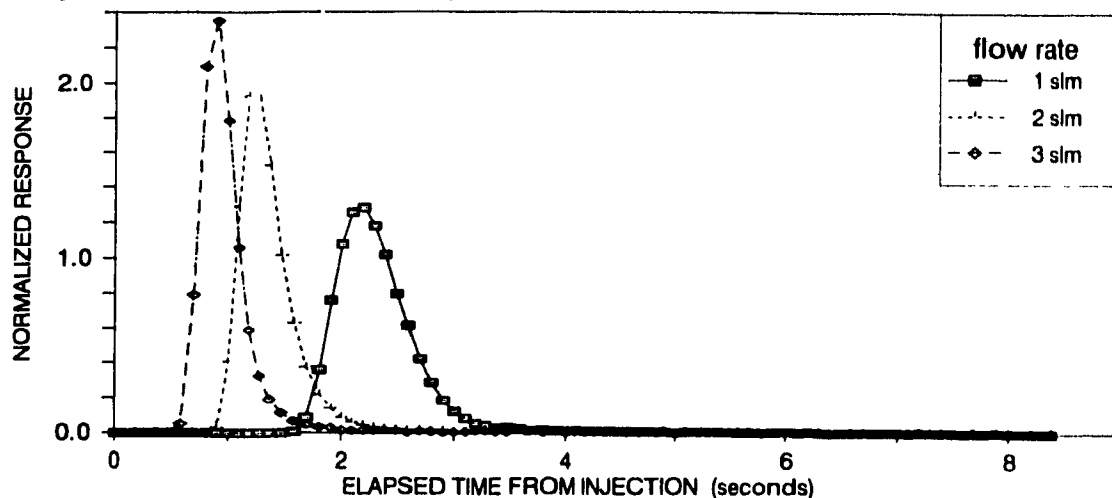


Figure 4.15 Normalized system impulse responses to CO injected at the midpoint of the tube furnace. Furnace temperature of 700°C with helium carrier gas flow rates as noted

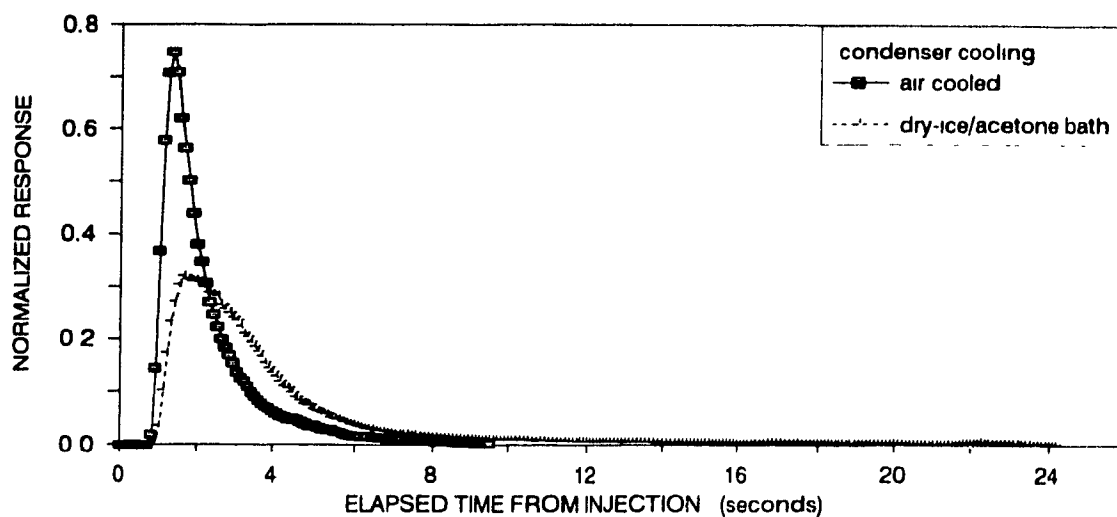


Figure 4.16 Normalized system impulse responses for dimethyl sulphide showing the effect of condenser cooling. Furnace at 700°C with a carrier gas flow of 2.0 slm helium

Fast Fourier Transform Deconvolution of Data

In order to generate models which accurately describe the rates of processes which

occur during the pyrolysis of droplets, one needs to know the rate at which gases are being produced by the droplet as a function of time and the droplet temperature as a function of time. Experimentally the latter is easier to achieve as the sample can simply be placed in direct contact with a thermocouple as was done in this study. Although there is some response lag in the thermocouple, it is not significant in terms of the rate that the droplet temperature changes. However, the determination of the rates at which gases are produced during black liquor droplet pyrolysis by the present mass spectrometer method is not straight forward, despite the superior response time of the mass spectrometer as compared to other continuous measuring techniques such as IR. The data obtained with the MS is distorted in two ways. Firstly, there is transport time between when an event occurs at the drop and when the gas reaches the detector. The second effect is the dispersion of events due to flow mixing, concentration gradient induced diffusion, adsorption on surfaces, and instrument response. The impulse response curves reported above include all these effects. For example, the time to the initial rise of the concentration in Figure 4.15 is a measure of the transport time while the width of the impulse response peak and the calculated variance are indicative of the dispersion effects. The time of the initial rise in concentration does not vary significantly from gas to gas in the present system, and therefore nonsymmetrical dispersion effects such as adsorption and instrument response are much stronger than the symmetrical effects such as diffusion and flow mixing, and thus the time to the concentration peak is not an appropriate measure of the transport lag.

The net effect is that responses measured by the instrument are delayed and smoothed versions of the actual processes occurring at the droplet. The measured response is said to be the convolution of the real response and the system response (62). If the system response is known, the real response can be calculated by deconvolution using Fourier transforms. For discrete data, the process is efficiently implemented by utilizing the FFT (Fast Fourier Transform) algorithm and its inverse.

If the system response can be represented by a function $r(t)$ and the actual response at the drop by $s(t)$, then the response measured at the instrument, $i(t)$, is the convolution $r*s(t)$ given by equation [4.9] (62), where t is time and τ is a dummy variable in the integration. The transform of the convolution $r*s(t)$ is simply the product of the transforms of the individual functions $r(t)$ and $s(t)$ as given by equation [4.10], where f is frequency, capital letters represent transforms of lower case functions, and $\langle === \rangle$ represents the transformation between the time and frequency domains.

$$r*s(t) = \int_{-\infty}^{\infty} r(\tau)s(t-\tau)d\tau \quad [4.9]$$

$$i(t) = r*s(t) \quad <====> \quad R(f)S(f) = I(f) \quad [4.10]$$

$$s(t) \quad <====> \quad S(f) = I(f)/R(f) \quad [4.11]$$

Whereas convolution is multiplication in the frequency domain, deconvolution is simply division so that $S(f)$ can be calculated by equation [4.11] and $s(t)$ is calculated by its inverse transform. Thus the procedure to determine the actual response is to calculate the transforms of $i(t)$ and $r(t)$ using the FFT algorithm, $S(f)$ by complex division of $I(f)$ by $R(f)$ in the frequency domain, and then $s(t)$ using the inverse FFT (62).

Since convolution by its very nature tends to smooth data, deconvolution tends to make data more abrupt. If the discrete data being deconvolved contain noise, the result is that the noise is amplified. Thus, to ensure the success of deconvolution, data should be free of noise. A good strategy is to sample at a frequency sufficiently higher than the frequency of events occurring so that digital filtering can be employed to eliminate higher frequency noise. Unfortunately the sampling rate of the mass spectrometer, when monitoring 16 channels, was about the same frequency as the events occurring in the process, and thus response data could not be filtered and was quite abrupt and sometimes very noisy. For the present data, deconvolution was not optimal, but as shown in Figure 4.17, it does provide some insight into the processes actually occurring at the droplet. For example, the deconvolved data show: the actual time elapsed to both the initial concentration rise and the maximum concentration peak; that there are two distinct maximums in the rate of CH_4 and CO_2 formation; and that formation rates rise and fall very rapidly. Figure 4.18 shows the discrete response curve used as the system response in deconvolving the data shown in Figure 4.17. While for a continuous response curve the appropriate normalization is to make the area under the curve equal to one, for discrete data the sum of the discrete responses must be equal to one. Sums greater than or less than one would provide amplification and attenuation respectively.

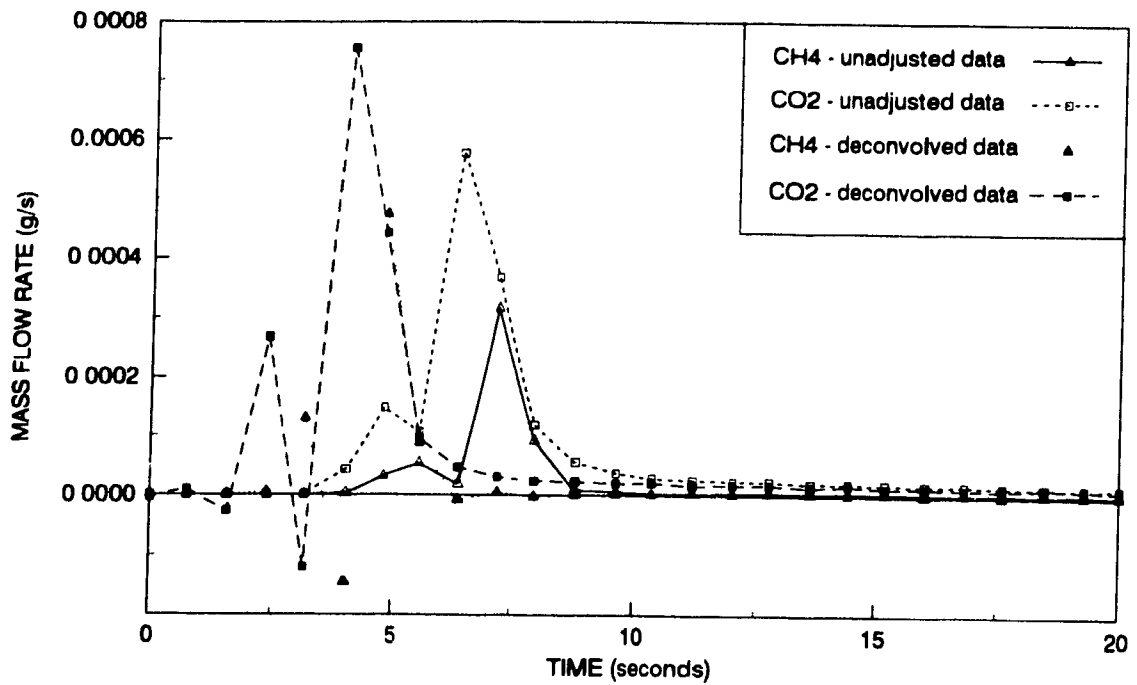


Figure 4.17 Example of deconvolution results showing how the deconvolved data is shifted to the left and more abrupt

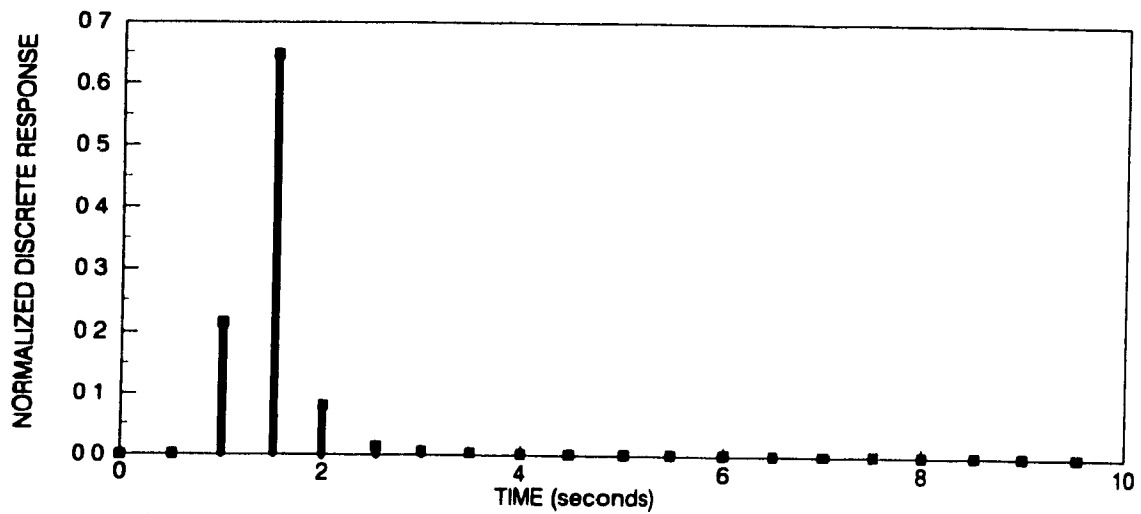


Figure 4.18 Normalized discrete response of fast pyrolysis apparatus for H₂S. Non-adsorbing gases are quite similar

CHAPTER 5 FAST PYROLYSIS EXPERIMENTAL RESULTS

Introduction

This chapter presents the results from an experimental program which was designed both to test the equipment and experimental procedures described in Chapter 4, and to obtain fundamental data for single droplet pyrolysis of kraft black liquor. The experiments were performed predominantly under inert conditions with a helium carrier gas of Ultra High Purity grade (UHP, 99.999+ % purity) over the temperature range 500-900°C. A few experiments were also performed under partial CO and CO₂ atmospheres with the balance being helium.

Experimental

Experimental Procedures

The first step in performing the fast pyrolysis experiments was to calibrate the mass spectrometer (MS) following the procedure described in Chapter 4. Since this procedure required approximately two full days, it was not possible to calibrate the instrument on every day which experiments were performed, and as a necessity it was assumed that the calibration remained constant during the experimental period. Two calibrations were made during the period of time in which experiments were performed. The sensitivities differed by about 10% between these calibrations for the primary response peaks of the gases, with the sensitivities increasing for some compounds and decreasing for others. Since at each new calibration additional compounds were included, as was deemed necessary to unscramble the MS results, only the final calibration was used to calculate the results presented.

The initial step in each experiment was to ensure that the MS, the thermocouples, the limit switches, and the synchronization signal from the personal computer (PC) to the MS were functioning properly. This was achieved by using a calibration and testing program provided with the A/D board on the PC.

The next step was to purge the system with a low flow rate - approximately 0.300 slm (litres per minute at 1 atm. and 0°C) - of helium until it was observed on the MS that the nitrogen peak at the m/z (mass/charge) ratio of 28 was relatively small and steady. At room temperature, the purging procedure required 30 to 60 minutes to allow nitrogen to desorb from the surfaces of the apparatus.

While maintaining the low helium flow, the furnace was disassembled so that the tube, and subsequently the drop thermocouple probe, could be removed. The probe was tared on the balance and an approximately 20 mg drop of black liquor applied to the thermocouple junction. The exact drop mass was then determined and subsequently the

probe was quickly installed in the apparatus and retracted into the sample cooler, which was under the helium purge and cooled indirectly to ca. 15 to 17°C - as indicated by the drop thermocouple. The furnace was then quickly reassembled so as to minimize the re-adsorption of nitrogen from the air onto the tube surfaces.

Immediately following assembly, the furnace was heated to the desired temperature using the PID controller in about 30 minutes. Once the steady state temperature had been reached, the nitrogen background at mass 28 was monitored to check if it was low and steady. Low background levels at m/z 28 were essential to achieving meaningful responses for CO and other gases contributing to this peak. The desired gas flow rates and composition were then established. At this point the cooling for the condenser was established, either a dry-ice and acetone or an ice and water bath, and the time recorded. The small amount of drying of the liquor droplets, which inevitably occurred during this heating and purging period, was neglected so that the solids content of the drop was taken to be the initial solids content in determining the amount of water produced by pyrolysis. This can be justified as a film forms on black liquor when it dries, thereby greatly impeding further evaporation.

When the temperature in the condenser and downstream tubing had reached steady state, as determined by the low and steady response of the MS for water at m/z 18, the MS was switched to the multiple ion monitoring (MIM) mode and the background levels subtracted using high averaging to ensure best accuracy. The MS, limit switches, and PC were then prepared for the experiment and the PC control and data acquisition program started. The MS was then activated at the maximum sampling rate, about 2 Hz with all 16 channels, and - provided the background subtracted levels were still zero - the sample was inserted after approximately five seconds. The movement of the sample triggered the temperature data acquisition, causing the synchronization channel on the MS to be set high, and switched the exhaust gas flow from the vent to the sampling bag (when the valve was enabled). After the prescribed pyrolysis time the sample - now char - was withdrawn from the furnace back into the sample cooler. The temperature data were collected by the PC for 30 seconds longer than the pyrolysis time in order to record the full time-temperature history of each experiment.

Next the sampling rate of the MS was reduced to one sample every 2-5 seconds and the condenser coolant removed and the time noted. The water, and any other volatiles collected in the condenser/demister were then evaporated and carried away by the carrier gas to the MS which continued to collect response data. This water response on the MS was later integrated to determine the amount of water collected in the condenser. Figure 5.1 is an example of the mass flow rate for water for an experimental run and shows the

relative magnitude of the water peaks during the black liquor pyrolysis and the evaporation of the water collected in the condenser/demister. Thus, the total amount of water detected by the MS, from the beginning of the experiment to the end of evaporation, is equal to the sum of the water evaporated from the drop, the water produced by pyrolysis, and the water condensed out of the carrier gas while the cooling was in place.

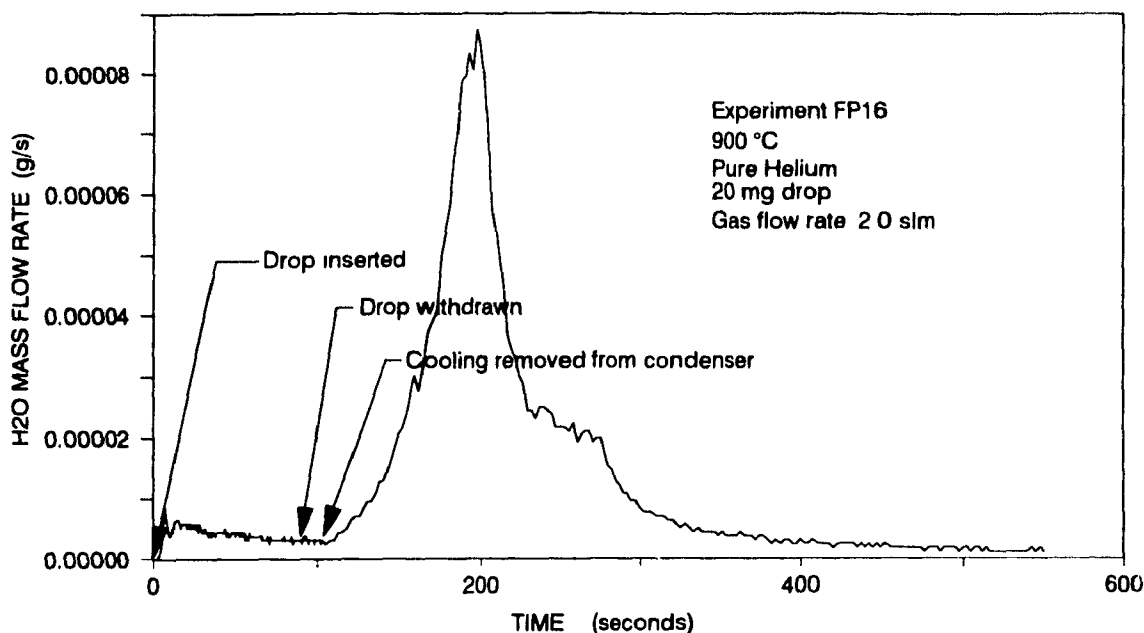


Figure 5.1 Typical mass flow rate curve from which water production was determined

Although one would expect this latter quantity to be insignificant when a high purity gas is deep-cooled, this was not the case as a condensation rate of 0.05mg/min was determined experimentally with a flow of 2.00 slm. Assuming that the gas temperature in the condenser reached -78°C , the temperature of the dry-ice acetone bath, the saturation vapour pressure of water would be 0.00056 mm Hg (84), or 0.74 ppmv. Assuming that this is the vapour pressure of water in the gas exiting the condenser, 31.3 ppmv of H_2O in the gas entering the condenser would be sufficient to produce the observed rate of condensation. During a typical experiment of 10 minute duration, about 0.5 mg of water is condensed out of the carrier gas.

After the water concentration of the purge gas had dropped to an insignificant level, the MS sampling was stopped, the furnace cooled, and the helium flow rate reduced. When the tube was cool enough to handle, it was removed from the furnace, allowing the drop thermocouple to be lowered and removed. The mass of the probe and char was then

determined and the char yield by difference. Normally, the char was scraped off the probe into a sample bottle for later analysis. The furnace tube and condenser/demister were washed with solvent to collect the condensible chars trapped on the lower furnace and the condenser/demister as described below.

Analysis of Black Liquor and Black Liquor Char

The black liquor used for the experiments was an unoxidized mixed hardwood and softwood mill kraft liquor, of approximately 70% dry solids content, and was in the as fired state. To prevent oxidation, the liquor was obtained hot from the mill and immediately stored under argon. It was subsequently frozen until the experimental program had begun, when it was thawed and kept under refrigeration. The approximate species composition of the chip supply from which the liquor was produced is shown in Table 5.1 and the chemical composition of the liquor is shown in Table 5.2. The distribution of the major inorganic ions in the liquor can be seen in Table 5.3.

Table 5.1
Approximate Chip Composition of Cook from which
the Studied Kraft Black Liquor was Obtained

	Weight %
Maple	50%
Beech	8%
Elm	2%
Poplar	20%
Basswood	7-8%
Birch	7-8%
Softwood (black spruce)	5-10%

Table 5.2
Kraft Black Liquor Ultimate Chemical Composition

	Weight %
Na	19.68
K	3.02
C	34.14
H	3.22
N	0.11
Cl	0.53
S	3.98
O	35.32 *

* Oxygen determined by difference

Analyses for sodium and potassium were performed by atomic absorption spectrometry (AAS - Smith-Heftje). Two methods of dissolution of the species were performed for comparison. In one method the black liquor solids were dissolved in deionized and deoxygenated water and then the solution was analysed. In the other method, the solids were oxidized using the Schöninger combustion technique and the resulting solution was diluted and analysed. The analyses by both methods gave the same

results within analytical error ($\pm 1\%$), indicating complete dissolution of the sodium by the first method, which was subsequently used. For the char, leaching with deionized water in a warm (about 50°C) ultrasonic bath, the combustion technique, and 60°C nitric acid digestion were evaluated. Compared to acid digestion and combustion, sodium recovery by warm water leaching was 97.9% and 97.3% efficient respectively, and thus its subsequent use introduced little error.

Table 5.3
Kraft Black Liquor Composition of Inorganic Ions
and Distribution of Organic and Inorganic Sulphur

Species	wt%	wt% as S
Na^+	19.68	----
K^+	3.02	----
Cl^-	0.53	----
CO_3^{2-}	6.18	----
HS^- (as S^{2-})	1.54	1.54
SO_4^{2-}	2.75	0.92
$\text{S}_2\text{O}_3^{2-}$	1.11	0.63
SO_3^{2-}	0.7 *	0.28*
Total Inorganic Sulphur Detected	3.37%	(84.7% of S)
Total Organic Sulphur	0.61% **	(15.3% of S)

* - approximate due to poor separation from SO_4^{2-}

** - by difference from total sulphur

Determination of anions in the black liquor solids and char was achieved by dissolution of the samples, as described above, and then analysis by ion chromatography (IC) on a Dionex System 2000i (85). Chlorine ions (Cl^-) were separated on an HPIC-AS3 column using 2 mM Na_2CO_3 eluent, with detection by conductivity using 25 mM H_2SO_4 regenerant for the anion membrane-suppressor. Carbonate was also separated by IC on an HPIC-AS1 column with deionized water eluent and detection by conductivity.

Hydrosulphide (HS^-), sulphate (SO_4^{2-}), thiosulphate ($\text{S}_2\text{O}_3^{2-}$), and sulphite (SO_3^{2-}) ions were all separated by IC on an HPIC-AS4A column using an eluent composed of 1 mM Na_2CO_3 , 5 mM NaOH , and 0.8 mM 4-paracyanophenol. Electrochemical detection (ECD) was used for hydrosulphide, while sulphate, thiosulphate, and sulphite were detected by conductivity using a membrane suppressor with 25 mM H_2SO_4 regenerant. Analysis of the char and liquor for these sulphur species was performed immediately after dissolution in order to minimize oxidation of HS^- to $\text{S}_2\text{O}_3^{2-}$ and SO_4^{2-} , and of SO_3^{2-} to SO_4^{2-} . The determinations for SO_3^{2-} were only approximate due to the small quantities present and difficulty separating sulphite from sulphate.

Total sulphur in liquor and tar samples was determined using the Schöniger combustion technique, whereby the sulphur is catalytically (with Pt) oxidized to SO_2 , absorbed into a potassium hydroxide solution, and then subsequently oxidized in solution

to SO_4^{2-} with hydrogen peroxide. The solution was then analysed for sulphate by IC on an HPIC-AS4 column using a 2.25 mM Na_2CO_3 and NaHCO_3 eluent, with detection by conductivity using 25 mM H_2SO_4 regenerant. Total sulphur in the char was determined by leaching in deionized water in a warm (about 50°C) ultrasonic bath, oxidizing the sulphur species to SO_4^{2-} with hydrogen peroxide, and then determination of sulphate by IC as described above. This was verified by Li (34) to give accurate determinations in comparison to the Schöniger combustion technique.

Carbon, hydrogen, and nitrogen in the liquor solids were determined on a CHN analyzer, model CEC 240XA. The carbon determinations from this analysis assume that all of the Na_2CO_3 in the sample decomposes such that all the carbon is converted to CO and CO_2 . The Na_2CO_3 decomposes under the extreme conditions in the analyzer of 1100-1200°C, as made evident by the sodium vapour etching on the quartz tubes, but whether this decomposition is complete is uncertain.

The oxygen content in the black liquor solids of 35.32% was determined by difference, but is in agreement with typical published values of 33-38% (1,9,34,42).

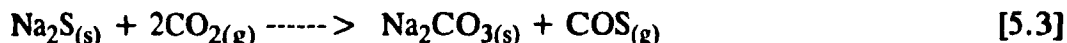
The fixed carbon in the pyrolysis char, typically present as microcrystalline graphite (66), was determined by gasifying the samples in a 15% CO_2 (anaerobic grade), 85% He (UHP or HP grade) atmosphere below 800°C. Since it has been shown that below 800°C CO_2 suppresses the decomposition of Na_2CO_3 in black liquor char (18), the fixed carbon in the char can be determined from the total CO produced by



Thus, the total quantity of carbon gasified can be calculated by equation

$$m_c = \frac{MW_c}{2MW_{\text{CO}}} \int_0^{t_g} Q [\text{CO}] dt \quad [5.2]$$

in which Q is the total gas flow rate, [CO] is the concentration of CO, MW_c and MW_{CO} are the molecular weights of C and CO respectively, and t_g is the time for complete gasification. Fixed carbon in char cannot be determined accurately from weight loss alone during CO_2 gasification since Na_2S reacts with CO_2 to produce COS and Na_2CO_3 via



Although this reaction is favoured at lower temperatures (34), COS was detected at mass 60 on the MS during gasification.

A modified arrangement of the pyrolysis apparatus, shown in Figure 5.2, was used for the fixed carbon analysis by gasification. CO was determined by an infrared (IR) analyzer, and the furnace temperature was controlled semi-manually by adjusting the set point. Both the furnace temperature and the CO concentration were recorded via the A/D board using a BASIC program. This same program digitally filtered the data and then

calculated and integrated the mass flow rate for CO.

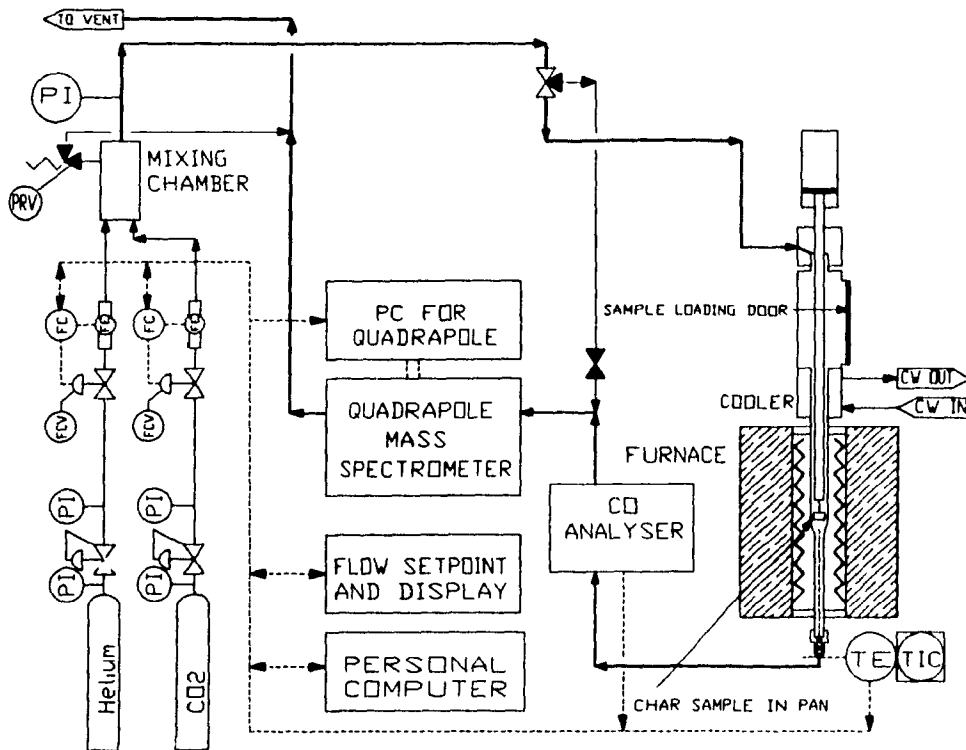


Figure 5.2 Char gasification apparatus

The procedure employed was to place a thoroughly dried char sample of 3 to 5 mg in a 10 mm diameter by 4 mm deep alumina pan. The pan was then suspended in the tube furnace from a gold wire and the furnace purged with helium for several minutes, after which the furnace was preheated to 500°C. At this point the helium flow rate was adjusted to 1.70 slm (standard litres per minute at 1 atm and 0°C) and a CO₂ flow of 0.300 slm was added to establish the desired gasification atmosphere. After about three minutes, the furnace temperature was increased gradually to 780°C in such a fashion that the CO concentration remained below the 2500 ppm maximum of the analyser. Figure 5.3 shows a typical example of the furnace temperature profile and CO concentration for an analysis. Note that at 1000 seconds, when the CO₂ flow was started, a relatively small CO peak is generated. This is the so-called "CO over-shoot", due to the rapid exchange of oxygen between the CO₂ and the fixed carbon in the char (56). Because of this phenomena, which forms an oxidized carbon complex plus CO via



the temperature of the furnace was not increased to gasification temperatures until after this peak had decayed, and its contribution to the integral [5.2] was subtracted in determining the mass of carbon gasified. However this overshoot did not always occur.

Also shown in Figure 5.3 is the MS response at m/z 60 due to COS formation, but the MS was not calibrated for COS. The amount of sulphur volatilized as COS was estimated to be 0.15 mg by assuming that the instrument sensitivity to COS can be approximated by that of CO_2 . Weight loss determinations were also made for several analyses and gave on average 20% greater values than those produced by integrating the CO concentration.

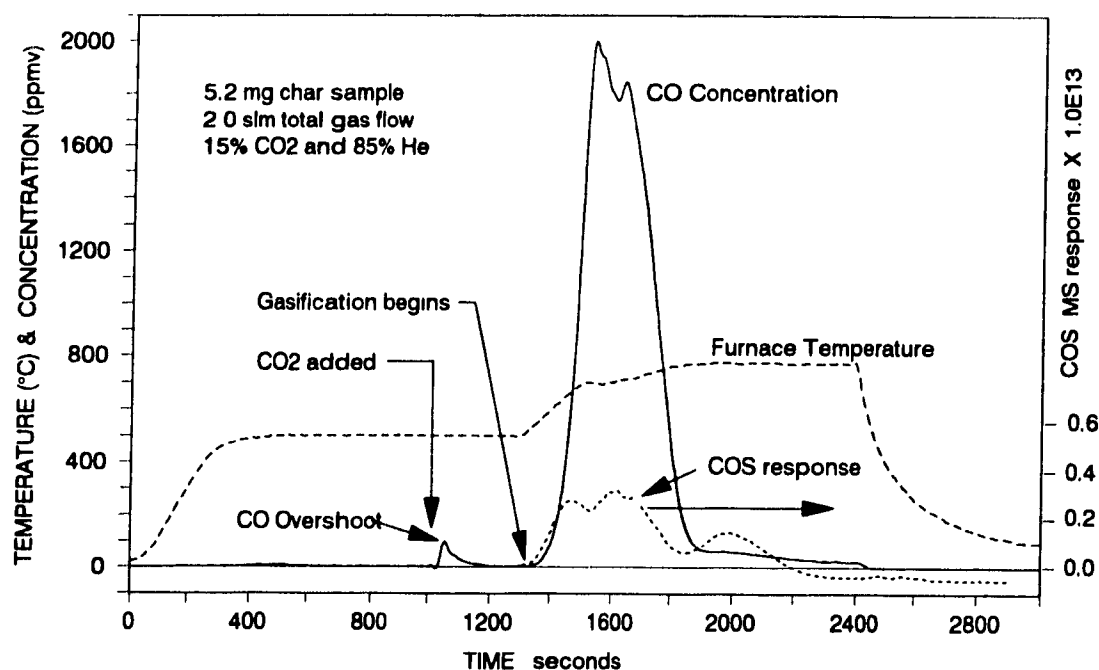


Figure 5.3 Fixed carbon gasification - typical result

As described in Chapter 4, the analysis and collection of the condensable tars presented several difficulties. Most of the experiments were performed with the condenser cooled by a dry-ice and acetone bath as this afforded better condensation and collection, and thus better protection of the MS. The tar which condensed and was subsequently trapped in the bottom of the tube furnace, the condenser, and the demister, was collected by rinsing these items thoroughly with methylene chloride, as done by others (31,67). The solvent was filtered into a pre-weighed and cleaned sample bottle, allowed to evaporate under a fume hood, and the tar yield determined by the weight gain of the bottle. Filtering was necessary as insoluble chips of alkali silicate, a reaction product of volatilized sodium and the quartz tube in the furnace, were sometimes washed out of the tube furnace and condenser along with the tar residue. The methylene chloride was HPLC grade with insignificant residue.

Since only very small quantities of tar were collected, typically 1 to 4 mg, it was

only possible to analyse for one element. Sulphur was chosen since the distribution of sulphur is the most important variable in evaluating alternative recovery processes. The total sulphur content of the tars was determined as follows. A small piece - approximately 20 mg - of ashless filter paper was weighed, wetted with methylene chloride, and then used as a sponge to wipe the tar out of the sample bottle. After the methylene chloride had evaporated, the paper was reweighed to determine the amount of tar on it. This tar soaked paper was then analysed for sulphur in the same manner as the black liquor solids.

For carbon mass balance purposes the tar was assumed to have the overall molecular formula of guaiacol (2-methoxyphenol), $C_7H_8O_2$, as this is the predominant tar component reported for lignin (63,68) pyrolysis.

Experimental Strategy

Since to a large degree the objective of this experimental program was to troubleshoot and verify the apparatus and techniques, a rigorous experimental design was not implemented. Instead, the strategy was to first experiment under relatively simple conditions, and to then test more severe conditions. Thus several runs were made at 700°C under helium until the results achieved were deemed satisfactory. The objective was then set to obtain two sets of data at each of 500, 600, 700, 800, and 900°C under helium. At 600 and 800°C, no special problems were encountered compared to 700°C. However at both 500 and 900°C difficulties were encountered, which are discussed below.

In addition to the experiments outlined above, three runs were made under partial CO atmospheres, four runs under partial CO₂ atmospheres, and two for extended times under helium atmospheres. Five more experiments were also completed with ice-water cooling of the condenser, instead of dry-ice and acetone cooling, to obtain gas production rate data closer to the true processes occurring in the furnace. During these five experiments the exhaust gases were also run through CO and CO₂ infrared analysers as a check on the MS calibration for these gases. Very little tar was trapped in the condenser during these 5 runs and thus tar analyses were not performed.

Results and Discussion

The results and discussion for the experiments are separated into seven sections. The first section discusses the mass balances obtained for carbon and sulphur (sodium is discussed in Chapter 6). The following section presents and discusses the yields of the tar, gas, and char fractions and the yields of their components. Next the possible routes for CS₂ formation and the effects of CO and CO₂ are discussed. The final three sections present and discuss data relating to kinetic evaluation of pyrolysis, that is the time-

temperature histories, the transient production, of gaseous compounds, and the correction of data for system response by using Fast Fourier Transform deconvolution.

Table 5.4
List of Fast Pyrolysis Experiments and Conditions

Exp	Temp. (°C)	Time (s)	Carrier Gas	BLS Sample Size (mg)	Char Yield (mg)	Comments
FP1	700	---	He	4.71	---	Acid used in moisture trap
FP2	700	---	He	30.94	---	Sample too large
FP3	700	---	He	14.90	8.8	Ice water cooling/no acid
FP4	700	---	He	14.72	9.3	Tar collection problems
FP5	700	---	He	14.23	8.4	Tar collection problems
FP6	700	60	He	14.16	---	New TC probe/Flow obstructed
FP7	700	60	He	13.74	6.3	Final tar collection method
FP8	700	60	He	14.37	9.0	
FP9	700	60	He	14.30	9.9	
FP10	700	60	He	14.44	9.4	
FP11	600	60	He	14.23	9.5	
FP12	600	---	He	14.23	9.8	Char stuck to tube/serpentine swelling
FP13	800	60	He	14.09	5.1	
FP14	800	60	He	14.09	6.6	
FP15	900	60	He	14.09	1.6*	*Ash - char pyrophoric
FP16	900	60	He	14.23	---	char pyrophoric - ash dissolved in water
FP17	900	60	He	14.23	---	char immersed in H ₂ O- 95% red. eff.
FP18	900	60	He/15%CO ₂	14.47	3.6*	* only solidified smelt
FP19	900	30	He/15%CO ₂	14.40	6.5	almost complete gasification
FP20	900	15	He/15%CO ₂	21.04	12.6	large sample - only partial gasification
FP21	900	20	He/15%CO ₂	14.26	7.8	only partial gasification
FP22	500	60	He	14.47	---	char stuck to tube
FP23	500	60	He	14.26	---	char stuck to tube
FP24	500	60	He	13.98	9.5	no tar data
FP25	500	60	He	14.12	10.2	spread BL along thermocouple
FP26	900	60	He/5%CO	14.47	---	char pyrophoric
FP27	800	150	He/10%CO	14.33	8.1	char not pyrophoric
FP28	800	150	He/10%CO	14.33	---	char analysed for Na ₂ S
FP29	800	150	He	13.98	---	char pyrophoric
FP30	800	150	He	14.05	---	char analysed for Na ₂ S
FP31	800	60	He	14.56	---	ice-water cooled condenser
FP32	700	60	He	14.35	---	ice-water cooled condenser
FP33	600	60	He	14.63	---	ice-water cooled condenser
FP34	900	60	He	14.42	---	ice-water cooled condenser
FP35	800	60	He	14.42	---	ice-water cooled condenser

Flow of 2.0 slm in all experiments

Table 5.4 is a complete list of the experiments performed with the fast pyrolysis apparatus and indicates the conditions and some observations. Experiments FP7 through FP30 were performed using dry-ice and acetone to cool the condenser. Experiments FP31 through FP35 used ice water to cool the condenser. Prior to FP6 a drop thermocouple probe with a much higher thermal inertia was used, so that sample heating was much slower. The first experiments are thus not included in the results presented. These runs

were also used to troubleshoot the tar collection and water trapping method. At 500°C extreme serpentine swelling of the black liquor droplets during pyrolysis produced difficulties as the char often stuck to the furnace tube. At 900°C under both pure helium and partial CO atmospheres the chars self-ignited upon contact with air and thus only the resulting ash was recovered.

Mass Balances

Carbon and sulphur mass balances were computed on those experiments for which gas and char analyses were performed. Overall mass balances were not performed since hydrogen was not determined. Carbon and sulphur closures are presented in Tables 5.5 and 5.6 respectively. The last three columns on the right of Table 5.5 are the gas yield, total yield, and closure for carbon when the calculated amount of CO produced is reduced by a factor of two. The rationale for this is explained below.

Table 5.5
Carbon Mass Balance

exp.	temp. (°C)	BLS mg	char mg	tar mg	gas mg	tot. mg	closure	With 50% of calculated CO		
								gas mg	tot. mg	closure
fp24	500	4.773	3.156	---	1.187	4.343	91.0%	1.187	4.343	91.0%
fp25	500	4.820	3.434	0.677	1.123	5.234	108.6%	0.904	5.015	104.0%
fp11	600	4.858	3.471	0.339	1.258	5.068	104.3%	1.126	4.936	101.6%
fp12	600	4.858	3.418	0.948	1.017	5.383	110.8%	0.854	5.220	107.4%
fp8	700	4.906	3.267	1.490	1.721	6.477	132.0%	1.543	6.300	128.4%
fp9	700	4.882	3.397	2.980	1.609	7.986	163.6%	1.355	7.732	158.4%
fp10	700	4.930	2.530	2.777	2.696	8.002	162.3%	2.168	7.474	151.6%
fp13	800	4.810	1.793	0.880	2.013	4.686	97.4%	1.474	4.174	86.2%
fp14	800	4.810	2.073	1.151	1.938	5.162	107.3%	1.535	4.760	98.9%
fp15	900	4.810	0.059*	1.016	13.044	14.119	293.5%	8.263	9.337	194.1%
fp16	900	4.858	0.092*	1.896	10.579	12.567	258.7%	6.981	8.969	184.6%

* - from CO₃²⁻ in the ash, char burned upon contact with air

At 500 and 600°C the carbon mass balances are remarkably good considering the approximations made in calculating the gas composition, the fraction of carbon in the tar, and other experimental error. However, at higher temperatures the carbon mass balances are off substantially on the high side. At 900°C they are as much as 200% high even though the fixed carbon is the char was lost due to self-ignition. At 900°C the error in the mass balance is almost entirely due to over estimation of the gas concentrations and in particular that of CO. As will be shown in the following section, the amounts of CO calculated are unrealistically high at this temperature. This is due to overlap at m/z 28 which is not accounted for in the analysis method and is particularly aggravated by the relatively low sensitivity of the MS to CO. When only one half of the calculated CO is included in the balance calculations the closures are more reasonable at 800°C, however at

900°C the results are still unrealistic. The closures of the carbon mass balances at 700°C are too high most likely due to unrealistically high carbon yields for the tar. Carbon closures for the experiments in atmospheres containing CO and CO₂ cannot be determined reliably because the increases in CO and CO₂ concentrations due to pyrolysis are small compared to the feed concentrations.

Table 5.6
Sulphur Mass Balance

exp.	temp. deg C	BLS mg	char mg	tar mg	gas mg	tot. mg	closure
fp24	500	0.556	0.171	---	0.127	0.298	53.6%
fp25	500	0.562	0.204	0.008	0.087	0.299	53.1%
fp11	600	0.566	0.187	0.013	0.105	0.305	53.9%
fp12	600	0.566	0.418	0.034	0.074	0.525	92.7%
fp8	700	0.572	0.198	0.019	0.072	0.289	50.5%
fp9	700	0.569	0.233	0.065	0.092	0.390	68.5%
fp10	700	0.575	0.185	0.118	0.093	0.396	69.0%
fp13	800	0.561	0.223	0.077	0.042	0.342	61.0%
fp14	800	0.561	0.237	0.125	0.053	0.416	74.1%
fp15	900	0.561	0.352	0.046	0.082	0.480	85.6%
fp16	900	0.566	0.372	0.074	0.108	0.554	97.8%
fp17	900	0.566	0.236	0.010	0.092	0.338	59.6%
fp18	900	0.576	0.349	---	0.065	0.414	71.9%
fp19	900	0.573	0.261	---	0.085	0.346	60.4%
fp20	900	0.840	0.185	---	0.192	0.377	44.9%
fp21	900	0.568	0.156	---	0.122	0.278	49.0%
fp27	800	0.570	0.254	---	0.076	0.330	57.9%
fp28	800	0.570	0.242	---	0.102	0.344	60.3%
fp30	800	0.559	0.250	---	0.089	0.339	60.7%

As a check on the accuracy of the quantitative MS results, CO and CO₂ IR analysers were connected in series after the MS during several experiments. The CO and CO₂ calculated using the IR and MS analysers, and their ratios are presented in Table 5.7.

Table 5.7
Comparison of IR and MS CO and CO₂ Determinations

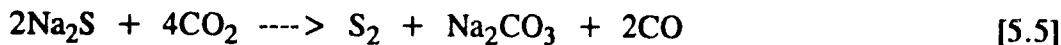
exp.	temp. deg C	CO			CO ₂		
		IR mg	MS mg	MS/IR	IR mg	MS mg	MS/IR
fp32	700	---	1.168	---	1.198	1.151	0.961
fp33	600	0.506	0.924	1.826	0.912	0.920	1.008
fp34	900	5.271	9.569	1.815	1.700	1.734	1.020
fp35	800	3.292	5.325	1.618	1.624	2.128	1.310

While the agreement between the CO₂ analyses is excellent for all but FP35, validating the method used to calculate CO₂ and the sulphur gases, the CO determinations by the MS are high by a factor of about 1.8. This error in CO accounts for much but not all of the discrepancy in the carbon closures. The CO yields calculated for FP15, FP16, and FP17 at the pyrolysis temperature of 900°C are 22.3, 16.7, and 14.7 mg respectively, and would be expected to be about the same as the 5.3 mg of FP34 (as determined by the

IR CO analyser), and thus one can conclude that sometimes the correction factor for the mass spectrometer CO data is substantially higher than 1.8. The CO₂ yields calculated for these same experiments were 4.8, 5.1, and 5.1 mg respectively and again are substantially higher than the 1.7 mg of FP34 (determined by the IR CO₂ analyser), suggesting that CO₂ is overestimated in some instances as well.

The sulphur balance closures are on average 69.6% for the experiments with char, tar, and gas analysis and are reasonable considering the small sample sizes used in the experiments. For experiments FP18 through FP21, which were performed in CO₂, the balances are poorer most likely due to the formation of undetected COS, via reaction [5.3]. The lack of tar analysis for FP18 to FP21, and for FP27, FP28 and FP30, contributes to the poorer sulphur closures for these runs.

Since the quantity of sulphur in 20 mg droplets is small, only small losses are necessary to cause incomplete closure of the sulphur mass balance. Several possible explanations for the missing sulphur follow. Firstly, a small fraction of sulphur may have escaped detection as compounds which were neither detected by the MS nor trapped in the condenser as tars. Although COS formation was found to be non-detectable at 700°C in He, at other conditions, particularly low temperatures, COS may have been formed in small quantities. Li (34) found that at very low CO partial pressures, the reaction of CO₂ with Na₂S to produce sulphur via



is thermodynamically favoured. Elemental sulphur condensing prior to the condenser or passing through the condenser would go undetected. Some adsorption of sulphur compounds may have occurred on the PTFE tubing between the condenser and the analyser, as well as condensation of compounds which may not have been trapped in the condenser/demister assembly. A final possible contribution to the sulphur imbalance is analytical error, and in particular calibration error of the mass spectrometer.

Tar, Char, and Gas Yields

Total tar, char, and gas yields are presented in this section as fractions of the starting black liquor solids, while the sulphur yields of the tar, char, and gas are expressed as fractions of the sulphur in the black liquor solids. The graphs, Figures 5.4 through 5.22, show experimental data points, their means, and confidence intervals for the means for each experimental temperature and gas composition. Unless noted the gas atmosphere is helium. CO-800 refers to those experiments performed in 10% CO/90% He at 800°C while CO₂-900 refers to those performed in 15% CO₂/85% He at 900°C. Since more data points were available for gas yields, 95% confidence intervals were plotted for gas

phase results, whereas for tar and char often only two were available, and thus 90% confidence intervals are shown for these products.

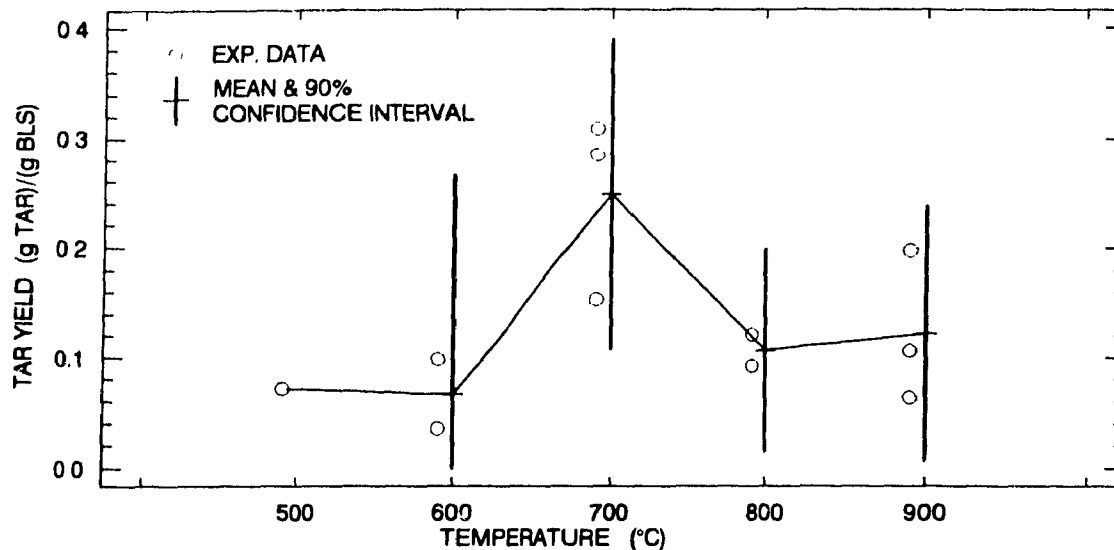


Figure 5.4 Tar yield for fast pyrolysis with 20 mg 70% solids droplets

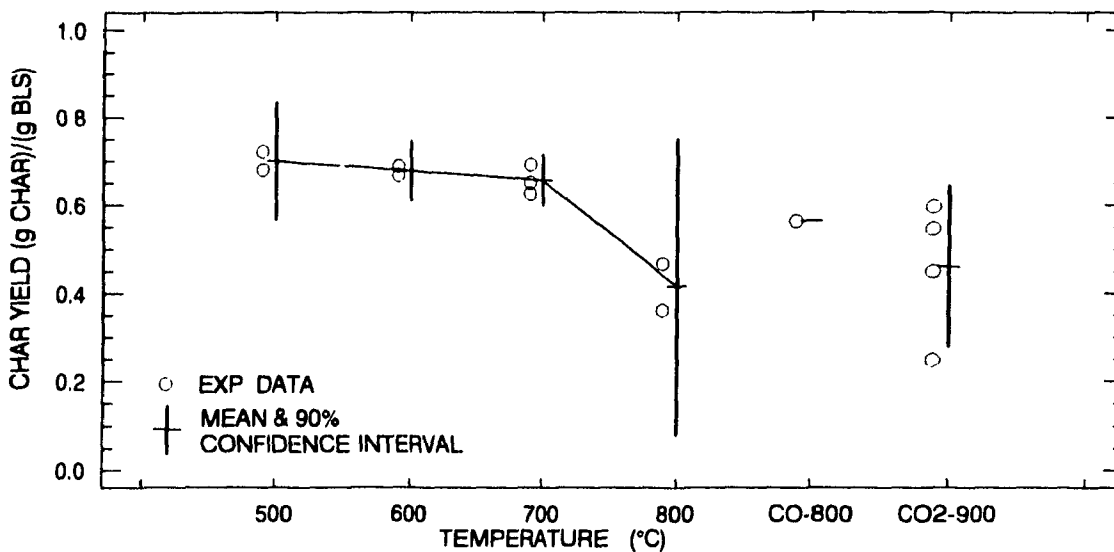


Figure 5.5 Char yield for fast pyrolysis with 20 mg 70% solids droplets

The tar yields in Figure 5.4 show a maximum at 700°C with 25% yield. While there is substantial scatter in the data, the trend towards high yields at 700°C appears significant, but the increase from 800 to 900°C is likely due to the anomalous upper data point at 900°C. Figure 5.5 indicates quite clearly that char yield decreases gradually up to a temperature of 700°C and then decreases strongly at 800°C. Conversely, total gas yield gradually rises with temperature up to 800°C, but increases sharply at 900°C as depicted in Figure 5.6. Char data at 900°C in He was not obtained as the char self-

ignited on exposure to air. While individual gas yields show much scatter (see below), the total gas yield data are quite repeatable. When the calculated amount of CO is reduced by a factor of two to account for the over estimation of the CO concentration, the total gas yields are those shown in Figure 5.6(b).

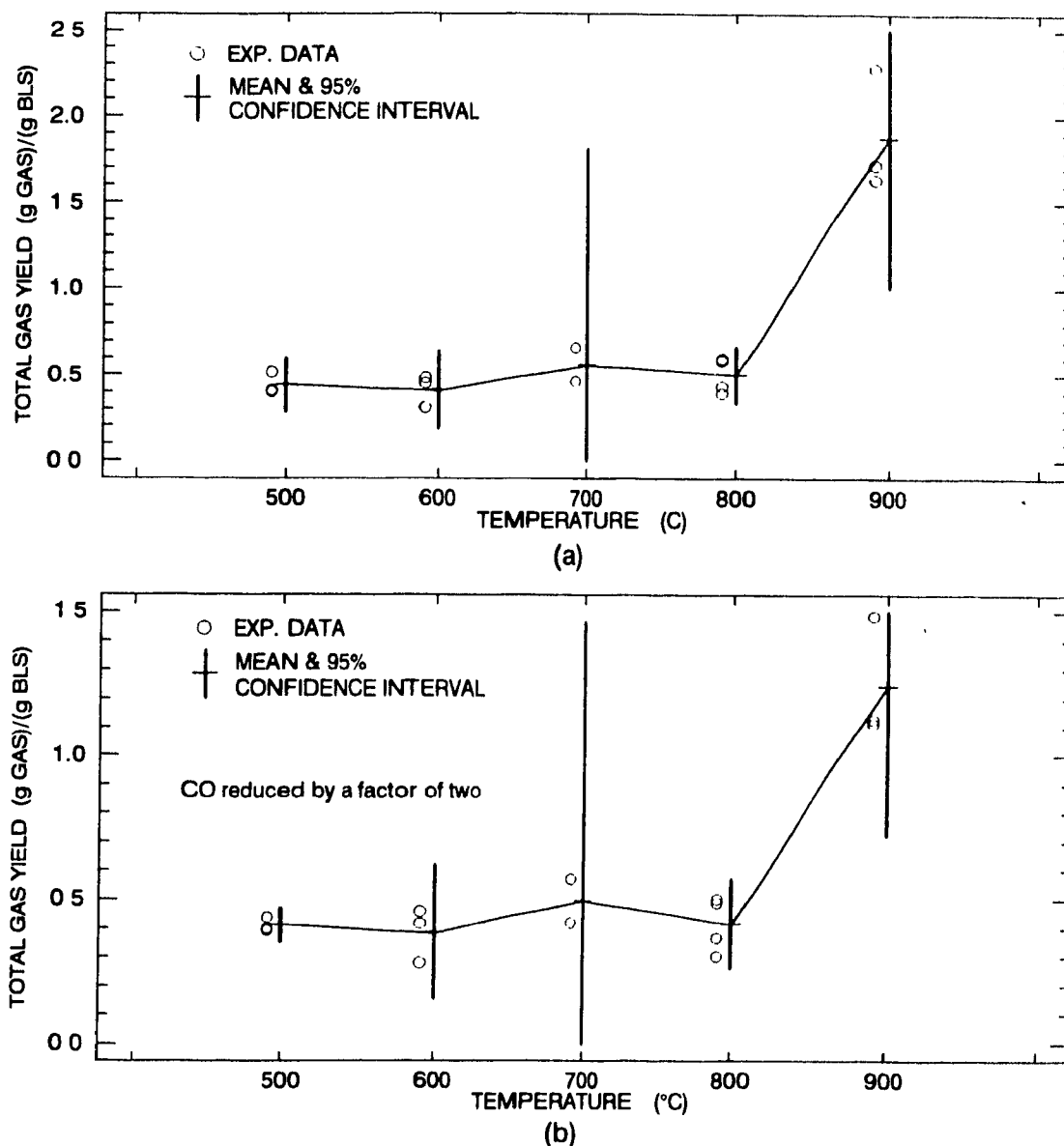


Figure 5.6 Total gas yield for fast pyrolysis with 20 mg 70% solids droplets.
 (a) as calculated (b) with CO reduced 50%

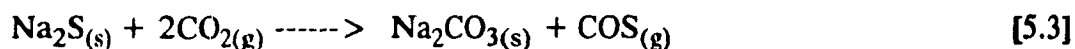
The decrease in char yield is expected with increasing temperature, since the volatiles are more rapidly produced and transported out of the pyrolysing material and thus fewer condensation reactions take place to form char (28). In addition, thermodynamics predict low char yields at higher temperatures due to greater gasification

of carbon (Figure 3.4(a)). The sudden decrease in char yield at 800°C is due to increased reaction rates for the reduction of both Na₂SO₄ to Na₂S and Na₂CO₃ to Na by carbon in the char (10,34), producing CO and CO₂. As is evident from the above discussion, decreasing char yields go hand-in-hand with increasing gas yields. However, the behaviour of the tar yields with temperature can not be explained so simply.

The increase in tar yield with temperature is consistent with the results of Feuerstein *et al* (14), but Bhattacharya *et al* found very little variation with temperature (17). Feuerstein's yields were constant above 600°C. These previous works were both for large samples which were heated relatively slowly. Rapid heating rate data for coal pyrolysis show increasing tar yields with final pyrolysis temperature (31) when the products are rapidly quenched to prevent secondary reactions. In the present apparatus the products of pyrolysis are typically exposed to the furnace temperature for about 3/10th of a second before they are quenched in the condenser. This allows unstable products time to decompose, for example dimethyl disulphide (DMDS) during the impulse response tests described in Chapter 4. Thus, an explanation for the increase and substantial decrease in tar yield is that more condensible products are indeed produced at higher temperatures, but they are further decomposed to non-condensable gases at 800 and 900°C. At 700°C the reaction kinetics of the secondary decomposition reactions are slower and thus the tar yields are higher.

The yield of sulphur in char, Figure 5.7, increases with temperature as can be expected from thermodynamic considerations (see Chapter 3), and conversely the sulphur gas yield, Figure 5.8, decreases as predicted with increasing temperature. The sulphur yield in the tar, Figure 5.9, increases to 800°C, and then falls off sharply. The increase parallels that expected for total tar yield. The high concentration of sulphur in the 800°C tar, indicated by the high sulphur yield yet low tar yield, suggests that the sulphur containing condensables are more stable than other condensables, perhaps due to the presence of elemental sulphur. At 900°C, the thermodynamic force to bound the sulphur with sodium, in combination with rapid kinetics reduce the amount of sulphur in the tar.

The sulphur retention in the char for pyrolysis at 800°C is not significantly different from that in pure He. At 900°C under 15% CO₂, the char sulphur yield after 60 seconds pyrolysis is not significantly different from that under pure He. However, the char sulphur yield surprisingly decreases with decreasing pyrolysis time under these conditions. This apparently strange behaviour can be explained as follows. The dominant reaction to volatilize sulphur under CO₂ is



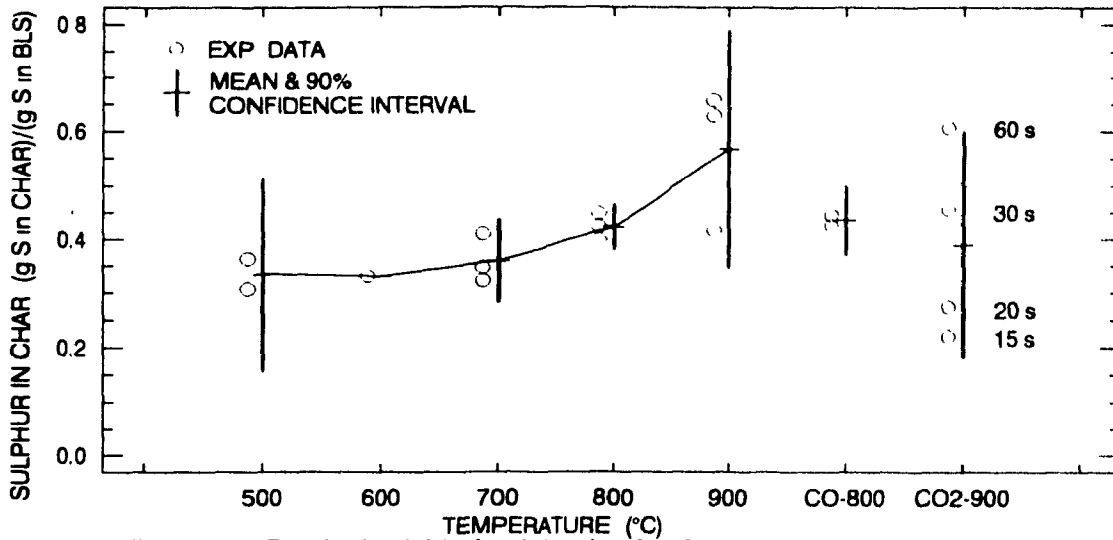


Figure 5.7 Pyrolysis yield of sulphur in char for 20 mg 70% solids droplets

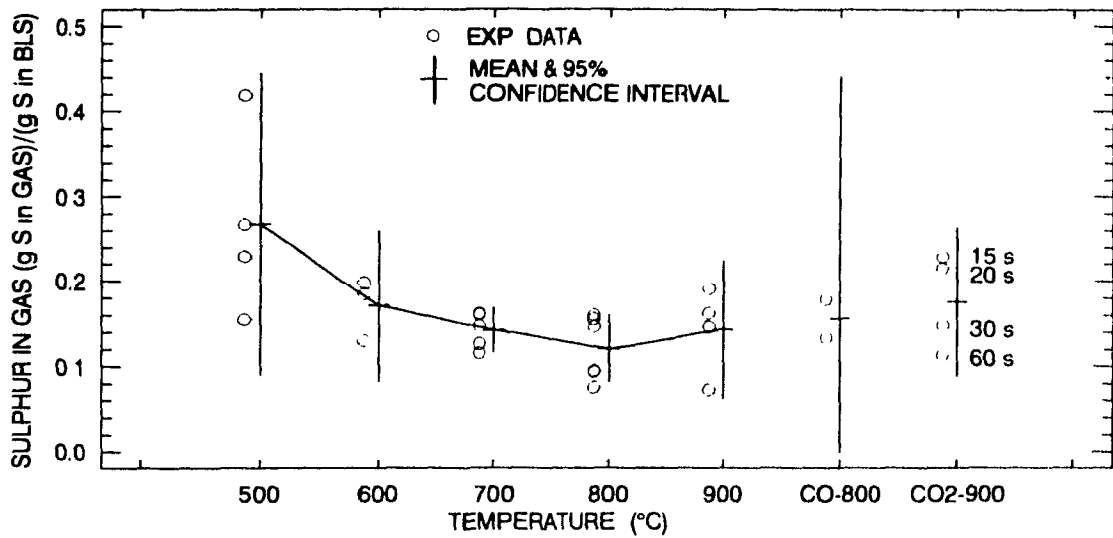


Figure 5.8 Pyrolysis yield of sulphur in gases for 20 mg 70% solids droplets

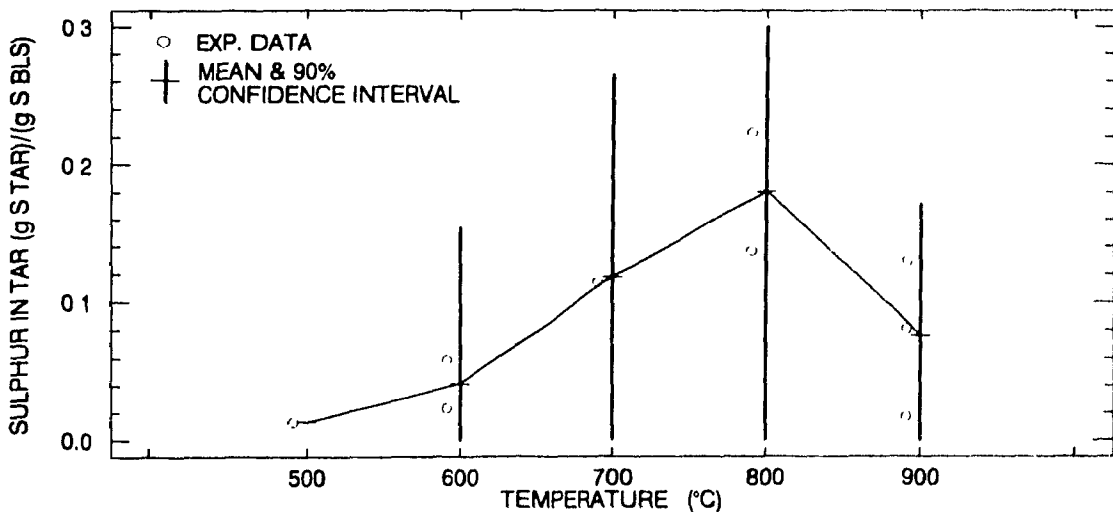
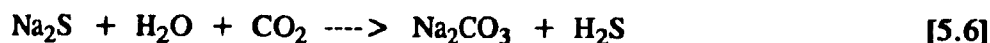


Figure 5.9 Pyrolysis yield of sulphur in tar for 20 mg 70% solids droplets

which is favoured at lower temperatures (34). The reaction



is also favoured at low temperatures and is important when water vapour is also present. These gas-solid or gas-liquid reactions require large surface areas to proceed quickly, and also require the presence of Na_2S . Thus the particle with the greatest amount of surface area and Na_2S available during cooling after pyrolysis will volatilize the greatest amount of sulphur. Since the reduction of Na_2SO_4 to Na_2S is largely complete in 15 to 20 seconds for a droplet at 900°C in 15% CO_2 (see below), the char surface area should be the dominant factor for sulphur loss after 15 to 20 seconds pyrolysis, and indeed explains the results depicted in Figure 5.7. Carbon gasification by CO_2 was complete after 60 seconds leaving only a drop of molten smelt of low surface area. After 30 seconds a small amount of carbon remained, thus increasing the surface area. The char samples at 15 and 20 seconds were only partially gasified and thus had high surface areas and experienced high sulphur losses.

The yield of fixed carbon in char, i.e. the carbon not associated with inorganic salts, is shown in Figure 5.10. As expected the fixed carbon yield decreases with temperature in the same trend as total char yield. The presence of CO does not affect the fixed carbon yield at 800°C . The carbonate and sodium yields for the char are presented in Chapter 6.

The yields of the individual gas compounds determined are presented in Figures 5.11 through 5.22. Acetylene and acetone yields, shown in Figure 5.23, were only detected for those conditions shown. General trends are that the yields of higher molecular weight compounds decrease with increasing temperature, while concurrently those of compounds with smaller and unsaturated molecules increase. These trends are to be expected as none of the larger molecules are thermodynamically stable under the present experimental conditions, as shown by their absence from the thermodynamic predictions of Chapter 3. At higher temperatures the kinetics of the decomposition reactions become sufficiently rapid that conversions are closer to those of equilibrium. The individual gas trends for pyrolysis in helium are discussed below, with the effects of CO and CO_2 discussed in a later section.

The yield of ethane, shown in Figure 5.11, clearly decreases with increasing temperature, from a significant 4.5% at 600°C to 1% at 900°C . The yield of ethylene is virtually a mirror image of ethane yield, Figure 5.12, and increases from 0.5 to 4.5% over this temperature range. Castillo *et al* (32) showed that C_2 hydrocarbons are mainly due to cellulose and hemicellulose degradation during ligno-cellulose pyrolysis, with some being produced by aromatic ring rupture. Thus in black liquor pyrolysis, C_2 hydrocarbons should be produced primarily from the organic acids formed from the

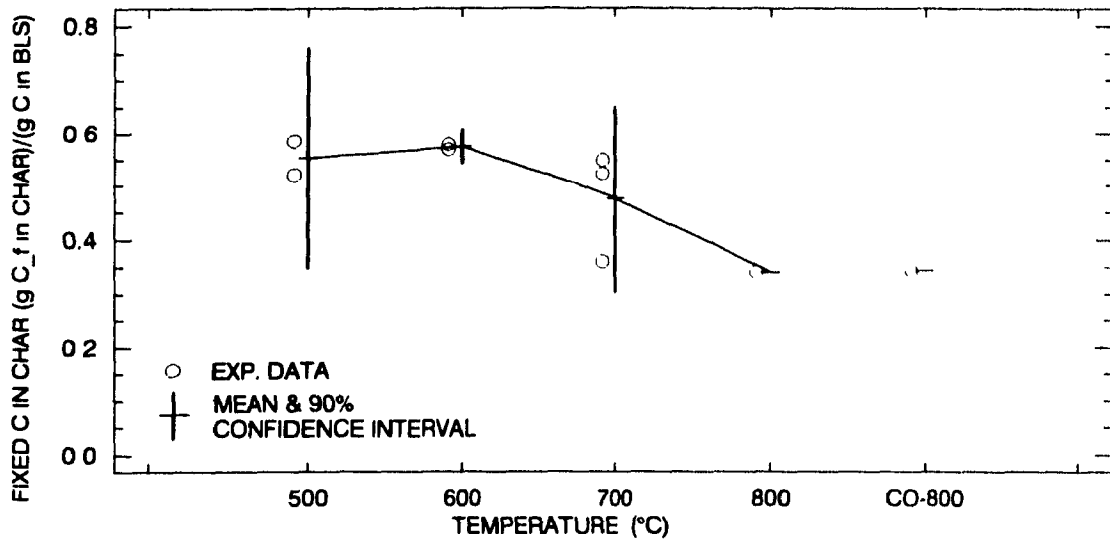


Figure 5.10 Pyrolysis yield of fixed carbon in char for 20 mg 70% solids drops

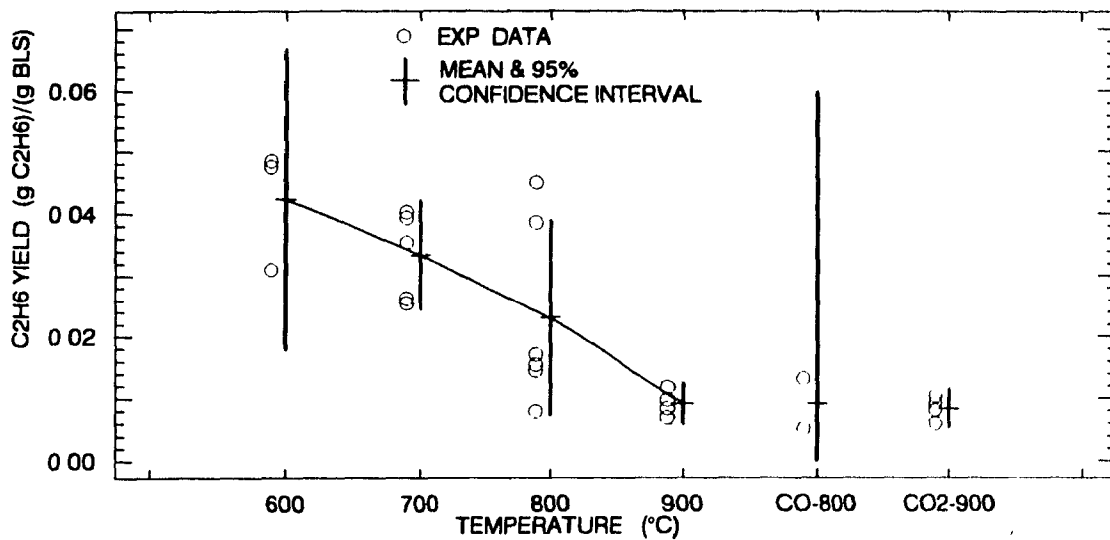


Figure 5.11 Pyrolysis yield of ethane for 20 mg 70% solids droplets

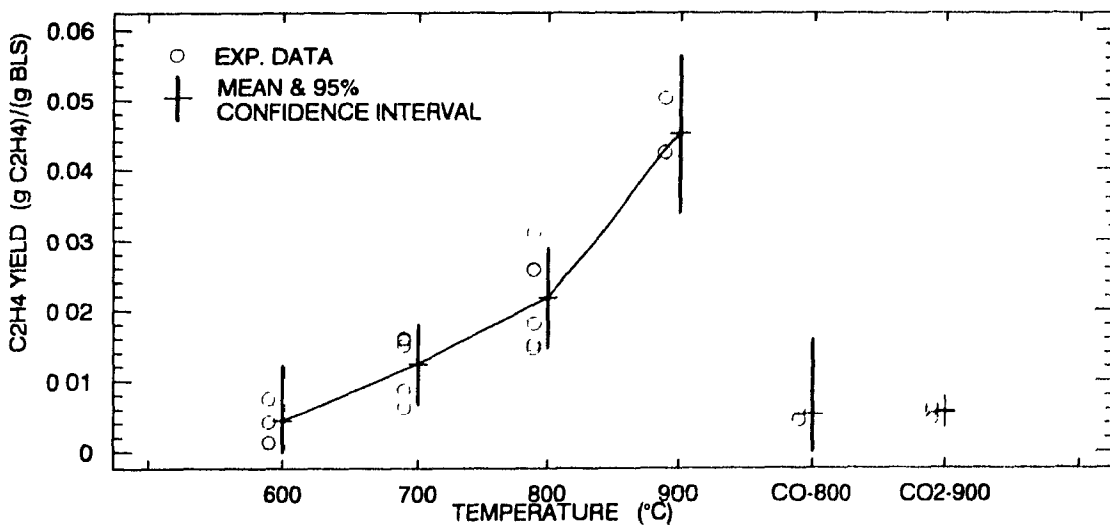


Figure 5.12 Pyrolysis yield of ethylene for 20 mg 70% solids droplets

cellulosics during kraft cooking, with some being formed via lignin ring rupture. While C_2H_4 becomes more favoured at high temperatures (69), it is still not thermodynamically stable at the present experimental conditions (Chapter 3). This suggests that greater fragmentation resulting in higher levels of free radicals (31), as compared to lower temperatures, is responsible for the increased yield of ethylene with increased temperature. Presumably, high free radical concentrations are also responsible for the onset of acetylene formation, shown in Figure 5.23(a), at 900°C.

The yield of methane in Figure 5.13 increases gradually from 2% at 500°C to 4% at 800°C and then dramatically to 12% at 900°C. The increase in CH_4 production can be attributed to greater fragmentation and less condensation at higher temperatures, and to being a product of secondary decompositions of larger molecules. Very rapid reaction kinetics could account for the large jump in yield at 900°C, although 12% yield is probably unrealistically high.

Figure 5.14 shows that the methanol yield is similar to that of ethane in Figure 5.11, decreasing from about 2% at 500°C to less than 0.5% at 900°C. Methanol likely is formed from lignin methoxy groups during pulping and is typically present at about 1% in black liquor obtained from softwoods. Since the liquor used was predominantly from hardwoods, which have many more methoxy groups in their lignin, close to 1.5% methanol may have been present in the liquor.

The yield of CO in Figure 5.15 increases gradually to 800°C and then jumps dramatically to high levels at 900°C. Although the calculated yields are unrealistically high, for reasons previously discussed, the trend shown by the graph is informative. CO is produced during pyrolysis through degradation of ether linkages (17), methoxy groups (32), and methanol; through gas phase reactions such as methane reforming and the water-gas shift; and as a product of Na_2SO_4 and Na_2CO_3 reduction (10,34,38). At lower temperatures CO is produced mostly through the degradation reactions mentioned above, some of which are more complete at higher temperatures. At 800 and 900°C sulphate reduction in combination with methane reforming and the shift reaction cause the large increase in yield. Because of the interdependence of methane, CO, and CO_2 through the methane reforming and water-gas shift reactions, it is difficult to determine which compounds are formed early and which are secondary products through equilibrium reactions. The transient gas production curves to be presented later will be used to help solve this dilemma.

Similarly, the yield of CO_2 also increases at higher temperatures as shown in Figure 5.16. Decarboxylation of carboxylic and hydroxy acids (17), α linkage breakage (32), and H_2S capture by Na_2CO_3 are the primary sources of CO_2 during black liquor

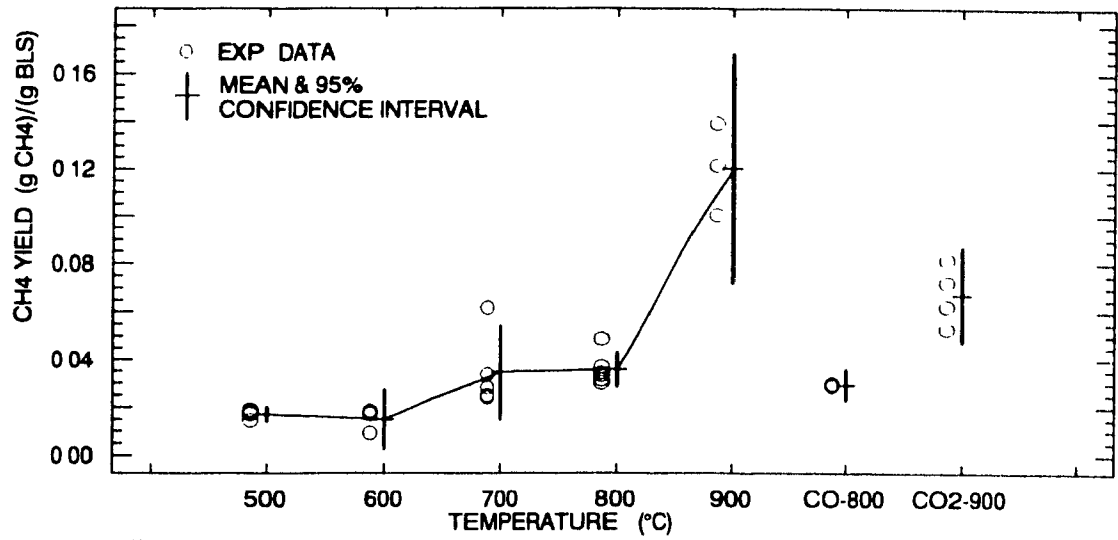


Figure 5.13 Pyrolysis yield of methane for 20 mg 70% solids droplets

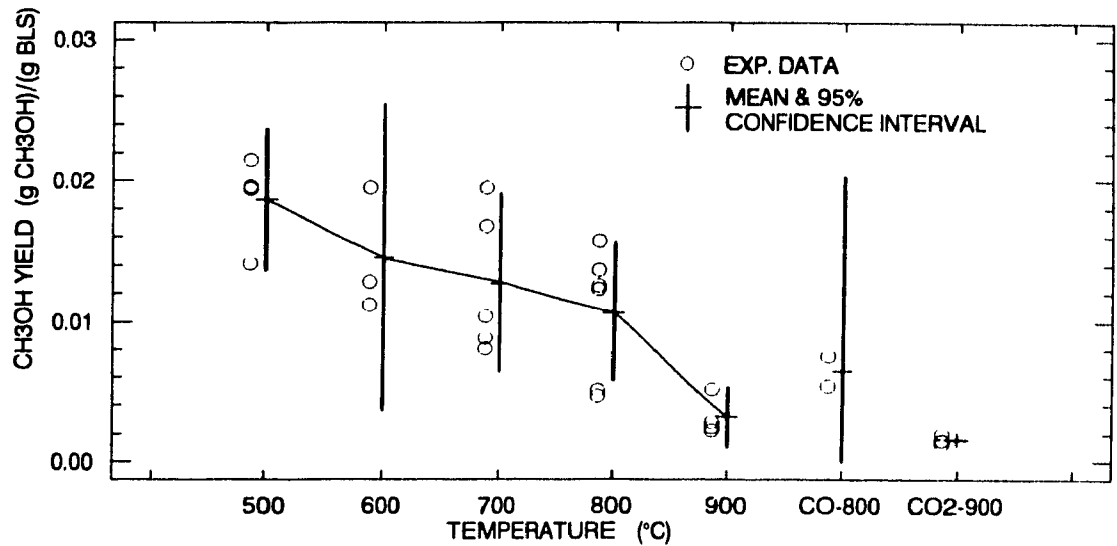


Figure 5.14 Pyrolysis yield of methanol for 20 mg 70% solids droplets

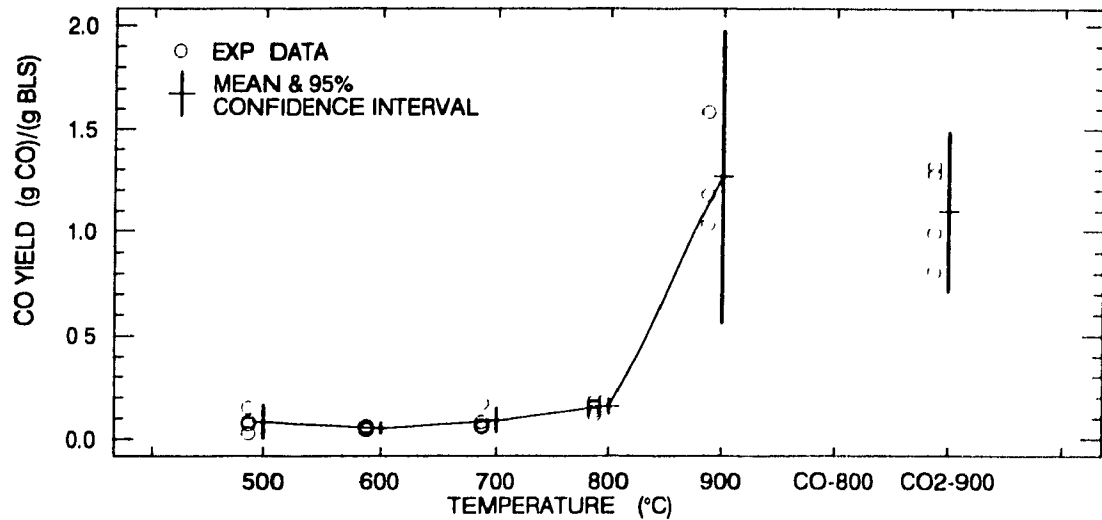


Figure 5.15 Pyrolysis yield of carbon monoxide for 20 mg 70% solids droplets

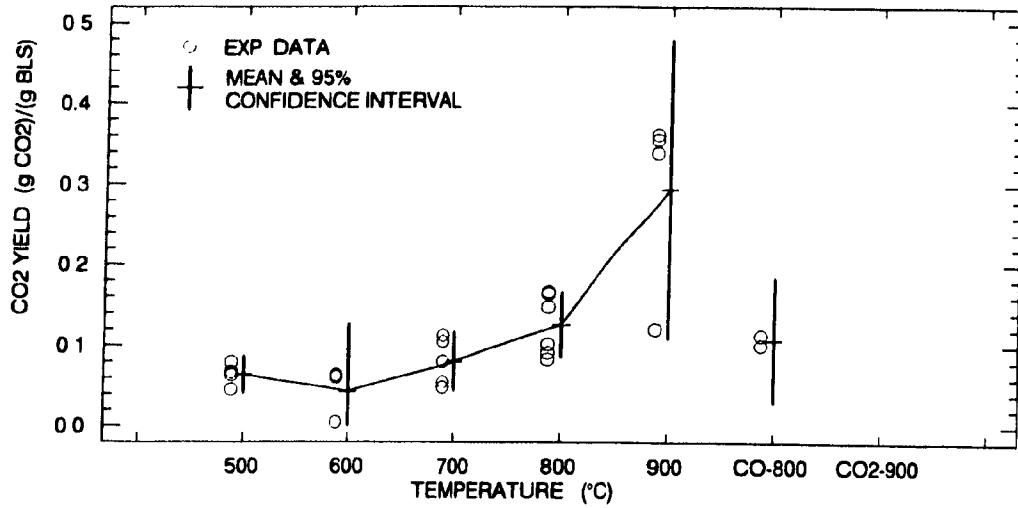


Figure 5.16 Pyrolysis yield of carbon dioxide for 20 mg 70% solids droplets

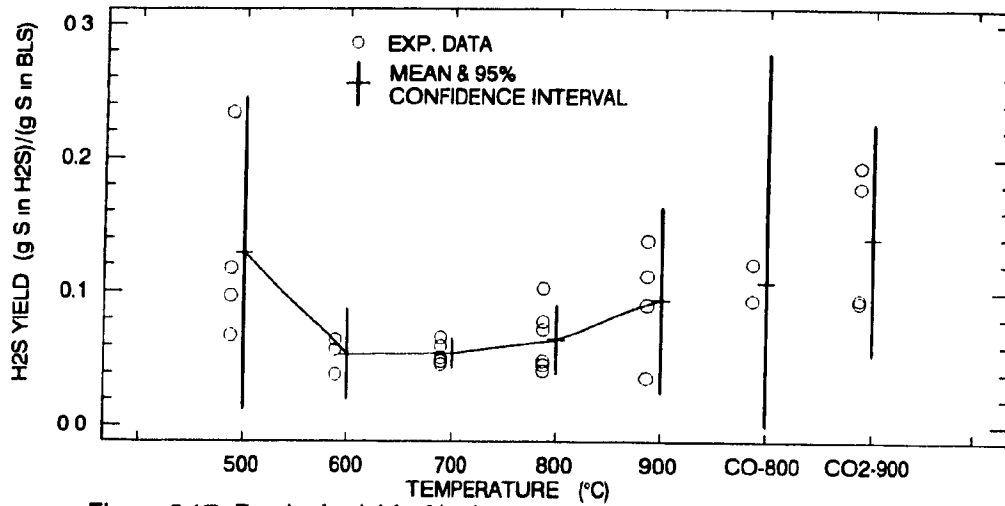


Figure 5.17 Pyrolysis yield of hydrogen sulphide for 20 mg 70% solids droplets

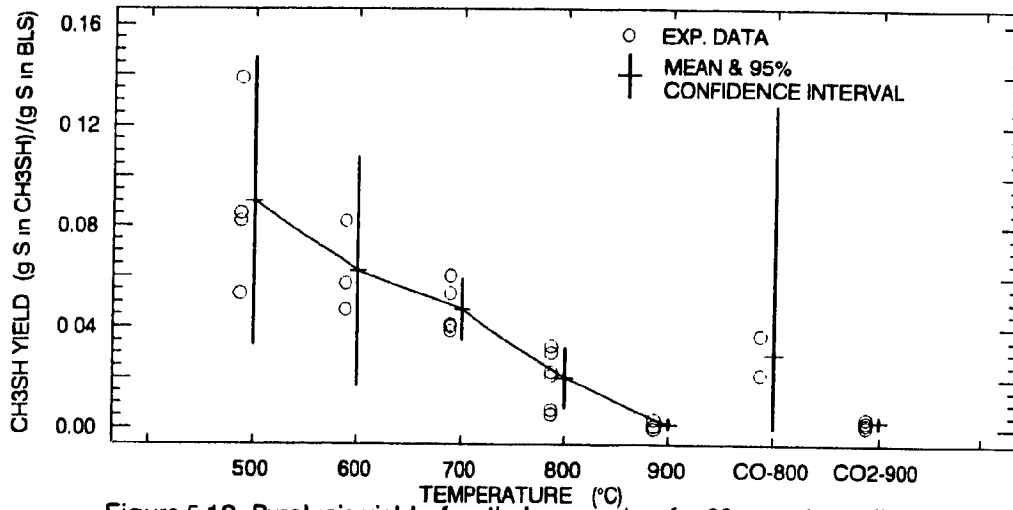
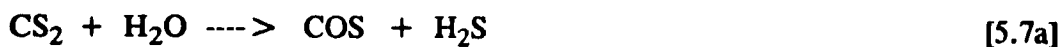


Figure 5.18 Pyrolysis yield of methyl mercaptan for 20 mg 70% solids droplets

pyrolysis. Relatively high CO₂ yields at low temperatures result from the ease with which the weak carboxyl group bonds are broken. Increasing yields at 800 and 900°C are primarily due to increased CO formation and the subsequent shift reaction. CO₂ does not increase as much as CO at 900°C as the CO/CO₂ ratio increases with temperature due to the shift reaction.

Figure 5.17 shows the yield of H₂S, which decreases as expected thermodynamically from 500 to 700°C, but then unexpectedly rises at 800 and 900°C. Since H₂S is the dominant sulphur gas its yield is very similar to that of total sulphur gas shown in Figure 5.8, except that the minimum yield of the latter is at 800°C. H₂S can be produced via thiolignin and mercaptan degradation (17), reaction of Na₂S with CO₂ and H₂O via [5.6], from CS₂ via reactions [5.7] and [5.8] (69), and reaction of CH₃SH and H₂O via [5.9] (69).

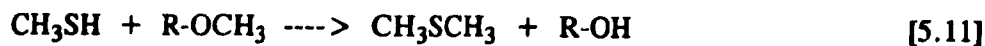


At 500°C H₂S production is high as the reaction of CO₂ and water vapour with Na₂S present in kraft black liquor (see Table 5.3) is thermodynamically favoured throughout the experiment. Additional H₂S is produced from organically bound sulphur. By 600°C thermodynamics favour the retention of sulphur in the char as Na₂S (Figure 3.5(b)), and the substantial drop in H₂S yield supports this prediction. The reason that H₂S production does not continue to drop as predicted may be because of the production of H₂S from the secondary decomposition of mercaptans and thioalkanes. The increases in H₂S yield at both 800 and 900°C appear to follow those of CS₂, or vice versa, indicating reactions [5.7] and [5.8] may contribute to its formation along with [5.9] and dimethyl sulphide decomposition.

The yield of methyl mercaptan in Figure 5.18 decreases linearly from about 9% of the sulphur in the BLS at 500°C to less than 1% at 900°C. CH₃SH is produced predominantly from thiolignin and in particular from reaction of HS⁻ with methoxy groups (35,36). Some CH₃SH is probably dissolved in black liquor, like methanol, and some produced during pyrolysis. Strohbeen (13) reports CH₃SH production during pyrolysis of inorganic sulphur with vanillic acid but found none during runs with sodium gluconate, and this supports the methoxy group being the source of CH₃SH. The decrease in CH₃SH yield with increased temperature can be attributed to more rapid kinetics providing more complete decomposition via [5.10], which is thermodynamically favoured, or to more complete reforming via reactions such as [5.9] above.



In Figure 5.19, the trend of the yield of dimethyl sulphide (DMS) is similar to that of methyl mercaptan, but the decrease is less extreme. DMS is generally believed to be formed during kraft cooking via reaction [5.11]. Under pyrolysis conditions a free radical reaction such as [5.12] could take place, thus it is reasonable that DMS formation follows that of CH_3SH , its precursor.



At 500°C CS_2 sulphur yield is minimal, whereas at 900°C it is a significant 2% as shown in Figure 5.20. The strong increases at 800 and 900°C indicate that the kinetics of formation are substantially enhanced at higher temperatures. The increase in CS_2 yield at 900°C , and the corresponding increase in H_2S yield, might be related to the decrease in tar sulphur yield at this temperature. Possible formation routes for CS_2 are discussed in the following section.

After rising from 0.5% at 500°C to 1% at 600°C , the sulphur yield as dimethyl disulphide (DMDS) in Figure 5.21 remains constant at this level through to 900°C . Dimethyl disulphide is generally known to be produced in kraft cooking by oxidation of CH_3SH via [5.13]. Similarly, oxidation of CH_3SH by CO_2 , such as [5.14], or by steam could be the mechanism for DMDS formation during pyrolysis. The reason for the yield of DMDS being insensitive to temperature may be that although more is produced at higher temperatures, it quickly decomposes due to secondary reactions, as was demonstrated at 700°C during the system response experiments (Chapter 4).

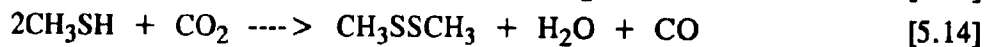
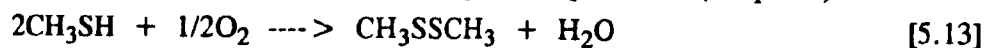


Figure 5.22 shows the produced water yield which was calculated by subtracting the water present in the original droplet and the estimated amount of water condensed out of the carrier gas from the total water detected. The yields of about 20% are in agreement with those of Feuerstein *et al* (14). The yield increases slightly with temperature which reflects increased devolatilization and then decreases at 800 and 900°C due to water being consumed by steam gasification, methane reforming, and the shift reaction.

Possible CS_2 Formation Routes

Early in this study a response was observed at the m/z ratio of 76 on the mass spectrometer during a preliminary pyrolysis run. Although CS_2 has not previously been reported as a pyrolysis product of kraft black liquor, it was felt that this was the likely contributor to this peak. The presence of CS_2 was later verified by gas chromatographic

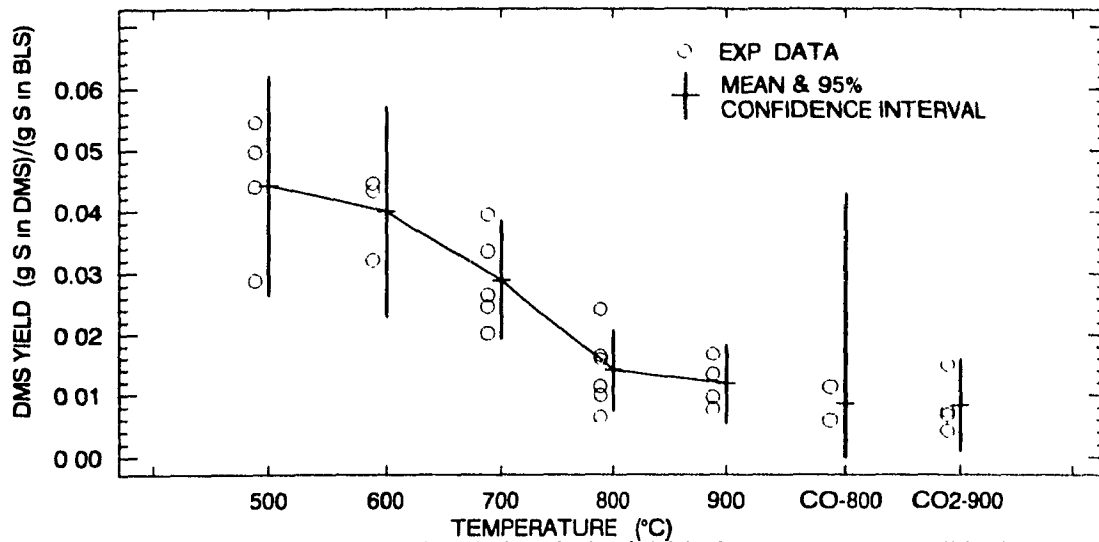


Figure 5.19 Pyrolysis yield of dimethyl sulphide for 20 mg 70% solids droplets

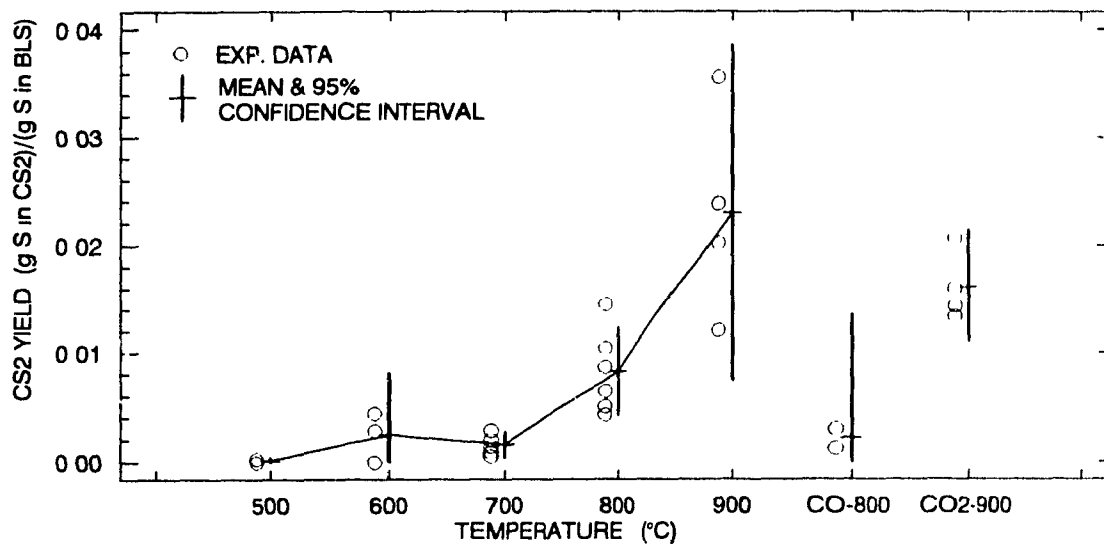


Figure 5.20 Pyrolysis yield of carbon disulphide for 20 mg 70% solids droplets

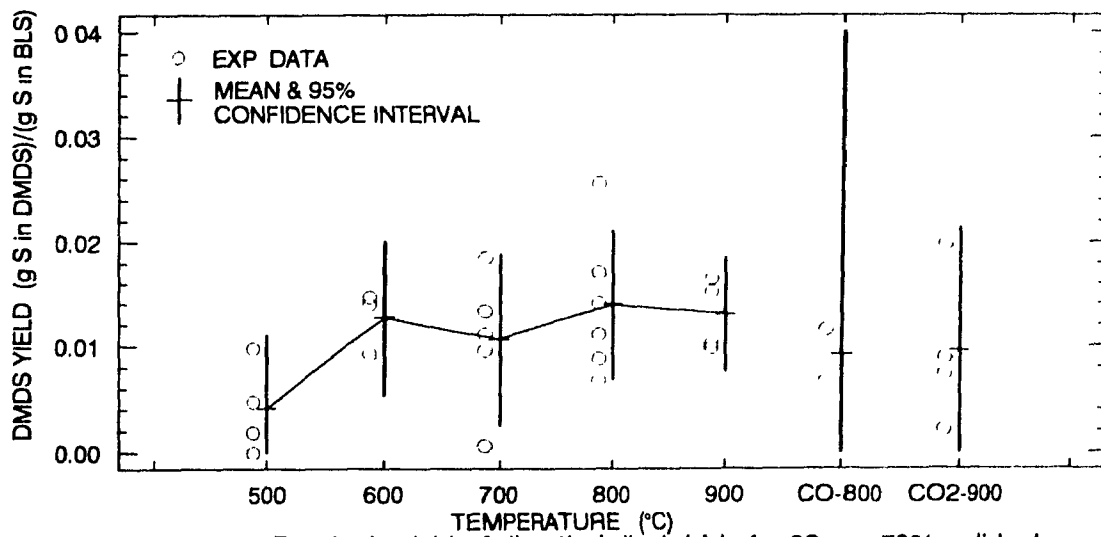


Figure 5.21 Pyrolysis yield of dimethyl disulphide for 20 mg 70% solids drops

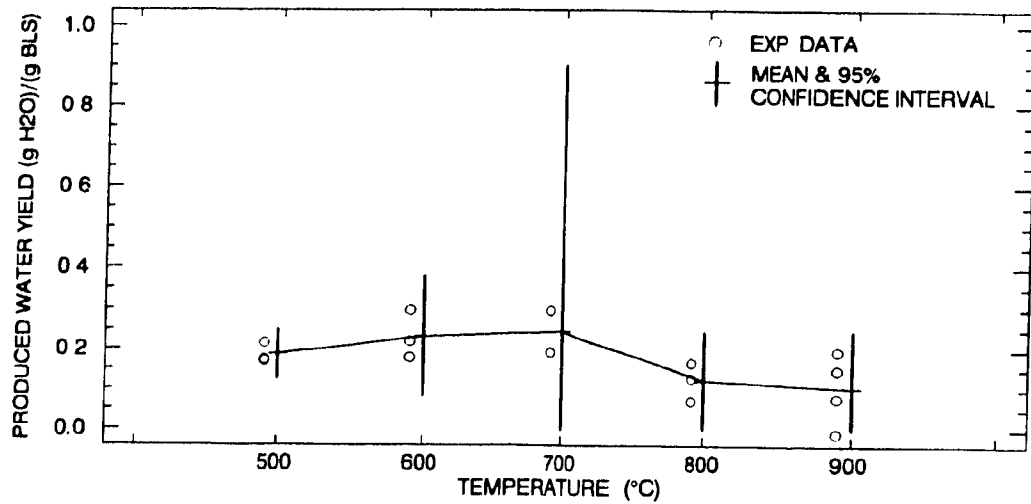


Figure 5.22 Pyrolysis yield of produced water for 20 mg 70% solids droplets

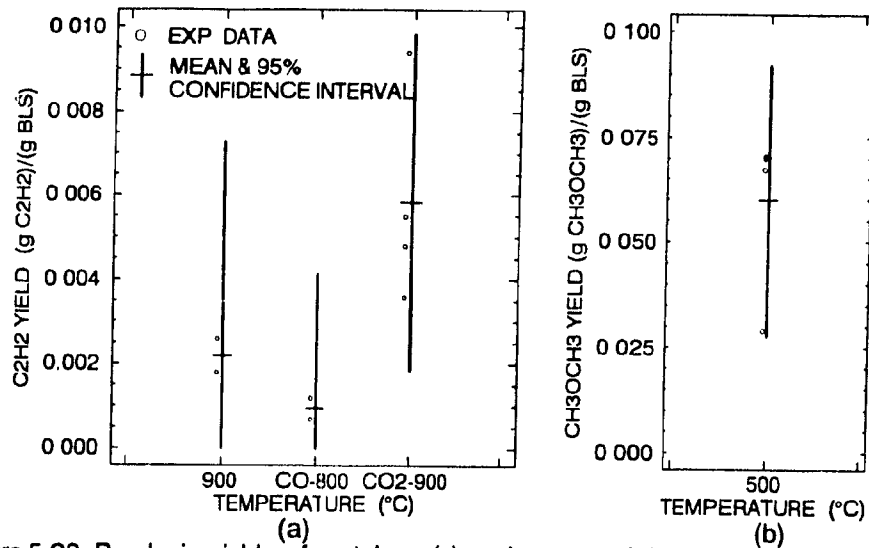
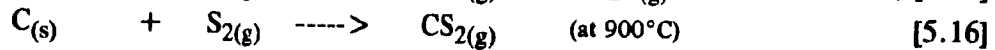
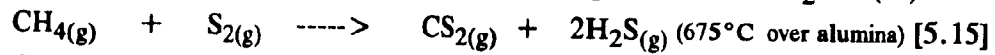


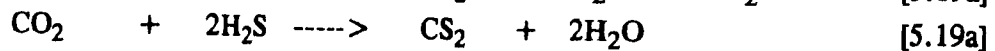
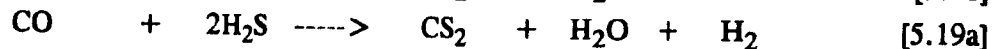
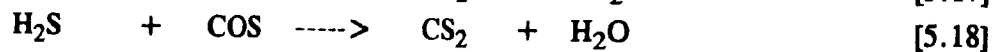
Figure 5.23 Pyrolysis yields of acetylene (a) and acetone (b) for 20 mg drops.

(GC) analysis using flame photometric detection.

Figure 5.20 shows that CS₂ formation increases quite strongly with increasing pyrolysis temperature. Two well known routes for the production of CS₂ are (66)



CS₂ can also be formed by the gas phase reactions (69)

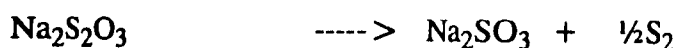
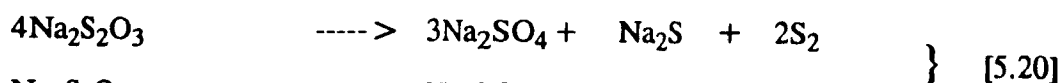


While both [5.15] and [5.16] are thermodynamically favoured over the range of temperatures in this study, see Table 5.8, reactions [5.18] and [5.19] are not (69). At 900°C the equilibrium constant for reaction [5.17] is close to one, making it a viable explanation for CS₂ production, as it explains both the sharp increase in CS₂ formation at the higher temperatures and the reduced yield when the CH₄ formation was lower, i.e. in CO and CO₂.

Table 5.8
Equilibrium Constants K_p for Reactions [5.15] and [5.16]
(calculated with data from (69))

Temperature (°C)	Reaction [5.15]	Reaction [5.16]
704	-----	12.02
760	1.55(10 ⁴)	10.97
816	1.42(10 ⁴)	10.00
871	1.33(10 ⁴)	9.35
927	1.24(10 ⁴)	8.71

The sulphur vapour necessary for reactions [5.15] and [5.16] could be produced by thermal decomposition of thiosulphate via [5.20] (13) as thiosulphate decomposition begins at 225°C and is complete by 470°C. Other possible routes for sulphur formation are reactions [5.21] and [5.22] below (34). Li's thermodynamic calculations showed that when the CO partial pressure is very low, S₂ can be produced in appreciable amounts. Reaction [5.22] is unlikely as no COS was detected by GC analysis of the pyrolysis gas from a run in helium.



Effects of CO and CO₂ on Pyrolysis

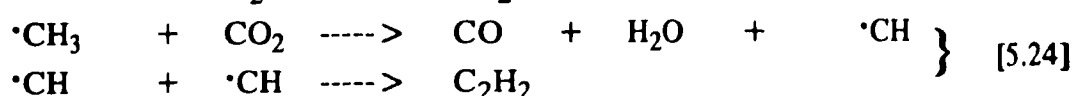
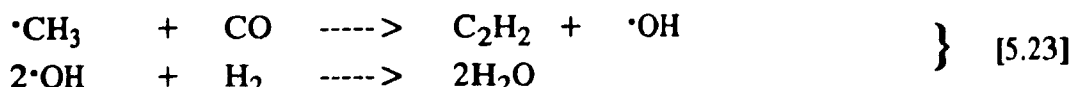
Even with the small number of experiments performed in partial CO and CO₂ atmospheres, it is evident that both CO and CO₂ substantially influence the yields of certain pyrolysis gases while having little or no effect on others. In the discussion below, the CO condition is 10% CO, 90% He at 800°C and the CO₂ condition is 15% CO₂, 85% He at 900°C. With reference to Figures 5.11 through 5.23, these effects are summarized as follows.

Ethane formation may be slightly reduced in CO but does not appear to be influenced by CO₂. Both CO and CO₂ significantly reduce the yields of ethylene and methane but in contrast CO and CO₂ substantially increase the yield of acetylene (without CO there is no acetylene produced at 800°C). The effect of CO and CO₂ on the yield of

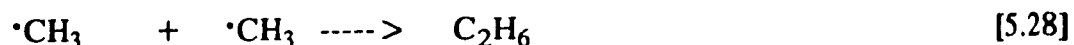
methanol is not statistically significant. The yield of CO₂ is also not significantly affected by CO. While the yields of the sulphurous gases H₂S, methyl mercaptan, DMS, and DMDS are not significantly influence by the presence of CO or CO₂, there appears to be a substantial decrease in the yield of CS₂ due to both CO and CO₂.

Thus, the largest changes due to the presence of CO and CO₂ appear to be in the yields of C₁ and C₂ hydrocarbons. According to Howard (31) it is well known that pyrolysis of coal produces radicals at temperatures as low as 300°C and that by 400°C a large increase in radical concentration has occurred. Most light hydrocarbons are also believed to be formed through secondary free radical reactions. It is also known (31) that a radical scavenger such as H₂ can substantially retard secondary reactions by combining with free radicals. Many of the effects that CO and CO₂ have on gas yields can be explained by considering that CO and CO₂ act as scavengers of hydrocarbon free radicals. The products of the reactions that could occur between CO and CO₂ and the free radicals are not obvious, but further investigation might reveal their existence.

The observation that the experiments in which C₂H₂ was formed in any appreciable quantities are those with significant CO₂ and CO partial pressures supports CO₂ and CO acting as radical scavengers, or promoting higher H₂ partial pressures since H₂ is a radical scavenger. Many possible paths exist by which this could occur. Reaction [5.23] below represents one such pathway for CO and [5.24] is a possibility for CO₂.



The lower yields of methane, ethylene, and ethane, with the addition of either CO or CO₂, can be explained by reduced concentrations of the radicals necessary for their formation, due to competition with reactions such as [5.23] and [5.24] for the available radicals. Possible reactions which yield these species as products are:



There are also many other routes by which these compounds could be formed via free radicals.

The observation that the presence of CO₂ has little if any effect on the calculated yield of CO, and may even reduce this amount (Figure 5.15), is in contradiction with the

increased carbon gasification and thus the expected increase in the formation of CO when CO₂ is present. This supports the suspicion that the response attributed to CO is actually corrupted by overlap with C₂H₄ and C₂H₆, which decrease under CO₂ offsetting the increased CO formation. The lack of influence of CO on CO₂ production is consistent with the CO₂ formation routes discussed in the pyrolysis literature and the discussion above.

The formation of CS₂ by reaction of sulphur vapour with methane or by H₂S with methane, as discussed above, is a possible explanation for the reduction in CS₂ yield in the presence of CO and CO₂ since less methane is formed, and thus less is available to react, under these conditions. In addition, any free sulphur normally available to react via [5.16], would likely react with CO₂ or CO to form COS. Increased H₂S yield under CO₂ is primarily explained by sulphur volatilization via reaction [5.6]. COS produced via reaction [5.3] may also contribute to increased H₂S via [5.29] and [5.30], both of which are thermodynamically favoured (69).



Droplet and Furnace Experimental Temperature-Time Histories

One form of information required to characterize rate processes during droplet pyrolysis is the droplet temperature as a function of time. This section presents such information for the experiments described earlier. The method of temperature measurement and recording has already been described in Chapter 4.

Figure 5.24 shows typical temperature-time profiles for 20 mg droplets of 70% solids kraft black liquor during fast pyrolysis experiments in helium at 500 through 900°C at a flow rate of 2.0 slm. Initial heating rates through the drying period to 150-200°C are relatively insensitive to furnace temperature, but after the end of drying at about 200°C the heating rates increase substantially with furnace temperature. At furnace temperatures of 700°C and below in helium, the droplet temperature rises continuously to the furnace temperature until withdrawn. However, at 800°C, and more pronouncedly at 900°C, the droplet temperature rises close to the furnace temperature in 5-10 seconds and then actually falls for a period before rising again to the furnace temperature (see Figure 5.24(a)). This decrease in temperature can be attributed to the endothermic reduction of sulphate by carbon to sulphide, which occurs rapidly at these temperatures (38). Production of CO corresponding to these temperature decreases is evident and is discussed further below. Figure 5.25 shows that the temperature decrease is even more pronounced in the reducing atmosphere containing 10% CO. While the temperature profiles for FP27

and FP28 show exceptional repeatability, other replicates also showed good consistency of heating profiles.

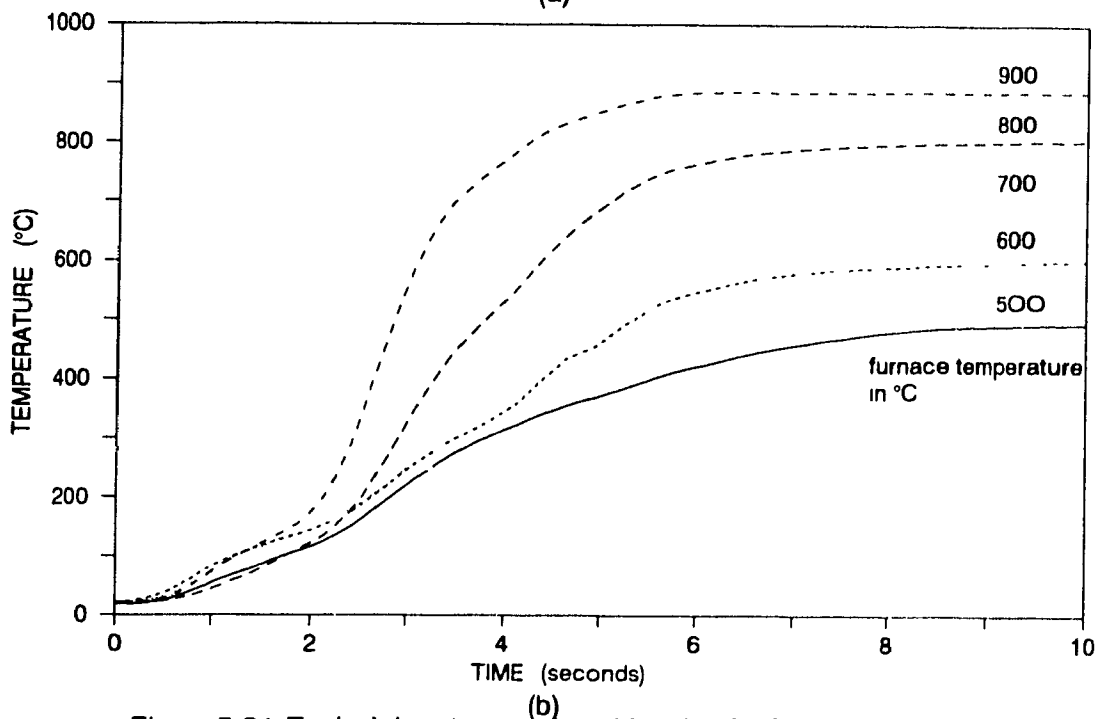
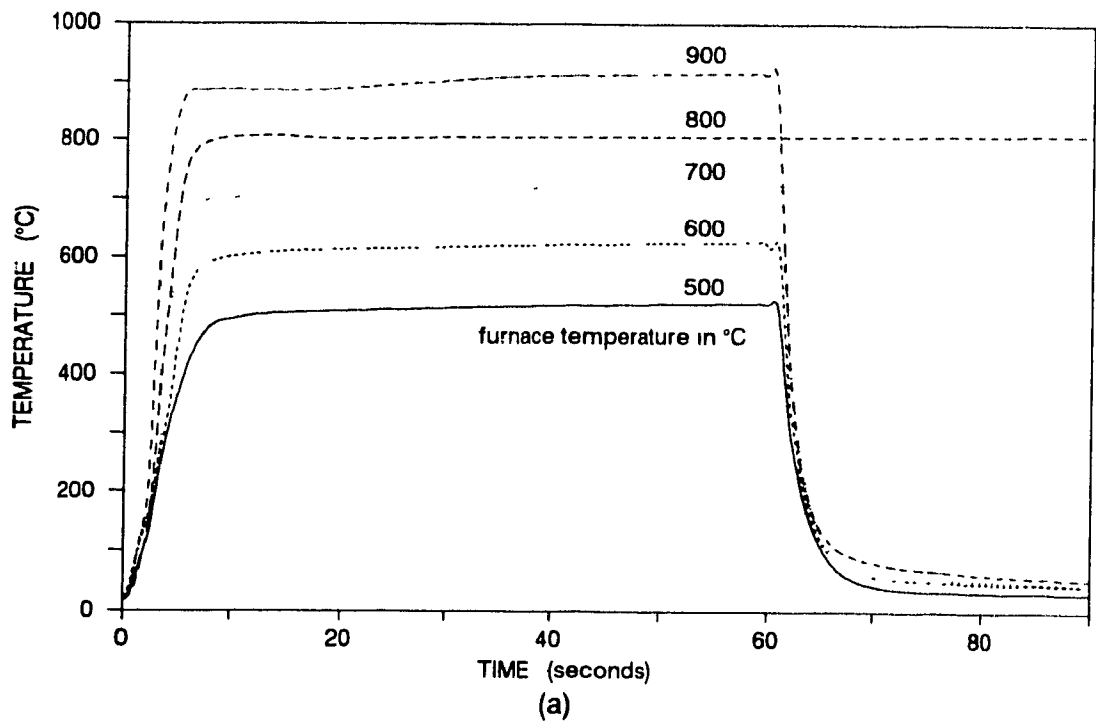


Figure 5.24 Typical drop temperature histories for fast pyrolysis experiments in helium. (a) 90 seconds (b) initial 10 seconds

Assuming that drying is complete when the droplet temperature reaches 200°C, the temperature at which decomposition begins, and subtracting the 0.7 seconds required for

the droplet to reach the centre of the furnace, the drying times for the droplets shown in Figure 5.24(a) are 2.2, 2.0, 2.0, 1.9, and 1.5 seconds at 500, 600, 700, 800, and 900°C respectively. These times are longer than those reported by others at the highest temperatures but shorter than those reported at the lowest temperatures (22,40). This may be due in part to the different criteria used to establish when drying is finished. Hupa *et al* (40) used the appearance of a visible flame, and Verrill and Nichols (40) used the onset of droplet swelling, to signify the end of drying. These two points are equivalent as described by Hupa *et al* (40). The data of Hupa *et al* (40) show that the droplet temperature can be significantly above 200°C at the end of their "drying phase", thus indicating that devolatilization has already begun. The different methods used to establish when drying are complete probably is responsible for the difference in drying times at the lower temperatures. The slightly longer drying times observed with the present apparatus at higher temperatures are likely caused by the relatively large droplets (20 mg of 70% solids liquor) used.

The effects at 900°C of carrier gas composition on both droplet and furnace temperature histories are shown in Figure 5.26. Heating in pure helium is more rapid due to its exceptionally high thermal conductivity, and the resulting high heat transfer coefficients. The decrease in temperature due to sulphate reduction is shown to be more pronounced with CO and CO₂ than in pure helium. The heating rate for 15% CO₂ in helium is somewhat lower than that for 10% CO in helium due to both the higher concentration of CO₂, and thus lower concentration of helium, and the endothermic gasification of carbon, which is very rapid at 900°C. The increase in heating rate after 20 seconds indicates the end of sulphate reduction, while the increase after about 35 seconds for the experiment in 15% CO₂ signifies that gasification is complete. The profile with CO₂ present is less smooth due to the disappearance of the carbon from and the migration of the smelt on the drop thermocouple.

Figure 5.26 also shows that the gas composition has a substantial influence on the ability of the furnace to maintain a constant temperature. With CO and CO₂ present the insertion of the sample causes the temperature to decrease 10 and 15°C respectively, whereas the change in pure helium is only about 2°C. This decrease is due to cooling caused by the thermal mass of the probe and the liquor as well as by the produced gases. The second decrease in furnace temperature is due to a combination of control oscillation and cooling caused by sulphate reduction.

Pyrolysis Gas and Volatile Formation Rates

In addition to the droplet temperature histories presented above, the rates of gaseous

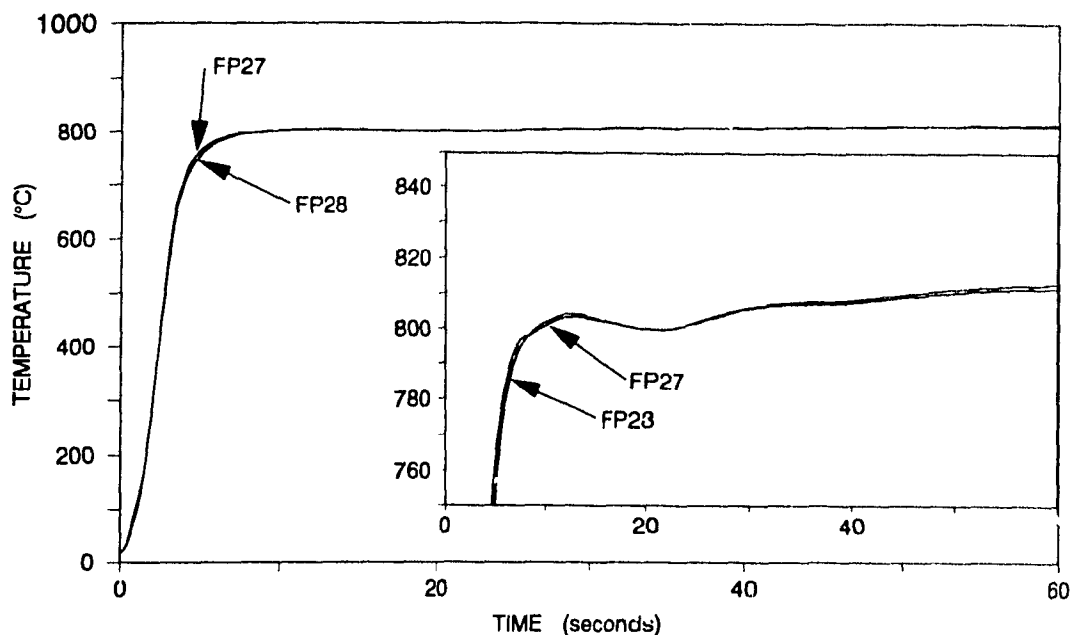


Figure 5.25 Replicate drop temperature histories for drop pyrolysis at 800°C in 10% CO and 90% helium showing temperature decrease due to the rapid reduction of sulphate by CO and carbon

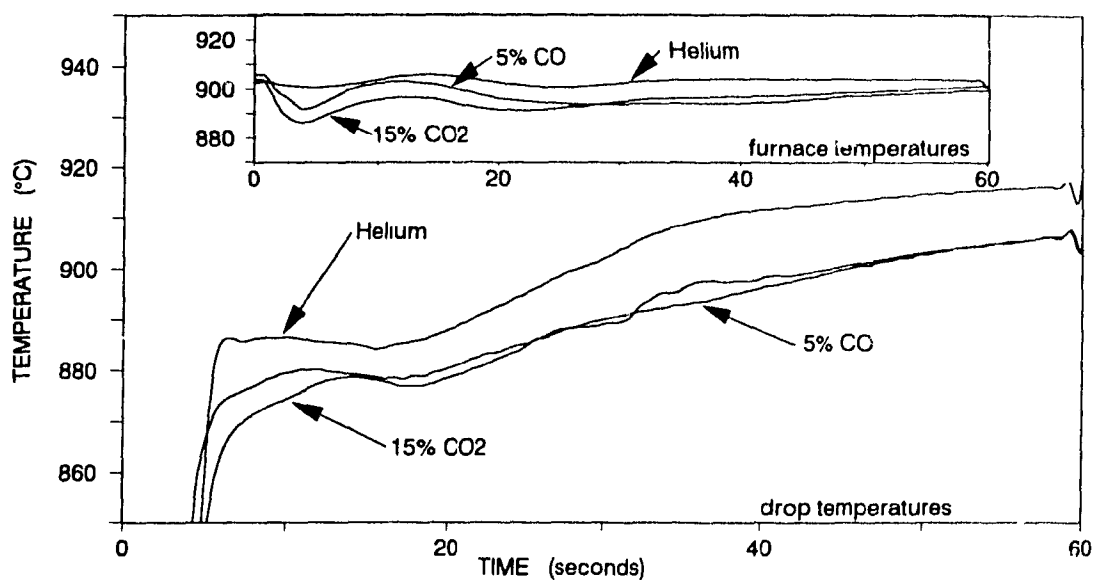


Figure 5.26 Effect of gas environment on drop and furnace temperature histories for liquor pyrolysis at 900°C.

and volatile product formation are required to characterize pyrolysis rate processes. The droplet-pyrolysis mass-flow-rate histories shown in Figures 5.27 through 5.38 are plotted parametrically against pyrolysis temperature for product gases and light volatiles with the exceptions of acetylene and acetone. The acetone formation was only calculated at 500°C and its mass flow history is similar to that of CH_3OH at this temperature. The profiles for acetylene are very similar to those of ethylene. The figures show mass flow rates as

determined with the mass spectrometer, using the methods described in Chapter 4. The time scale on the plots is synchronized with droplet insertion into the furnace. The figures have not been corrected for the lag time of about one second (Figure 4.16) due to the volume of gas between the instrument and the droplet, or for the compound specific dispersion caused by the mechanisms described in Chapter 4. However, selected examples of data corrected for these effects using deconvolution are presented later.

The plots shown are for the individual experiments FP24 and FP32 to FP35, of which the latter four were performed using ice-water to cool the condenser rather than dry-ice and acetone. Experiment FP24 at 500°C used the colder dry-ice and acetone bath coolant for the condenser because of concern that tar would condense in the instrument.

Table 5.9
Times for Onset of Formation and Peak Formation Rate
During Black Liquor Droplet Pyrolysis

Product	500°C		600°C		700°C		800°C		900°C	
	Onset	Peak	Onset	Peak	Onset	Peak	Onset	Peak	Onset	Peak
CH ₃ OH	5.0*	10.5*	3.0	7.0	2.0	5.75	1.0	4.75	1.0	4.25
CH ₄	7.0*	9.0*	4.0	6.5	2.0	5.0	1.0	4.0	1.0	4.0
C ₂ H ₄	5.0*	11.0*	5.5	7.0	2.0	5.5	0.5-1.0	4.0	0.5-1.0	4.0
C ₂ H ₆	---	---	3.5	6.5	2.5	5.0	0.5-1.0	4.25	0.5-1.0	4.1
CO ₂	5.0*	6.5*	3.0	5.75	2.5	5.0	0.5	4.0	0.5	4.1
CO	9.5*	12.0*	3.0	6.4	1.0	5.3	0.5	4.0	0.5-1.0	4.0
H ₂ S	1.5*	6.25*	2.0	5.5	1.0	4.75	0.5	3.5	1.0	3.75
CH ₃ SH	5.0*	7.0*	3.0	5.8	2.0	4.8	1.0	3.7	1.0*	1.5*
CH ₃ SCH ₃	---	---	3.5	6.4	2.0	5.2	1.0	4.2	2.0**	4.6
CS ₂	---	---	---	---	4.5	7.0	0.0-0.5	4.0	0.5-1.0	4.2
CH ₃ SSCH ₃	---	---	3.0	7.4	1.5	5.6	0.5-1.0	4.5	1.0	4.2
H ₂ O	3.0*	---	2.0	---	2.0	---	2.0	---	1.5-2.0	---

* - from experiments using dry-ice and acetone condenser cooling

** - shows as 4.0 on plot but part of response is cutoff

Two variables which can be used to characterize the formation rate history profiles are the time of initial formation, defined as the time when the mass flow rate becomes positive, and the time at which the maximum peak in the formation rate occurs. These values are listed in Table 5.9 and are corrected for the one second time lag of the system impulse response, but are not corrected for dispersion in the system. Some broad conclusions can be drawn by analysis of these parameters. At lower temperatures there is a fairly broad range of times for the onset of formation of different products as well as for when their maximum formation rates are reached. This reflects the fact that these droplets heat more slowly and that the products resulting from the most easily broken bonds are formed at lower temperatures than those formed from more stable bonds. At higher temperatures these differences become smaller as kinetics become less important and heat

and mass transfer dominate. The times for the onset of formation and the maximum formation peak in the alkanes, alkenes, and thioalkanes tend agree closely, reinforcing the suggestion that free radical formation reactions and hemicellulose and cellulose derivative decomposition are shared by these compounds.

Many compounds show a shoulder on the leading edge of their formation rate peaks. This indicates an early phase of pyrolysis which reaches a maximum very early in the overall process and overlaps with the main devolatilization peak. This phenomena was observed to varying degrees at all temperatures but 500°C, but most strongly at 800 and 900°C. The initial shoulder becomes even more pronounced when the data is corrected by deconvolution as shown below. The onset of formation times in Table 5.9 are very often associated with this initial peak and comparison between these times and the temperature histories in Figure 5.24(b) reveals that this phase occurs during droplet drying. If one considers droplet temperatures below 200°C as the drying phase, this period takes 2 to 3 seconds for all experiments. Since H₂S formation has commenced at all pyrolysis temperatures during the drying period, as has the formation of almost all other species at pyrolysis temperatures of 700°C and above, it can be concluded that there is a definite overlap between the drying and devolatilization phenomena. This initial devolatilization stage is likely due to pyrolysis of the dry "skin" of a droplet occurring while its interior is still drying. Miller found that droplet swelling was maximum at a pyrolysis temperature of 500°C and proposed that above this temperature a hard "skin" is formed during the initial stages of pyrolysis which restricts droplet swelling (11). His hypothesis is consistent with an overlap of the drying and devolatilization phenomena, and an initial devolatilization stage (of the dry "skin") before the dramatic swelling and devolatilization takes place.

Compound by compound the following comments can be made in reference to Figures 5.27 and 5.38. Methanol formation, in Figure 5.27, rises smoothly with the initial devolatilization phase evident at 600, 800 (a change in slope on the rising side of the peak), and 900°C. The tailing of the peaks is mainly due to condensation and adsorption in the condenser and the tubing. At the intermediate pyrolysis temperatures (600 - 800°C) the maximum formation rates correspond to a droplet temperature of 600-650°C. Figure 5.28 shows an initial devolatilization for methane formation at all pyrolysis temperatures. Peak formation rates correlate with droplet temperatures of 600 to 700°C for the intermediate pyrolysis temperatures. Ethylene and ethane formation profiles shown in Figures 5.29 and 5.30 are similar to those of methane except for substantial tailing of the ethane peaks. The tailing is likely due to interference from a condensible compound, such as methanol, and thus ethane yields are probably over

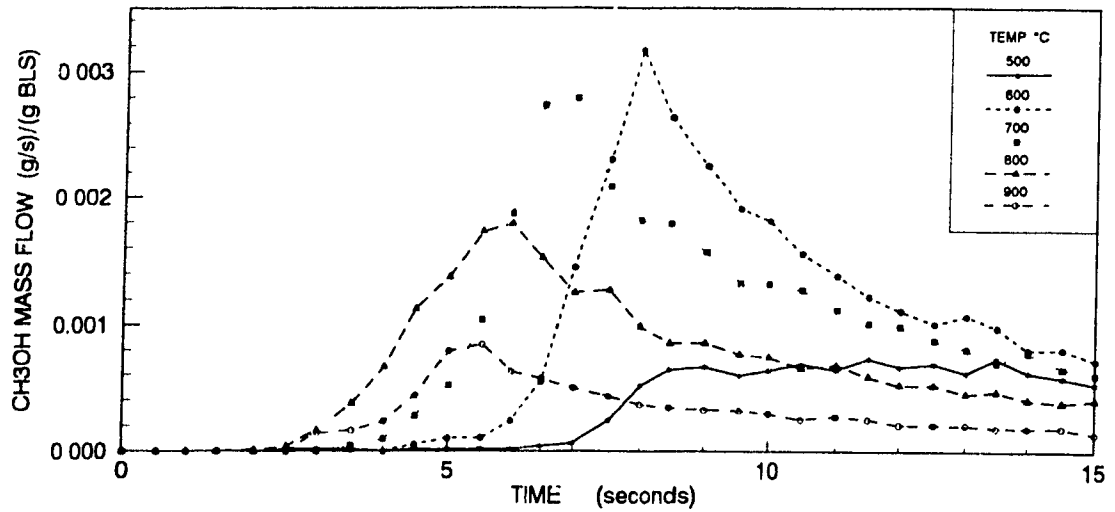


Figure 5.27 Methanol formation rate measured at MS for droplet pyrolysis

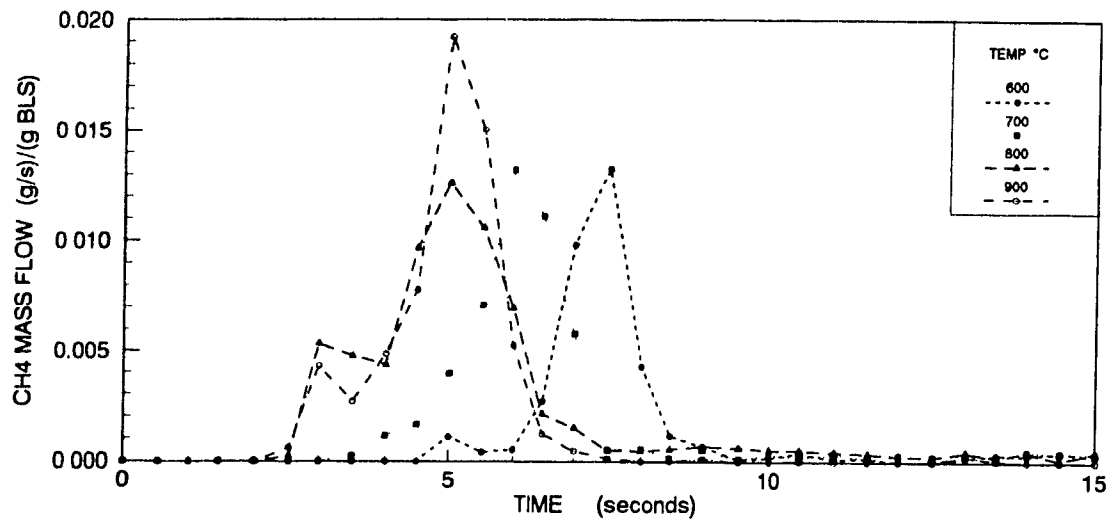


Figure 5.28 Methane formation rate measured at MS for droplet pyrolysis

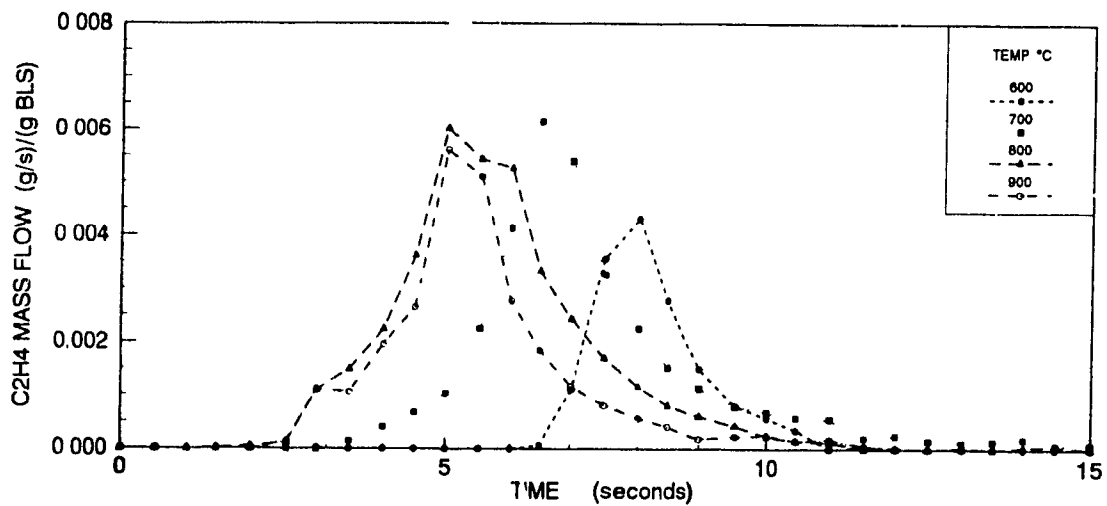


Figure 5.29 Ethylene formation rate measured at MS for droplet pyrolysis

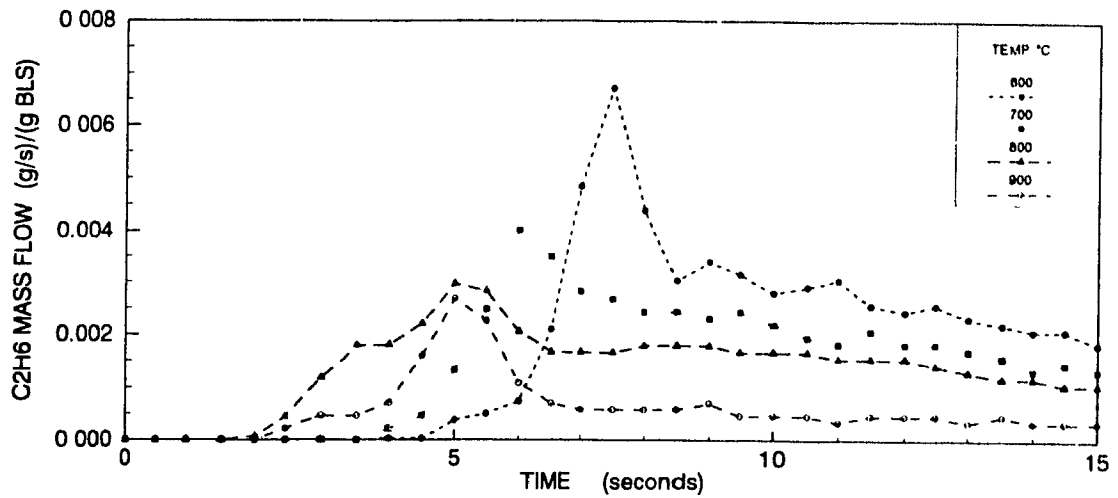


Figure 5.30 Ethane formation rate measured at MS for droplet pyrolysis

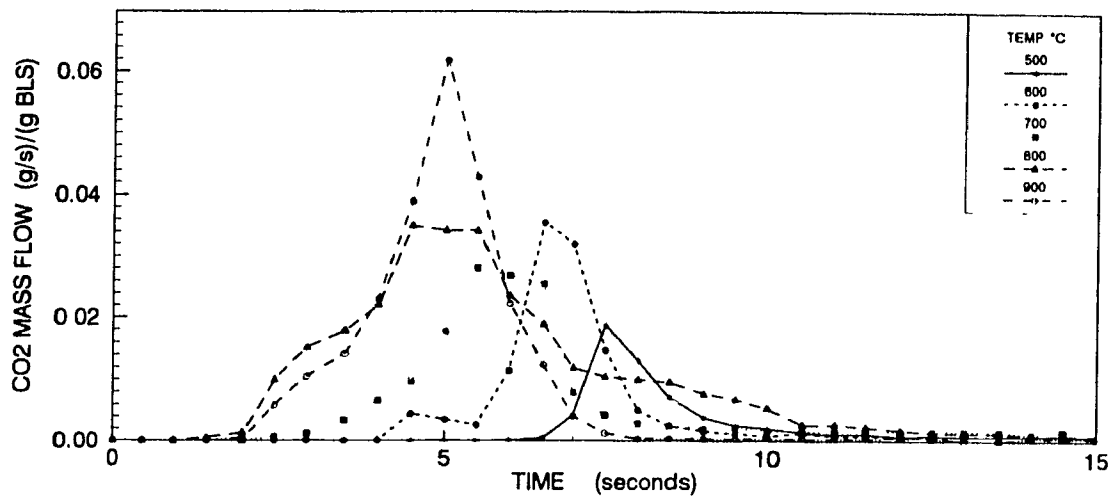


Figure 5.31 Carbon dioxide formation rate measured at MS for droplet pyrolysis

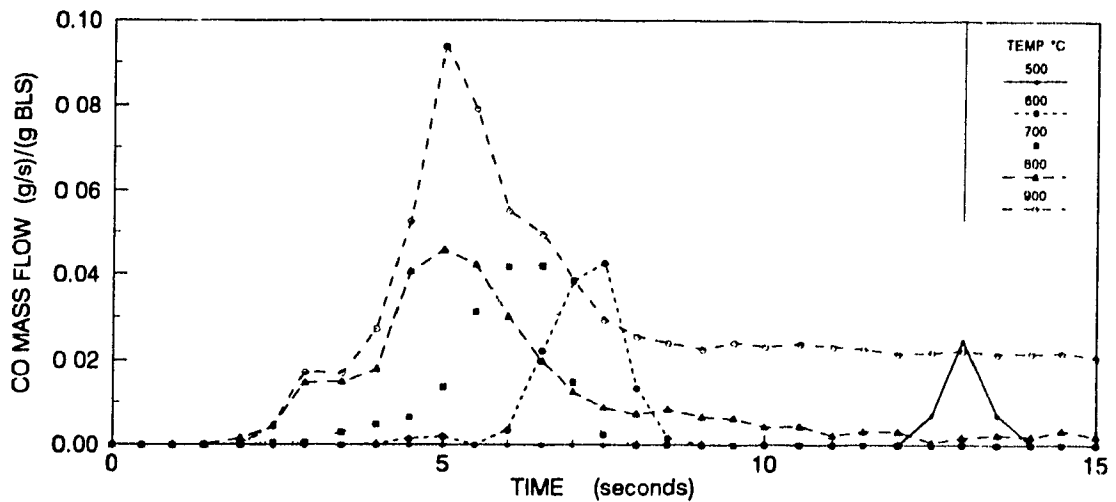


Figure 5.32 Carbon monoxide formation rate measured at MS for drop pyrolysis

estimated.

The initial formation of CO_2 , shown in Figure 5.31, occurs slightly earlier than that of the hydrocarbons due to CO_2 resulting from the cleavage of the relatively weak bonds between carbon and the carboxyl group (17). Initial devolatilization again occurs above 600°C . At a pyrolysis temperature of 500°C , the CO formation, shown in Figure 5.32, occurs much later than that of CO_2 as it results from the breaking of relatively strong ether linkages (17). Above 600°C , the times for the onset of formation and the maximum formation rate for CO coincide with those of CO_2 , suggesting that they are coupled through the water-gas shift reaction. The CO formation rate profiles at 800 and 900°C show three phases; the initial devolatilization period; the main devolatilization period; and the sulphate reduction period responsible for the tailing. At 900°C the CO production due to endothermic sulphate reduction begins after about 6.5 seconds and coincides closely with the time at which the droplet temperature ceases to increase, as shown clearly in Figure 5.26.

As discussed above and shown in Figure 5.33, the onset of formation of H_2S starts in all cases during drying. The formation of H_2S is also complete at an earlier time than that of other compounds. The early formation of H_2S is likely due to a combination of two factors. Firstly, organic sulphur bonds from which some H_2S originates break at relatively low temperatures (17). The second formation route is through devolatilization of sulphur from the residual Na_2S in black liquor by reaction with CO_2 and steam via reaction [5.6], which is very favourable at low temperatures. The latter route explains why H_2S formation occurs earlier than that of the organic sulphur gases. Finally, the H_2S formation rate maximum occurs earlier than those of other gases as H_2S formation via [5.6] is not favoured for droplet temperatures above about 600°C (Chapter 3).

The methyl mercaptan formation rate shown in Figure 5.34 is similar to that of H_2S except that the onset of formation and maximum formation rate are observed somewhat later. At 900°C the formation of methyl mercaptan is insignificant. The formation rates of dimethyl sulphide are shown in Figure 5.35 and very much resembles those of CF_3SH except that the maximums occur slightly later. With reference to Chapter 4, this is likely due to differences in system response rather than to differences in pyrolysis formation rates. Differences in system response could also account for some of the time lag between the formation rate maximums of CH_3SH and those of H_2S . As shown in Figure 5.37, dimethyl disulphide is similarly shifted with respect to DMS in most cases, presumably due to greater adsorption of dimethyl disulphide.

While formation of CS_2 , shown in Figure 5.36, is weak at 700°C , it is strong at both 800 and 900°C . Its early onset at 800 and 900°C coincides with that of H_2S and

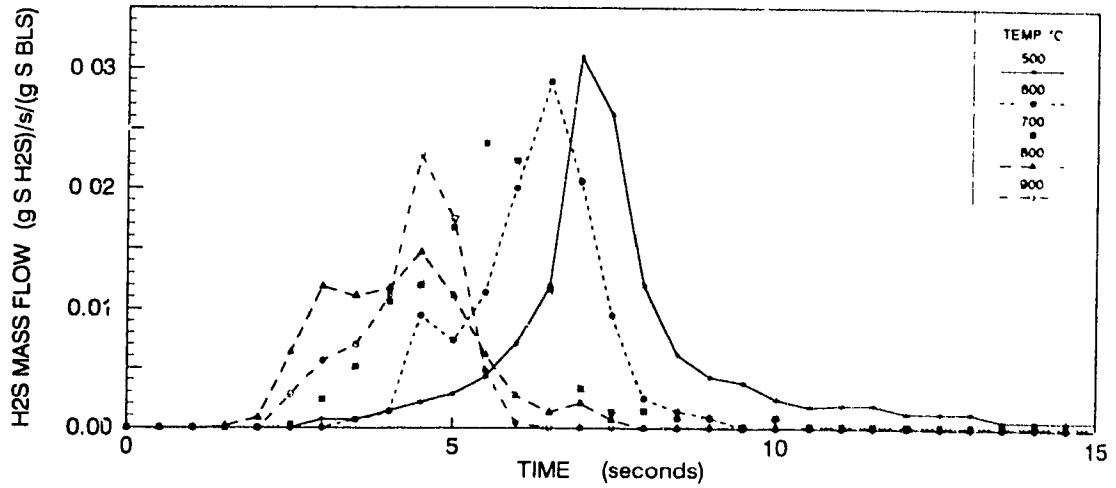


Figure 5.33 Hydrogen sulphide formation rate measured at MS for drop pyrolysis

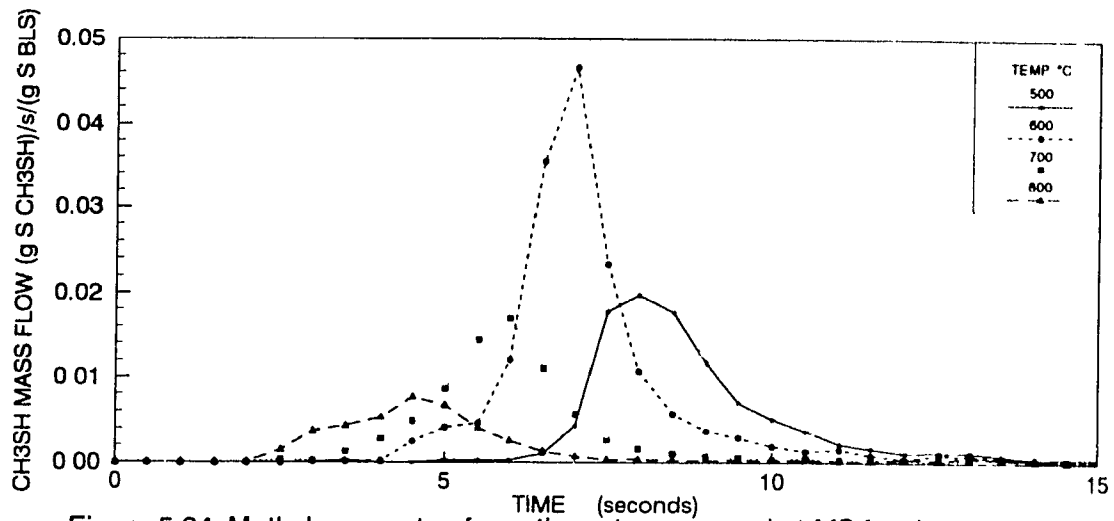


Figure 5.34 Methyl mercaptan formation rate measured at MS for drop pyrolysis

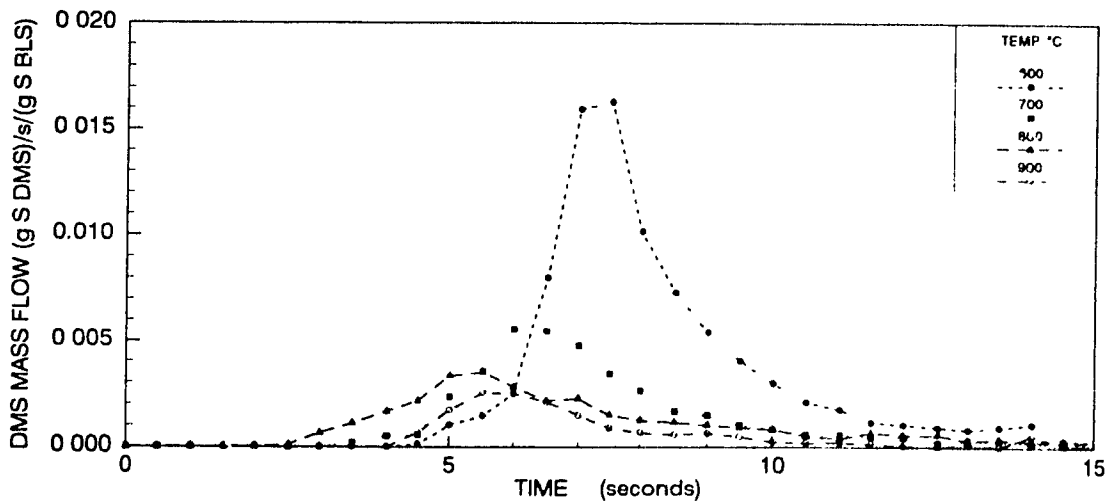


Figure 5.35 Dimethyl sulphide formation rate measured at MS for drop pyrolysis

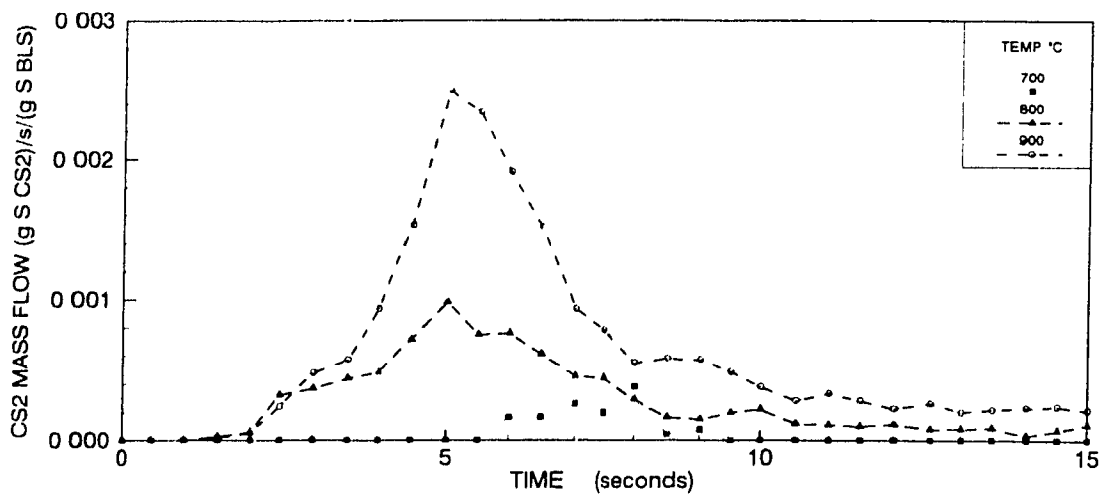


Figure 5.36 Carbon disulphide formation rate measured at MS for drop pyrolysis

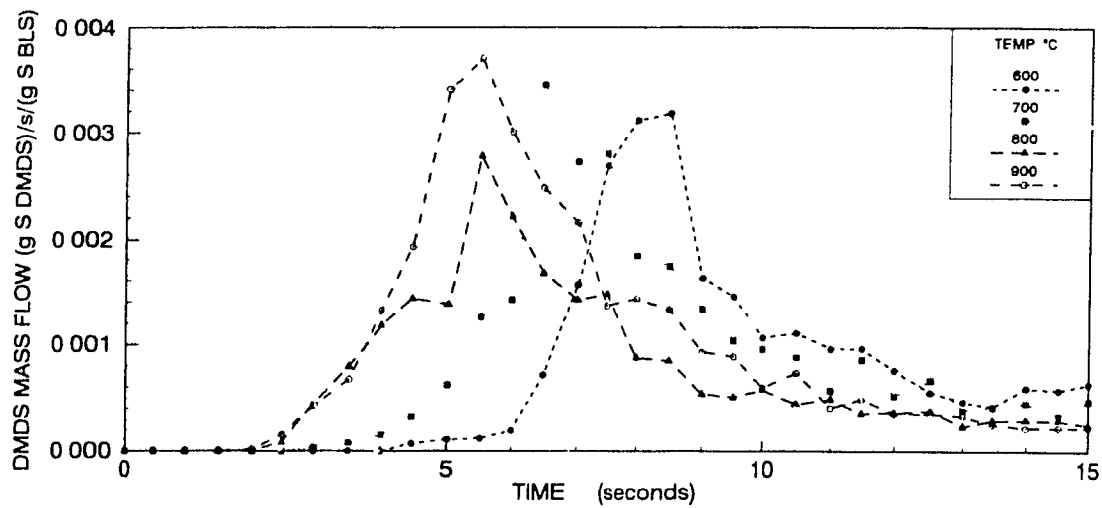


Figure 5.37 Dimethyl disulphide formation rate measured at MS for drop pyrolysis

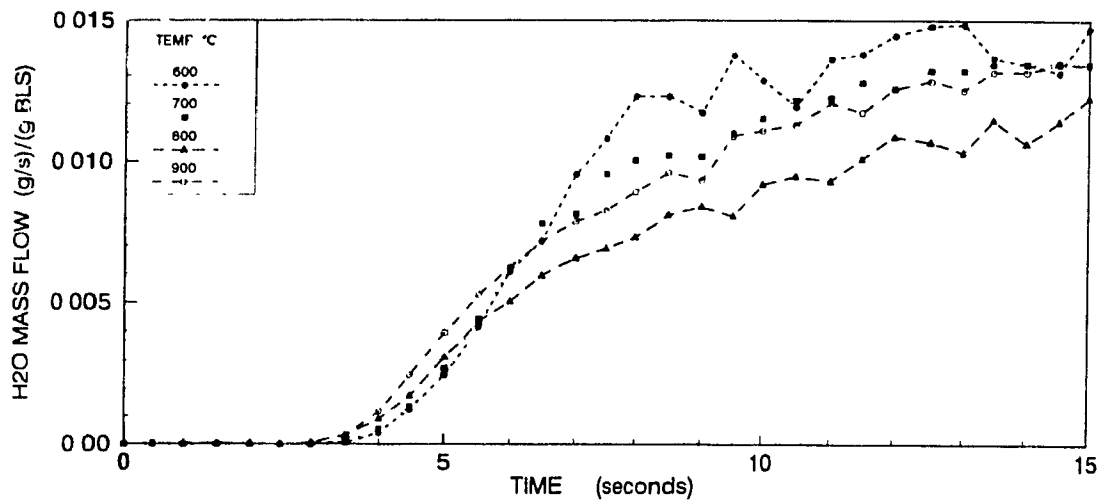


Figure 5.38 Initial water vapour flow measured at MS

supports the postulate that CS_2 is formed from H_2S , perhaps by reaction with methane via [5.17]. This is plausible as at these temperatures the times of maximum formation rate of H_2S , CH_4 , and CS_2 are approximately the same.

Figure 5.38 shows that the water vapour flow rate past the MS is not influenced much by the pyrolysis temperature during the initial six seconds of heating. Since the onset of evaporation is certainly before the time indicated by the plot, it can be concluded that condensation and adsorption in the condenser and tubing are responsible for the present response.

Formation Rate and Conversion Data Corrected by FFT Deconvolution

Figures 5.39 and 5.42 show production rate data for CH_4 and H_2S which have been deconvolved using the method described in Chapter 4 to correct for the time lag and dispersion caused by the apparatus and detection equipment. The initial devolatilization period is very evident on these plots, although there is amplification of the experimental noise. Figures 5.40 and 5.41 show methane conversion versus time plots for the deconvolved and non-deconvolved data respectively. Figures 5.43 and 5.44 are equivalent plots for hydrogen sulphide. These plots demonstrate that deconvolution is important for the analysis of experimental black liquor droplet pyrolysis data as the deconvolved plots show much more clearly the initial devolatilization phase and more accurately the conversion rate during devolatilization. If higher data sampling rates can be achieved, the results of this method will be improved substantially as then the primary signals will be much more accurate and digital filtering techniques can be employed.

Summary of Black Liquor Droplet Pyrolysis

Pyrolysis of kraft black liquor droplets is a complex process with many overlapping phenomena and competing chemical reactions. Based on the present results, the pyrolysis of a kraft black liquor droplet at pyrolysis temperatures of 600 to 900°C occurs as follows. Initially the bulk temperature of a droplet rises gradually as the solids content increases during the evaporation of water. During this drying period a "skin" forms on the outside of the droplet which then undergoes decomposition during an initial devolatilization phase, which is concurrent with the drying of the rest of the drop. H_2S is the first gas produced during the initial devolatilization phase due to the low strength of the carbon-sulphur bonds in the organic component of the black liquor. CO_2 is also produced early and along with H_2O reacts with Na_2S to produce additional H_2S when the droplet temperature is low (below 600°C).

When droplet drying is complete at a droplet bulk-temperature of about 200°C, the main devolatilization period starts as the droplet begins to swell substantially, rupturing

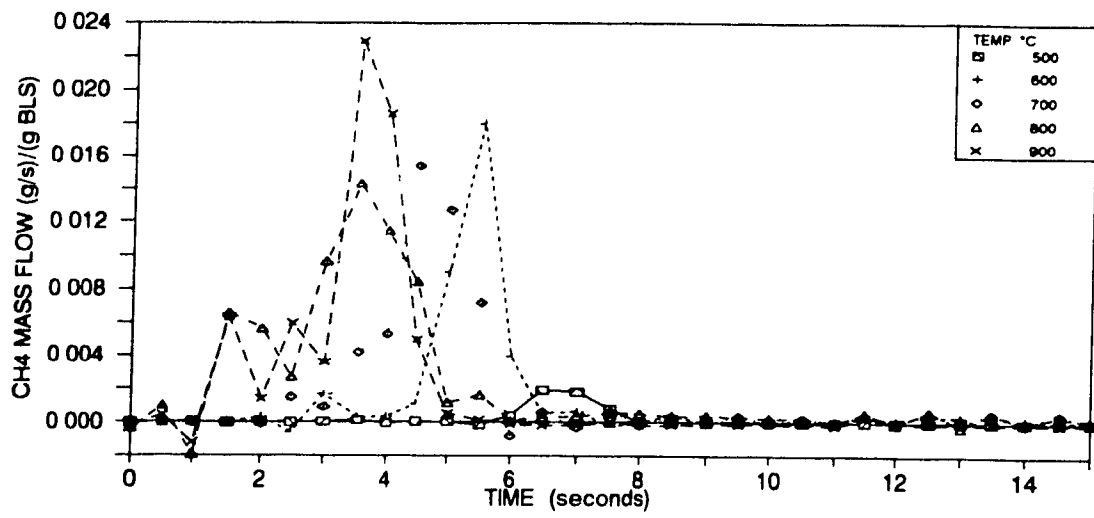


Figure 5.39 Methane formation rate at droplet calculated using deconvolution

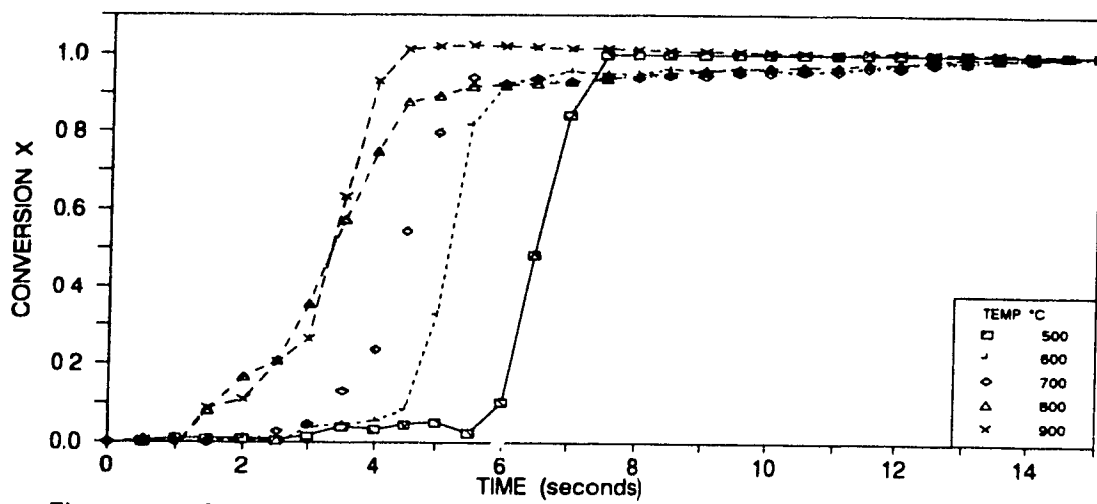


Figure 5.40 Methane conversions calculated from deconvolved formation rates

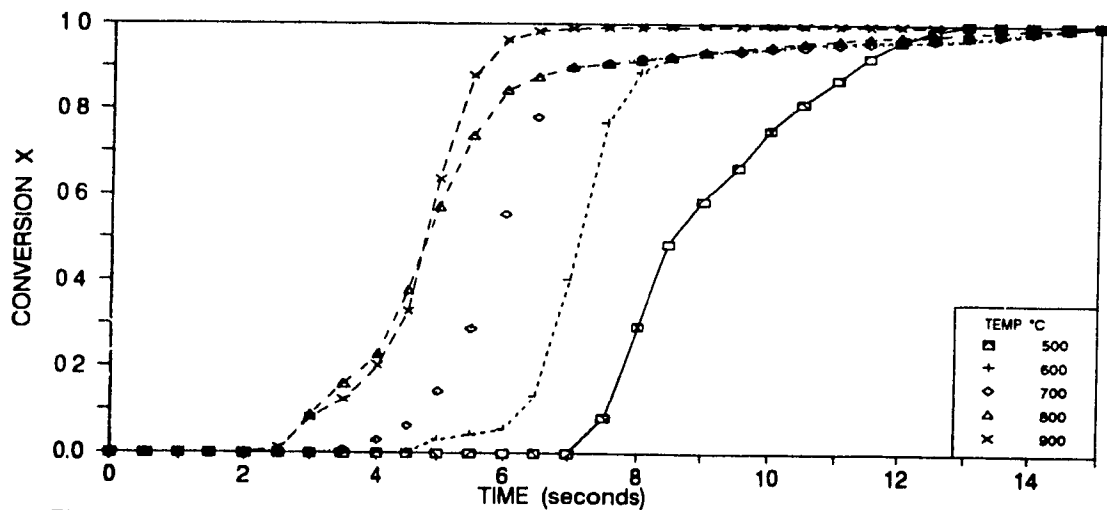


Figure 5.41 Methane conversions calculated from non-deconvolved formation rates

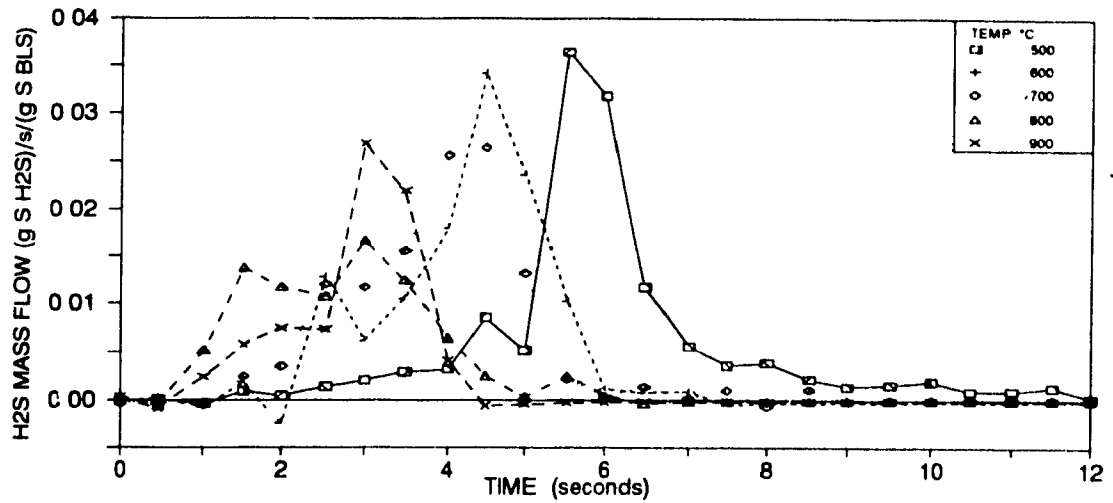


Figure 5.42 H2S formation rate at droplet calculated using deconvolution

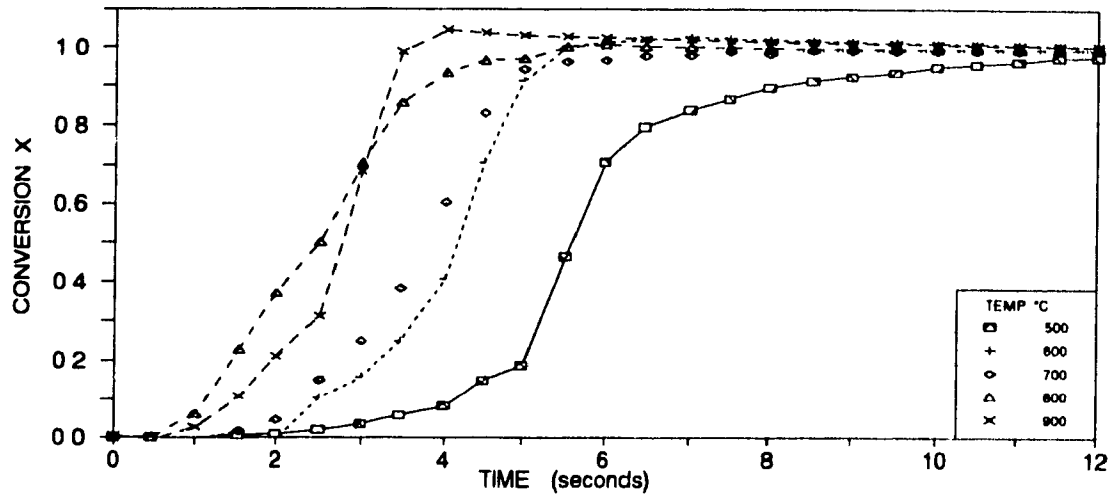


Figure 5.43 H2S conversions calculated from deconvolved formation rates

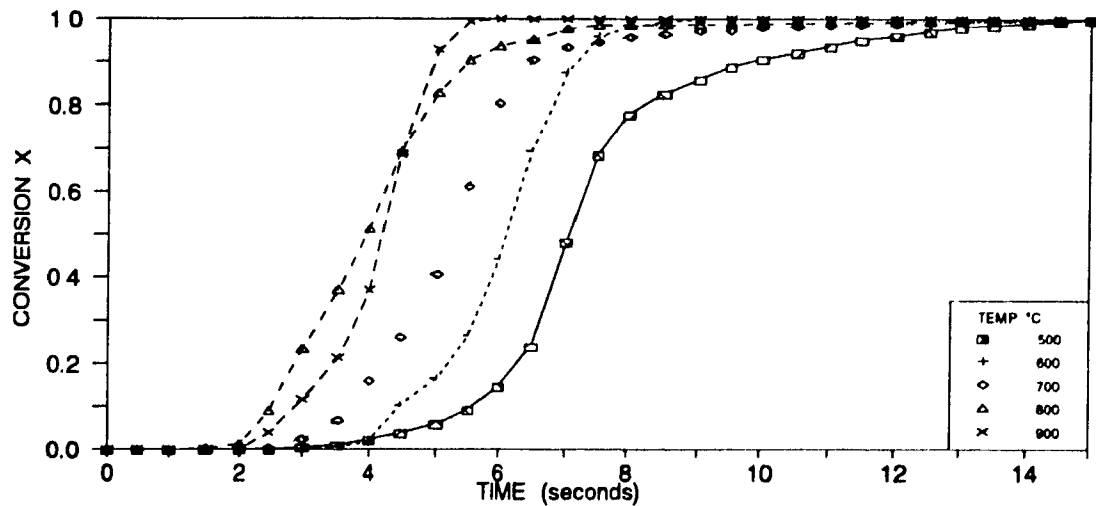


Figure 5.44 H2S conversions calculated from non-deconvolved formation rates

the hard "skin" and rapidly expelling pyrolysis gases. During the main devolatilization phase the droplet temperature rapidly approaches that of the furnace. For pyrolysis temperatures of 600 - 800°C the gas formation rate reaches its maximum for most gases at a droplet temperature between 600 and 650°C, before rapidly falling back to zero. The peak formation rate of CO occurs slightly later than that of the hydrocarbons, CO₂, and the sulphurous gases, due to it being formed from the breaking of more stable bonds. At pyrolysis temperatures of 800 and 900°C, the droplet temperature first attains a value close to that of the furnace temperature, before decreasing moderately because of the rapid endothermic reduction of Na₂SO₄ to Na₂S by carbon. The reduction produces CO and is complete at 900°C after about 20 seconds when the droplet temperature begins to rise again.

Conclusions

The following can be concluded for fast pyrolysis of kraft black liquor droplets, based on the results and discussions presented in this chapter.

- i) A mass spectrometer coupled to a tube furnace can be successfully used to collect data from the pyrolysis of single droplets of kraft black liquor and provides a powerful tool for kinetic analysis when rate data are corrected using Fast Fourier Transform deconvolution methods.
- ii) The sulphur yield of kraft black liquor char increases as expected thermodynamically with increasing pyrolysis temperature, but gas sulphur yield appears to be more influenced by kinetic and transport phenomena.
- iii) Yields of hydrocarbon gases increase with temperature for lighter and unsaturated molecules while decreasing for large molecules, including the thioalkanes, due to thermal instability.
- iv) Thermodynamics can explain much of the formation behaviour of CO, CO₂, H₂O, and CH₄ at 800°C and above, but free radical reactions are necessary to explain the behaviour of unsaturated hydrocarbons.
- v) CO and CO₂ appear to act as free radical scavengers, influencing the yields of unsaturated and light hydrocarbons.
- vi) Carbon disulphide is formed in appreciable quantities during droplet pyrolysis at 800 and 900°C and its source appears to be reaction of H₂S with CH₄.
- vii) At 800 and 900°C the rate of the endothermic reduction of sulphate by carbon is very rapid and causes droplet temperatures to decrease.
- viii) Three phases of devolatilization are present during black liquor droplet pyrolysis, an initial devolatilization phase, the main devolatilization, and finally CO production through sulphate reduction by carbon.

CHAPTER 6 BEHAVIOUR OF SODIUM AND FORMATION OF ELEMENTAL SODIUM DURING FAST PYROLYSIS OF KRAFT BLACK LIQUOR

Introduction

This chapter reports the investigation of whether fully reduced sodium is formed during the rapid pyrolysis of kraft black liquor and whether this "elemental sodium" is present in appreciable quantities in the resulting black liquor char. The term "fully reduced sodium" is generally used in preference to "elemental sodium" as the sodium is most likely present as a chemisorbed species, rather than as a species with the electronic structure of elemental sodium. Also presented are the sodium yield results of the rapid pyrolysis experiments reported in Chapter 5. The reasons for investigating the presence of fully reduced Na in black liquor char are presented, and the relevant literature is reviewed.

Sodium Loss During Black Liquor Pyrolysis

The fate of sodium during the pyrolysis of black liquor has recently been the subject of substantial investigation (18,19,21,22,23). Li and van Heiningen in their studies of slow pyrolysis of kraft black liquor in a thermobalance found that for samples heated to 675-775°C in an inert carrier gas, the sodium loss was 8-20%, increasing with increased final temperature. For heating to 800°C the loss was substantially greater at 40-45%. When they held the sample at the final pyrolysis temperature until no further weight loss occurred, they observed that almost complete decomposition of Na_2CO_3 occurred through reduction by carbon in the char, whereby CO and CO_2 were produced and Na was released from the char. They proposed that fully reduced sodium was formed which subsequently desorbed to enter the gas phase.

When Li and van Heiningen added 12% CO to the inert carrier gas, after initially heating to 550°C, they suppressed the carbonate decomposition at temperatures below 800°C. The sodium loss observed in these experiments of about 10%, which occurred during the initial heating to 550°C, was not explained in their discussion. They also report that no significant sodium loss was observed during the gasification (1.5% loss was reported) of black liquor char under a 20% CO_2 , 10% CO atmosphere at 750°C. However, their results indicate an 18% sodium loss during the heat up period, during which the char was formed via a pyrolytic process from black liquor solids. The sodium content in their liquor and char was determined by atomic adsorption spectroscopy (AAS), after leaching of the chars in warm deionized water and dilution of the liquor.

Li and van Heiningen's explanation for the suppressing effect of CO_2 and CO is based on research in the field of alkali-carbonate catalysed coal gasification. This research

has shown that alkali carbonates heated in the presence of activated carbons are reduced to form surface metal complexes, and that these complexes can exist in several stages of reduction: an unreduced state in which carbonate decomposes onto carbon sites to produce surface oxides (carboxylic), a partially reduced state (phenolic), and a fully reduced adsorbed form (70,71,72,73). This literature also indicates that the alkali metal catalyst is only lost by desorption of metal vapour from the fully reduced form, and that the vapour pressure increases asymptotically as the ratio of alkali to carbon M/C increases (74,75). The maximum value of these vapour pressures corresponds to the equilibrium vapour pressure for the carbothermic reduction of the carbonates to metals (74) and not to that of the liquid metals. Since CO is a product of the final reduction step, its presence in the gas phase suppresses the formation of the fully reduced form. It is also reported that CO₂ can oxidize the phenolic alkali metal form to its carboxylic form, and the fully reduced form to the phenolic form, producing CO in both these steps, thus explaining the suppressing effect of CO₂. This process of oxidation and reduction of the alkali metal complexes is believed to be responsible for their catalytic effect in carbon gasification.

The rapid increase in alkali metal loss around temperatures of 800°C is attributed to the rapid kinetics of the reduction reactions and not to increased vapour pressures (74,75). Thus it is probable that at temperatures of 800°C and above, CO is unable to suppress Na₂CO₃ decomposition because the kinetics of decomposition become too rapid. Since both reduction reactions produce a net increase in the number of gaseous molecules, CO is produced, these reactions must also become more thermodynamically favoured at higher temperatures (66). This is evident by considering the change in Gibbs free energy, $\delta G = \delta H - T\delta S$, where δH is the heat of reaction, T the absolute temperature, and δS is the change in entropy. An increase in the number of gaseous molecules in a reaction will generally produce a large positive δS . At high temperatures $T\delta S$ becomes large decreasing the algebraic value of the Gibbs free energy change for the forward reaction, thus making it more favourable provided that the changes in δH with temperature are small. The thermodynamic favourableness of complex oxidation by CO₂ would not be expected to change as much with temperature since no net change in gaseous molecules occurs.

Volkov *et al* (76) report sodium loss data for the combustion of black liquor droplets. Fine glowing particles were observed to be ejected during swelling.

Recent studies in black liquor pyrolysis by Frederick *et al* (19,21) and Verrill and coworkers (22,23,27) have investigated the initial sodium loss during rapid heating of single droplets of black liquor. Frederick *et al* (19,21) studied sodium loss during fast pyrolysis in a 95% N₂ and 5% CO atmosphere. They found that at 800°C and below, sodium loss was approximately 15% after 20 seconds, and then remained constant for the

duration of the 60 second exposure. They also observed that most of this loss occurred during the first five seconds and thus was associated with devolatilization of the black liquor droplets. At 900°C and above, significant sodium loss continued after devolatilization. They concluded that the quantity of Na released during pyrolysis at 800°C was sufficient to account for the majority of the fume produced in a recovery boiler.

Verrill and coworkers (22,23,27) investigated aerosol formation by black liquor droplets during pyrolysis in 95% N₂ and 5% CO, combustion in 7.5% O₂ and 92.5% N₂, and gasification in 5% O₂ and 95%. During gasification at 500°C and pyrolysis at 600°C for 30 seconds they report char yields of 75% based on the liquor dry solids content, while during pyrolysis at 900°C they found the char yield to be 60-70%. Char from samples pyrolysed at 900°C for 30 seconds and then cooled in N₂ combusted spontaneously on exposure to air. They attribute this combustion to the rapid oxidation of highly reduced char, but do not suggest which char compounds are oxidized. Similarly to Frederick *et al*, they found that 10-30% of the sodium in kraft black liquor droplets is released during the swelling stage of pyrolysis. They also found that sodium loss continues after swelling of the droplets for temperatures above 800°C. At 600°C under 20% CO₂, 5% CO, 75% N₂ the sodium loss was not significantly different from that in the CO and N₂ atmosphere at 600°C. Increased gas velocity significantly decreased sodium loss for droplet experiments under 5% CO and 95% N₂ at 750°C (27). Although no explanation was suggested for this effect, improved mass transfer of CO to the droplet and improved suppression of Na loss seems a probable explanation. Large samples (70 mg of BLS) of both liquor and solids were also pyrolysed in boats under these conditions for 60 seconds, with no significant loss of sodium (27).

Stewart *et al* (77) pyrolysed organo-sodium compounds in a TGA at relatively low heating rates and report that no sodium loss occurred during devolatilization but that sodium loss occurred by reduction of sodium carbonate in the char by carbon above 800°C.

Verrill *et al* (22,23,27) suggest two possible mechanisms for sodium release during pyrolysis. The first is vaporization of low vapour pressure organic sodium salts, which they suggest is unlikely due to the absence of sodium loss during the pyrolysis of the large samples (27). The second, physical ejection of sodium containing material through bubbling and jetting during drying and pyrolysis respectively, appears to be supported the most strongly by their data, that of Volkov *et al* (76), and related literature. However, the reduction of initial sodium loss with increased flow rate under a partial CO atmosphere suggests that chemical interaction is also important.

The pyrophoric nature of char has been reported in both the coal pyrolysis and gasification literature (74) and the black liquor combustion literature (78,22,23). Most authors have attributed this pyrophoric nature to the presence of reduced sodium or potassium in the char. Tromp and Cordfunke (74) have shown that the reduced alkali metal-carbon complexes discussed above are converted to carbonates upon exposure to air.

Matsukata *et al* (79) report that hydrogen was formed when a model coal char previously heat treated to 850°C was soaked in a HCl solution. They proposed that K was formed by reduction of K_2CO_3 by carbon in the char and that it reacted with water to produce hydrogen by the reaction



Smelt Water Explosions: History and Mechanism

Since the time of their development to the present, kraft recovery boilers have been susceptible to explosions (3,4). While some of these explosions are due to problems common to power boilers, such as hydrocarbon fuel explosions, the majority have been and continue to be due to smelt-water interactions (3,4). Despite the considerable combined effort by insurers, users, and manufacturers to reduce the number of accidents, incidents of smelt-water explosions still persist at only moderately reduced frequency.

The mechanisms of liquid-liquid explosions, the broader class of phenomena to which smelt-water interactions belong, have been the subject of considerable study by many industries. The pulp and paper industry has sponsored several experimental studies with the objective of finding ways to prevent smelt-water explosions. Shick and Grace (2) have compiled a comprehensive review of these studies. Liquid-liquid explosions are also known as rapid phase transitions (RPTs), as the explosive force results from the rapid vaporization of one of the two liquids (80). The general requirement for an RPT is that a relatively cold volatile liquid come into contact with a relatively hot non-volatile liquid. Under many conditions the volatile liquid will simply boil away and there is no danger of an RPT. Shick and Grace have summarized the four steps believed necessary for an explosive interaction. They are:

- i) A quasi-stable intermixed initial configuration in which the hot and cold fluids are coarsely premixed (film boiling prevents direct contact)
- ii) A triggering event that collapses the vapour film in a localized region and permits direct liquid-liquid contact (alternatively a pressure pulse may trigger explosive release of stored superheat in those systems without a vapour film)
- iii) Escalation of interaction by rapid heat transfer, vaporization, and pressurization
... (further fragmentation increases heat transfer surface)

- iv) Propagation of a fully developed detonation wave through the coarsely premixed system.

If the film boiling in step i). is very stable no explosion will occur and the cold liquid will gradually vaporize. Events which stabilize or destabilize the film boiling can dramatically change the probability of an explosion (2,80).

The literature clearly shows that chemical reaction is not a required step to produce the violent interactions which have been observed (2). However, chemical reactions may release additional heat and explosive gases making the explosion more severe or, non-condensable gases produced may have a stabilizing effect. Shick and Grace (2) report that many investigators found that smelt compositions which produced substantial amounts of CO_2 when in contact with water were less explosive than those smelts which produced little or no CO_2 when in contact with water. The evolution of CO_2 at the interface appears to stabilize film boiling suppressing the triggering event. It has also been suggested that evolution of gas may only temporarily extend the quasi-stable stage intensifying the premixing and leading to a more violent explosion (2). Therefore, the production of a gas at the interface is likely to affect the liquid-liquid interaction in some manner.

It is possible that the presence of a fully reduced sodium-carbon complex in the char bed of a recovery boiler could influence the occurrence or severity of smelt-water explosions, since hydrogen gas would be produced upon contact of water with the char (18), via a reaction analogous to [6.1] above. The hydrogen produced might effect the occurrence of a smelt water explosion if an explosive mixture was produced and subsequently detonated, thus triggering a smelt-water interaction, or effect the severity by increasing the magnitude of an explosion.

Thus, in addition to providing an improved understanding of the role of Na during black liquor combustion and gasification processes, the possible role of elemental sodium in smelt water explosions provides another reason for exploring its formation in kraft black liquor char.

Experimental

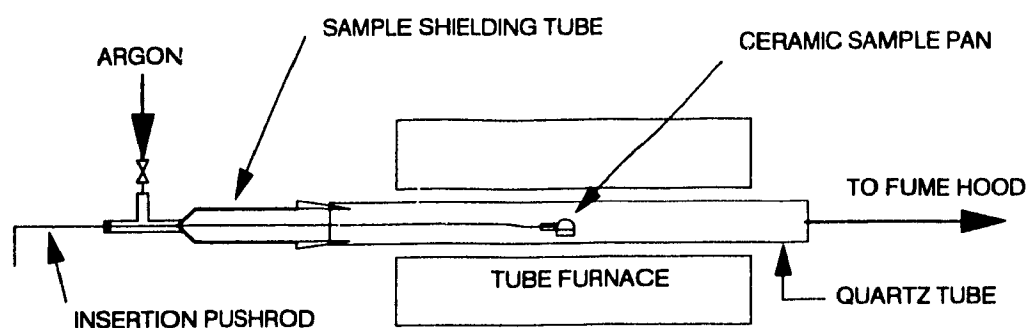
Two types of experiments are presented in this chapter. Firstly, the kraft black liquor (KBL) pyrolysis experiments of Chapter 5 are discussed in terms of the behaviour of sodium, and secondly, experiments are discussed which were specifically performed to confirm the presence and determine the quantity of fully reduced sodium in black liquor char.

Experimental Procedures

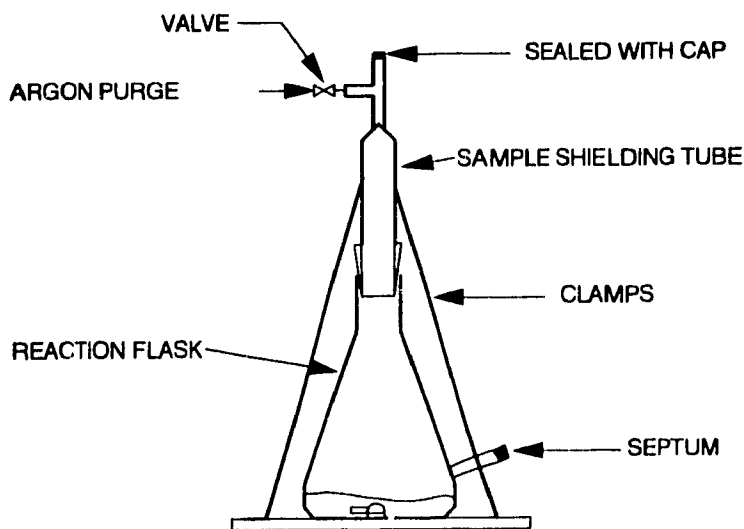
The basic experimental procedures for the first type of experiments have been presented in Chapters 4 and 5. Several of these experiments were performed to test the hypothesis that a reduced form of sodium is the cause of the pyrophoric nature of some black liquor chars. These experiments were carried out after it was discovered that chars formed during pyrolysis for 60 seconds at 900°C under He, and under 95% He and 5% CO, self-ignited upon contact with air. They included four experiments performed at 800°C for extended pyrolysis times of 150 seconds, since chars from earlier 60 second pyrolysis runs at this temperature were found in to be non-pyrophoric. Two of these experiments were performed with a 90% He and 10% CO atmosphere and two under pure helium. One experiment at each condition was used to observe whether the resulting char was pyrophoric, while the other was used to determine the reduction efficiency of the char. The reduction efficiency was determined to test whether the presence of sodium sulphide, and its subsequent oxidation, contributes to the pyrophoric nature of some black liquor chars. The sample treatment after pyrolysis differed from that presented in Chapters 4 and 5. First the samples were retracted into the sample cooler (see Figure 4.2), and then, with the helium purge maintained, the furnace was cooled and the quartz tube removed. The air piston was then used to rapidly move the sample from the helium environment in the sample cooler to either open air or into a small beaker of deoxygenated, deionized water. In the later case air exposure was for less than one tenth of a second. The air exposure experiments were performed to test the char for pyrophoric behaviour. Ultrasonic agitation was used to disperse the char in the water, and dissolve the soluble salts, in the beaker experiments. The resulting solution was immediately analysed for HS^- and SO_4^{2-} by ion chromatography using the methods described in Chapter 5.

The procedures for the second type experiments, which were performed with the objective of determining the presence and quantity of reduced sodium in black liquor char, are as follows. Black liquor solids (BLS) were prepared by first drying the liquor (see Tables 5.2 and 5.3 for liquor composition) at 105-110°C to constant weight, and then grinding the solids with a mortar and pestle. The ground solids were redried and then stored in a dessicator. Figure 6.1 shows schematically the pyrolysis tube furnace and sodium detection apparatus used. The first step was to measure about 10-50 mg of BLS into a ceramic pan, connect the pan to the push rod, and withdraw the sample into the shielding tube. Four sample pans of slightly different geometries were used. All were about 10 mm in diameter and 2 to 3 mm deep. They differed in that one was very thin walled alumina, another thin walled porcelain, and two were about 1 mm thick alumina.

The sample weighing was performed quickly to minimize the error caused by the rapid weight gain of the very hygroscopic BLS. The sample shielding tube was then connected to the tube furnace as shown in Figure 6.1. A minimum argon purge rate of 1.0 slm (litres per minute at STP, 0°C and 1 atm) was used. At this purge rate the flow in the shielding tube was sufficiently high to prevent back diffusion, as demonstrated in Appendix A. After a minimum of 3 minutes, the quartz tube was free of air, and the sample was quickly moved using the push rod from the shielding tube to the centre of the preheated furnace. The furnace temperature was maintained by a PID controller. The back pressure of the exhaust line provided a slight positive pressure which prevented air



(a) Pyrolysis tube furnace and sample shielding tube



(b) Char water reaction flask and sealing arrangement

Figure 6.1 Sodium detection apparatus

infiltration. The push rod passed through the centre of two compressed septa, providing a gland type seal between the shielding apparatus and the rod. After the desired pyrolysis time, the resulting char was carefully withdrawn into the shielding tube. Contact between the pan and the quartz tube must be prevented during insertion and retraction of the sample, since alkali silicate which forms by reaction between the quartz and the Na sodium vapour will contaminate the sample. When the char was visible through the quartz tube during this process, observations were made, and occasionally photographs were taken.

After retraction of the sample into the shielding tube, the gas purge rate was increased to 3.0 slm and the shielding tube disconnected from the tube furnace. It was then connected to the flask shown in Figure 6.1(b) with the flask horizontal and the septum cap off. The flask (nominal volume of 50 ml) was purged for a minimum of three minutes to ensure complete removal of air while the clamps were secured. The flask was then placed in a vertical position and the septum cap was secured in place. The sample pan was then dropped to the bottom of the flask by removing the push rod, allowing the purge gas to exit out through the top. Then the push rod opening was capped and the flask apparatus was leak tested to 10 psig using "Snoop", and subsequently depressurized through the valve via a long tube to avoid back diffusion of air into the flask.

Five ml of deoxygenated and deionized water was then injected into the flask through the septum with a syringe. Next the apparatus was placed in a warm ultrasonic bath to disperse the char in the water and to enhance the diffusion of any produced gases into the gas phase. It was found that with ultrasonic agitation the equilibrium H_2 concentration in the gas phase was reached after about after 90 minutes, while without ultrasonic agitation the concentration continued to rise many hours after water was injected. After 90 minutes air leakage into the apparatus was insignificant as determined by GC analysis. This implies that any leakage of hydrogen out of the reaction flask was also small 90 minutes after water injection. However, after several hours a significant air peak was present during GC analysis and the solution sometimes turned blue-green, indicating possible oxidation of sulphide to polysulphide (81). Figure 6.2(a) depicts the substantial increase in rate of H_2 concentration rise when ultrasonic agitation was used opposed to when it was not used.

Following ultrasonic agitation the hydrogen concentration in the gas space of the flask was determined by GC analysis with a Fischer Gas Partitioner using thermal conductivity detection. The separation was made using a 15'-0" x 1/8" Porapak QS column at 50°C with a high purity argon carrier gas flow rate of 3-4 cc/min. A short 1'-0" x 1/8" 5A molecular sieve precolumn was used to remove water vapour. The GC was

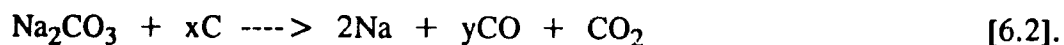
routinely calibrated using 50 and 100 ppmv standards of H₂ in argon. Standards in the order of 1000 ppmv H₂ in argon were used for calibration at higher concentrations. Argon was chosen as the carrier gas since the large difference in thermal conductivity between argon and hydrogen provides good detection sensitivity, and also since it allows air to be separated. Figure 6.2(b) shows a typical chromatogram with the retention times shown in minutes. The first peak is that due to hydrogen and the second is that due to air.

The methods used for the analysis of total sodium in the BLS and char are presented in Chapter 5.

Results and Discussion

Behaviour of Sodium During Single Droplet Fast Pyrolysis

The sodium yield of the char and the normalized CO₃²⁻ and total sulphur yields of the char for many of the experiments discussed in Chapter 5 are presented in Figures 6.3(a) and 6.3(b). The abscissa points CO-800 and CO2-900 correspond respectively to experiments performed at 800°C in 10% CO for 150 seconds and at 900°C in 15% CO₂ for the times noted. All other experiments were performed in pure helium atmospheres for 60 seconds. In agreement with the literature (18,19,21,22,23), the results in Figure 6.3(a) show that 10-20% of the initial sodium is lost during pyrolysis in He at temperatures below or equal to 700°C, while at 800°C and above sodium loss increases dramatically. Also as expected (18), the addition of 10% CO at 800°C greatly suppresses the loss of sodium to about 15% in 150 seconds compared to a loss of about 60% in only 60 seconds without the presence of CO. As discussed earlier in this chapter, the sodium loss during fast pyrolysis of KBL at temperatures of 700°C or lower appears to be primarily due to physical ejection during devolatilization, while the additional sodium loss at higher temperatures is due to decomposition of Na₂CO₃ as a result of its reduction by carbon according to the overall reaction (18)



At 800°C the addition of 10% CO reduces the rate of the above reaction to 5% of that without CO (18), so that for fast pyrolysis under these conditions, the sodium loss of the char is due primarily to processes occurring during devolatilization (see Figure 6.3(a)). When the quartz tube of the furnace was new and transparent, it was observed on occasion that debris from a pyrolysed drop was stuck to the tube. This supports that physical ejection contributes to the loss of sodium during devolatilization. The reported influence of the carrier gas flow rate on sodium loss in the presence of 5% CO at 750°C (27) indicates that CO is also able to lower sodium loss during devolatilization and that mass transfer of CO to the droplet is important.

The interesting result in Figure 6.3(a) is that in a CO₂ gasification atmosphere at 900°C, the sodium loss was completely suppressed. The four experiments at this condition were of time durations 15, 20, 30, and 60 seconds. During the 60 second run

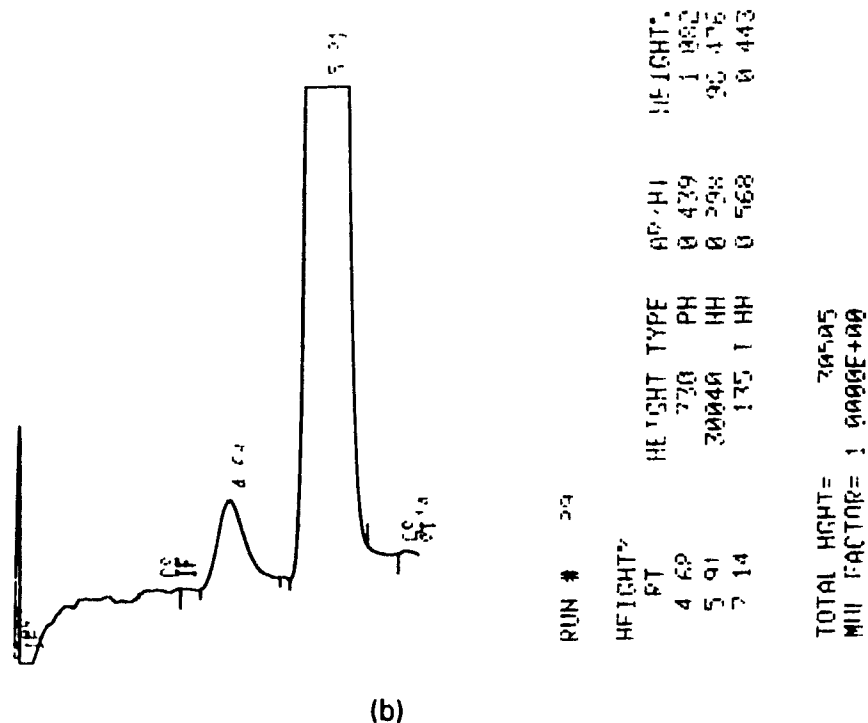
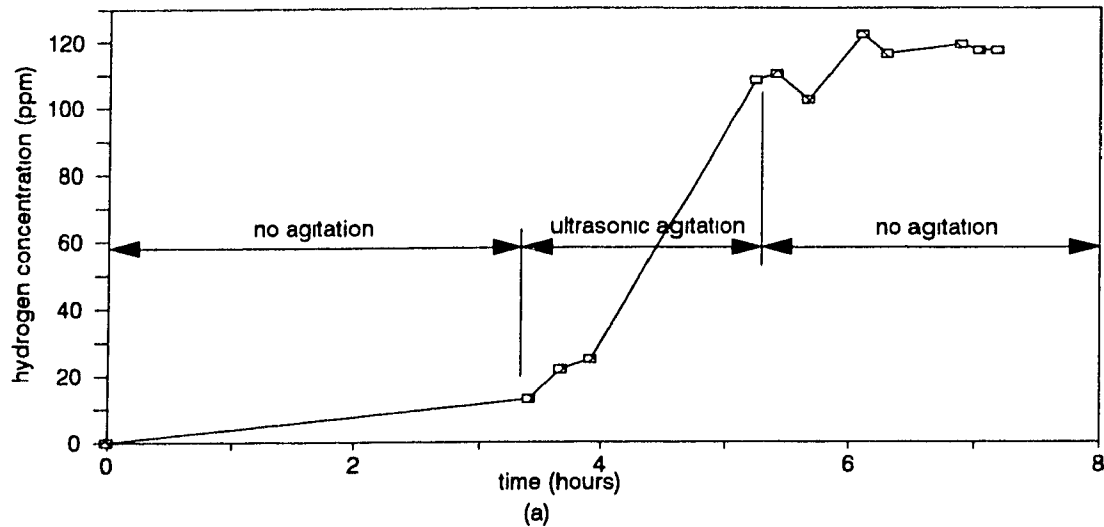
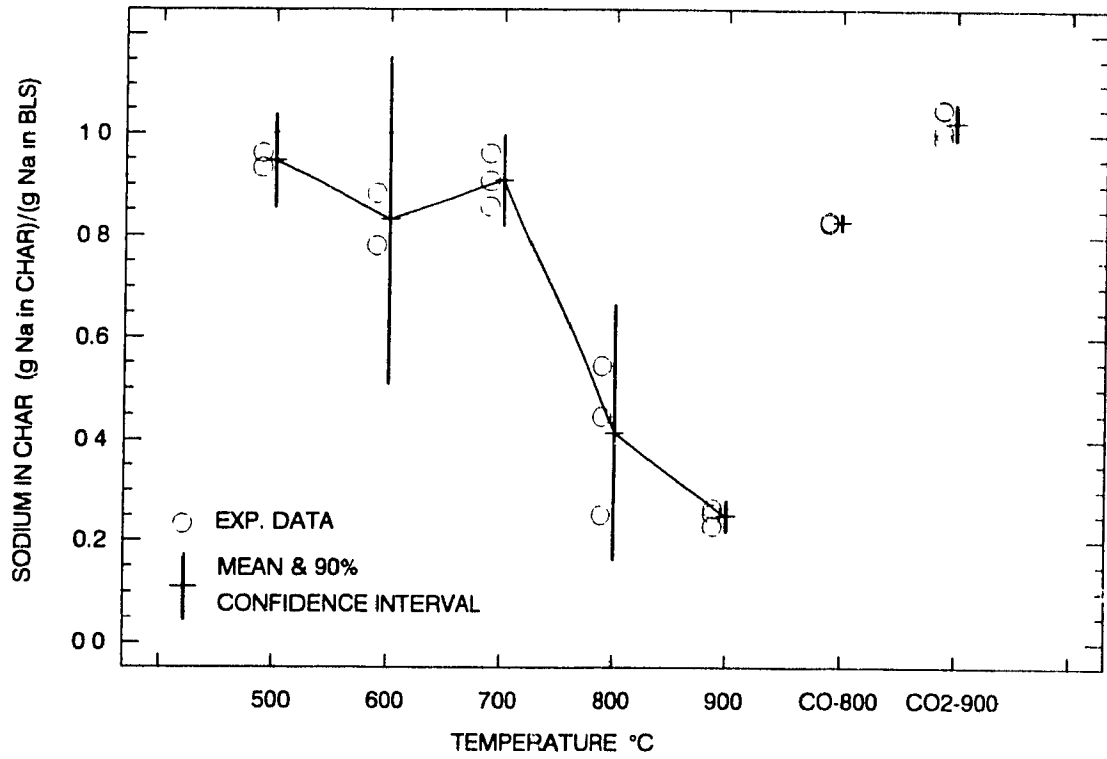
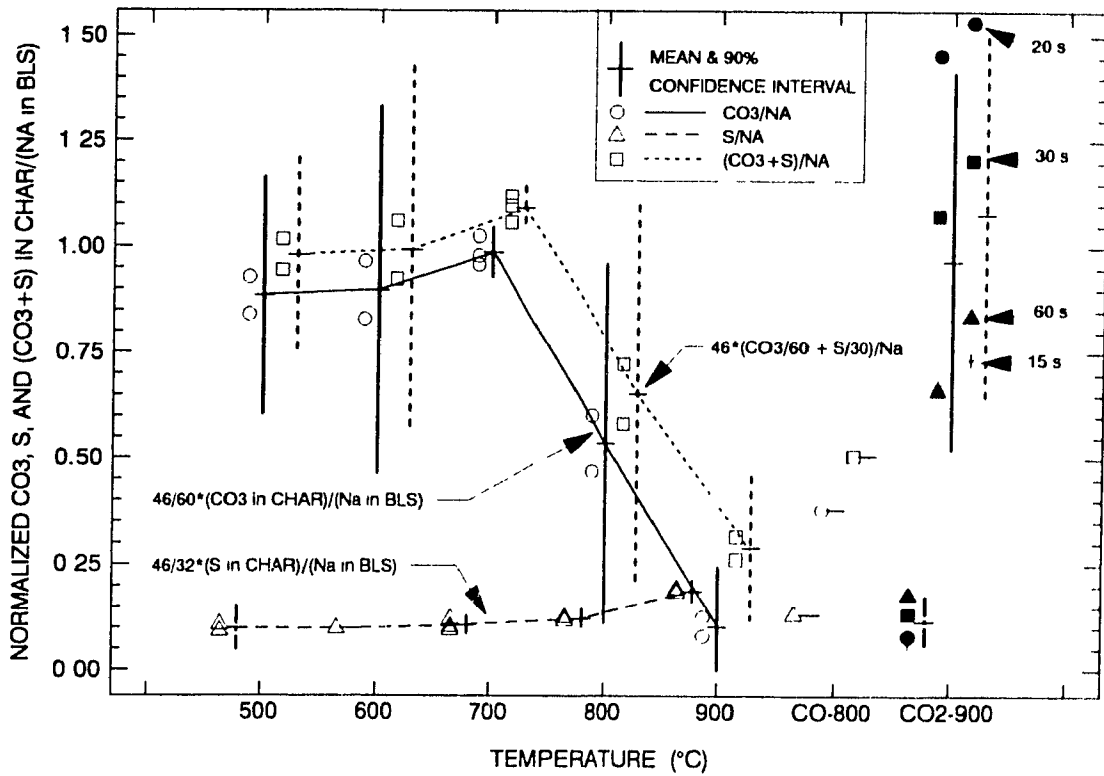


Figure 6.2 (a) Effect of ultrasonic agitation on hydrogen diffusion to the gas phase
(b) Typical gas chromatogram for hydrogen analysis

complete carbon gasification occurred, while after 20 and 30 seconds partial gasification had occurred, and after 15 seconds very little or no gasification had occurred. These



(a)



(b)

Figure 6.3 Char yields for fast pyrolysis experiments. Pure He unless noted.
 (a) Sodium yield (b) CO₃ and total S yields as fractions of sodium in BLS required to form Na₂CO₃ and Na₂SO_x (x = 0, 3, or 4) salts

results indicate that in addition to the known suppression of reaction [6.2] by the presence of CO₂ (70,18), at 900°C the sodium loss associated with devolatilization is eliminated when pyrolysis occurs in a gasifying atmosphere containing 15% CO₂ and 85% He.

The absence of sodium loss during fast pyrolysis of KBL under 15% CO₂ at 900°C could be interpreted as grounds for rejecting physical transport (ejection) as the mechanism of sodium loss during devolatilization. However, this would be presuming that the behaviour of black liquor droplets is the same during devolatilization under gasifying and non-gasifying conditions and experimental evidence suggests that this is not true. Firstly, Frederick *et al* (25) report much less swelling of black liquor droplets at 800°C under gasification conditions, as compared to inert conditions, but do not suggest an explanation. Secondly, at 600°C, a temperature too low for gasification to occur, Verrill *et al* (27) report no influence of 20% CO₂ addition on Na loss during pyrolysis, as compared to 5% CO in nitrogen. Thus, one explanation of the suppressing effect of CO₂ at 900°C is that under gasification conditions little or no jetting occurs which can transport sodium out of the droplet. Under CO₂ gasification conditions droplet heating is slightly more moderate due to the endothermic gasification reaction (see Figure 5.26). A lower heating rate combined with the more open surface structure produced by gasification could lead to lower velocity gas jets incapable of transporting Na containing particles.

An alternative to the physical transport mechanism for sodium loss during pyrolysis is the vaporization of sodium as elemental sodium (18), sodium hydroxide, or a low molecular weight organo-sodium compound (27). Based on this mechanism, a possible explanation for the elimination of the sodium loss during devolatilization is that CO₂ reacts very rapidly with vaporized compounds to form Na₂CO₃ which is then trapped in the char. Further experimental evidence would be required to verify either of the above mechanisms.

Figure 6.3(b) shows the char yields of CO₃²⁻, total sulphur, and total sulfur plus CO₃²⁻. Carbonate is expressed as the sodium required to form Na₂CO₃ divided by the sodium in the black liquor solids. Similarly total sulphur is expressed as the sodium required to form bisodium salts Na₂SO_x (x = 0, 3 or 4) divided by the sodium in the black liquor solids. The lines, data points, and error bars for each of total sulphur and sulphur plus carbonate are respectively shifted left and right with respect to the temperature scale for greater clarity. Each of the four experiments performed under CO₂ at 900°C is given a separate symbol as indicated on the graph. The reduction in carbonate yield follows the trend of the reduction in sodium yield and is in agreement with Li and van Heiningen's mechanism of sodium loss as a result of the reduction of Na₂CO₃ by carbon. The sum of the normalized carbonate and sulphur yields is very close to one at

500 and 600°C, but rises to 1.1 at 700°C. Considering that this ratio is calculated on the Na in the black liquor and not that in the char, the maximum value of this ratio should be about 0.9, since sodium loss is about 10% at 700°C and below under pure helium. Thus, ratios greater than 0.9 indicate that not all of the CO₃²⁻ groups and sulphur atoms are present as Na₂CO₃ or Na₂SO_x respectively. This could be due to the presence of chemisorbed oxygen groups or CO₂ in the amorphous char which are not associated with any sodium and which form carbonate ions on contact with water. At 800°C and above in a pure helium atmosphere the normalized carbonate yield decreases rapidly due the onset of rapid kinetics for the reduction of carbonate by carbon (18,75), while the normalized sulphur yield increases moderately. The addition of 10% CO at 800°C has no effect on the normalized sulphur yield although it decreases the carbonate yield moderately. This could be due to the partial reduction by CO of the Na₂CO₃-carbon complexes discussed earlier in this chapter.

Also shown in Figure 6.3(b) is that the addition of 20% CO₂ at 900°C greatly increases the carbonate yield while having only a small effect on the sulphur yield, and that carbonate yield is a strong function of exposure time. A possible explanation for the observed effect of time follows, although there are not enough data to confirm its validity. At early times (15 s) when devolatilization and sulphate reduction are not yet complete as shown in Figures 5.26 and 5.31, the carbonate ratio is low due to reduction of carbonate during these processes. After 20 seconds the carbonate yield is very high since gasification has begun and the large internal surface area of the porous char is now highly oxidized by the CO₂. As further gasification occurs (30 s) the quantity of carbon available to bind oxygen is greatly reduced, and thus the carbonate yield is lower. After 60 seconds virtually complete gasification has occurred and the carbonate is now only associated with sodium. It is unclear why the sum of the normalized carbonate and sulphur yields is not equal to one for the run with a duration of 60 seconds, since one would expect all the sodium in the resulting smelt to be present as Na₂CO₃, Na₂S, and Na₂SO₄. A possible explanation is the presence of Na₂S₂O₃ in the char, which has been reported (7), resulting from reaction during handling, possibly via



For the experiments in 95% He/5% CO and in pure He at 900°C the chars were pyrophoric even after thorough cooling under helium. The chars did not ignite instantaneously, but only after an induction period of 2-3 seconds. To test whether the pyrophoric nature of some black liquor chars is due to general oxidation of the char surface, which was suggested as a possible explanation by Verrill and Nichols (22,23), or whether it is due to the oxidation of a specific compound, four experiments were

performed at 800°C. In the first experiment black liquor was pyrolysed in 90% He and 10% CO for 150 seconds (for details see experimental procedures). The resulting char did not self ignite on contact with air. The second experiment was a duplicate of the first except that the char was immediately immersed in water to prevent sulphide oxidation. The sulphur reduction efficiency was found to be 97.4%. The first two experiments were repeated in a pyrolysis atmosphere of pure helium. The resulting char self ignited upon exposure to air in the first run and the char from the second run showed a reduction efficiency of 85.3%. Thus, the char produced under CO had a very high reduction efficiency but was not pyrophoric, while the char pyrolysed under pure He had a lower reduction efficiency but was pyrophoric. This indicates that the oxidation of sulphide is not responsible for the auto-ignition of some chars. As will be shown below, the pyrophoric nature of some chars is due to the presence of reduced sodium-carbon complexes in the char which are oxidized upon exposure to air.

Presence of Reduced Sodium in Black Liquor Chars

The second type of experiments used to produce black liquor char are described in the Experimental Procedures. Table 6.2 below summarizes the experimental conditions for this group of experiments. The char formed during most runs was nicely swollen and closely resembled the examples presented in Chapter 4. The physical characteristics of the char differed substantially in some experiments even though they were performed under seemingly identical conditions. In one or two experiments a smelt globule with a small amount of char was all that remained. In two others the char was as shown in Plate 6.1 where small smelt globules had migrated to the surface of the char particle, indicating the very mobile nature of the smelt in the char. The fact that these globules formed on both the upstream and downstream sides of the char mass indicates capillary action, rather than drag from the purge gas, causes this phenomena. The disappearance of carbon in some instances could have been caused by separation of the smelt and the char and then the latter being blown away by the purge gas.

For this second group of experiments, the reduced sodium content of the pyrolysed chars was determined by measuring the hydrogen content of the gas phase in the char-water reaction flask (see Figure 6.1) The amount of reduced sodium was calculated by assuming that all the hydrogen detected was formed by reaction [6.4] below.

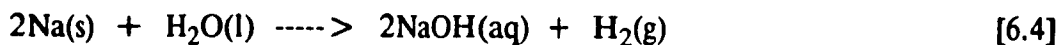


Figure 6.4 shows the amount of reduced sodium formed as a fraction of the original sodium in the BLS and sodium remaining in the char as a function of sample size for the experiments listed in Table 6.2. Since the sodium content of the char was not determined

Table 6.1
Reduced Sodium Formation Experiments

Exp. (mg)	BLS	Time (min)	Sample Pan
SEPT13	32.5	15.0	1
SEPT14	33.5	15.0	1
SEPT15	33.7	15.0	3
SEPT24	41.4	10.0	3
SEPT25	34.0	10.0	2
CW1	45.1	20.0	3
CW3	25.6	10.0	3
CW4	28.6	10.0	1
CW5	28.7	30.0	3
CW7	31.2	10.0	1
CW8	31.5	10.0	3
CW9	21.3	10.0	1
CW10	21.4	10.0	3
CW11	21.4	10.0	1
CW12	21.4	10.0	1
CW13	10.6	10.0	2
CW14	10.9	10.0	4
CW15	41.3	10.0	4

Pyrolysis at 800°C under pure argon.

Sample pan index 1 thin walled alumina pan
 2 porcelain pan
 3 thick walled alumina pan
 4 thick walled alumina pan - vertical tube furnace

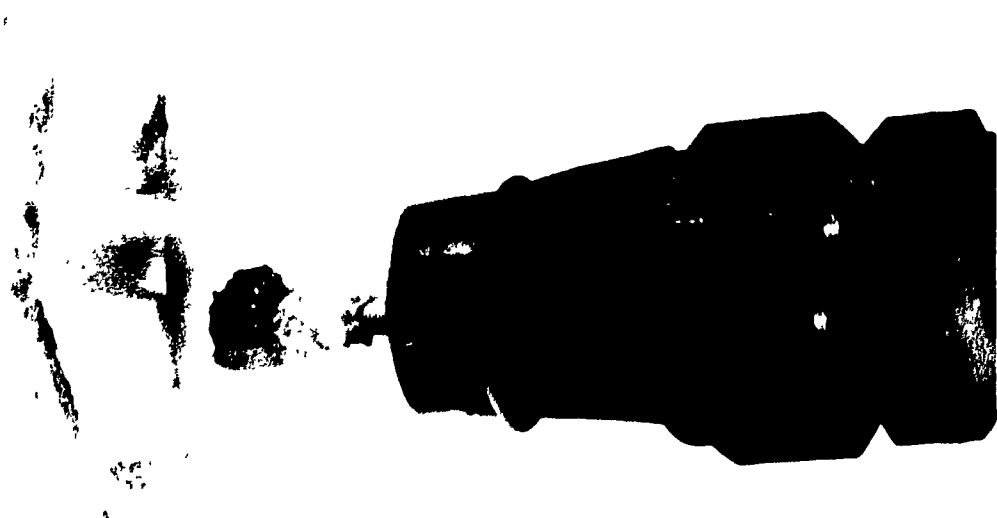


Plate 6.1 Char after 10 minutes of pyrolysis at 800°C in argon. Smelt nodules which have migrated to the surface are evident

for every experiment, there are fewer data points for the ratio of reduced sodium to char than reduced sodium to BLS.

Although the results in Figure 6.4 show much scatter, they do confirm that hydrogen is produced when chars pyrolysed under pure helium are contacted with water in the absence of oxygen. Blank trials, i.e. with an empty sample pan, did not produce hydrogen, indicating the hydrogen is produced by a reaction between char and water. Since these chars also auto ignite, it seems conclusive that reduced alkali metal is responsible for the formation of hydrogen and the pyrophoric behaviour.

Comparison of the reduced sodium yields plotted as a fraction of original sodium and as a fraction of sodium in the char indicate that the latter value is moderately higher, and that neither show a dependence on sample size. There also does not appear to be any effect of the type of sample pan, other than that both experiments performed with the tube furnace oriented vertically show lower reduced sodium yields than average. In comparison to the horizontal position, this difference could be due to more effective retention of CO produced by reduction of sulphate in the early stages of pyrolysis and the subsequent reduction of carbonate. Such CO will act to suppress further carbonate decomposition (18) and thus reduced sodium formation.

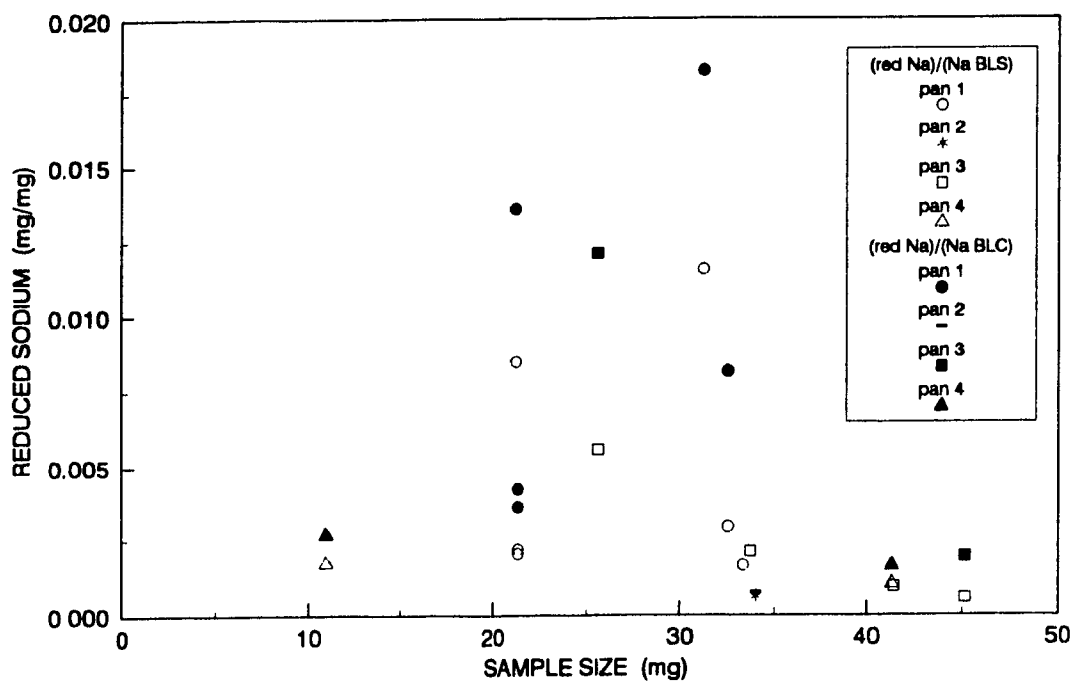


Figure 6.4 Reduced sodium - calculated from measured hydrogen

Figure 6.5 is a plot of the ratio of the reduced sodium to the sodium in the char versus total sodium yield and does not indicate an obvious relationship between them. The reduced sodium yield as a function of pyrolysis time is shown in Figure 6.6. Again no definite pattern is present, but it appears that reduced sodium yield is relatively constant with time. This is consistent with the mechanism of catalyst loss in alkali catalysed carbon gasification. In this mechanism alkali is lost by vaporization when it is present in a reduced form. The vapour pressure of this reduced form is a weak function of the alkali to carbon ratio (74). Thus, it appears that there is an equilibrium amount of reduced sodium present in the char and this quantity is a weak function of the Na/C ratio.

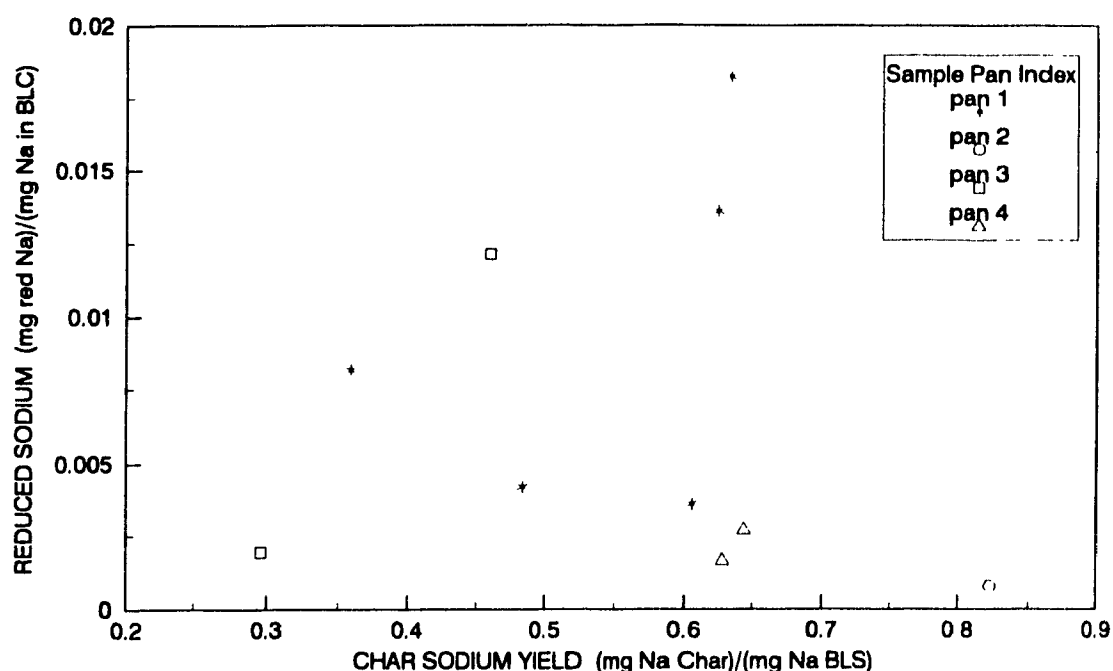


Figure 6.5 Reduced sodium as a function of sodium yield during pyrolysis

The pyrophoric nature of the char produced at 900°C with 5% CO indicates that at high temperatures ($\geq 900^\circ\text{C}$) reduced sodium is present even with CO in the gas phase. The complete suppression of sodium loss by the presence of CO₂ at 900°C suggests that reduced sodium is not formed under these conditions. The atmosphere inside a recovery furnace char bed is likely rich in CO from the reduction of sulphate by carbon and lean in CO₂ as a result of carbon gasification. Therefore, based on the results presented above, it is possible that the percentage of sodium in the reduced form in the char bed is of the order of one percent.

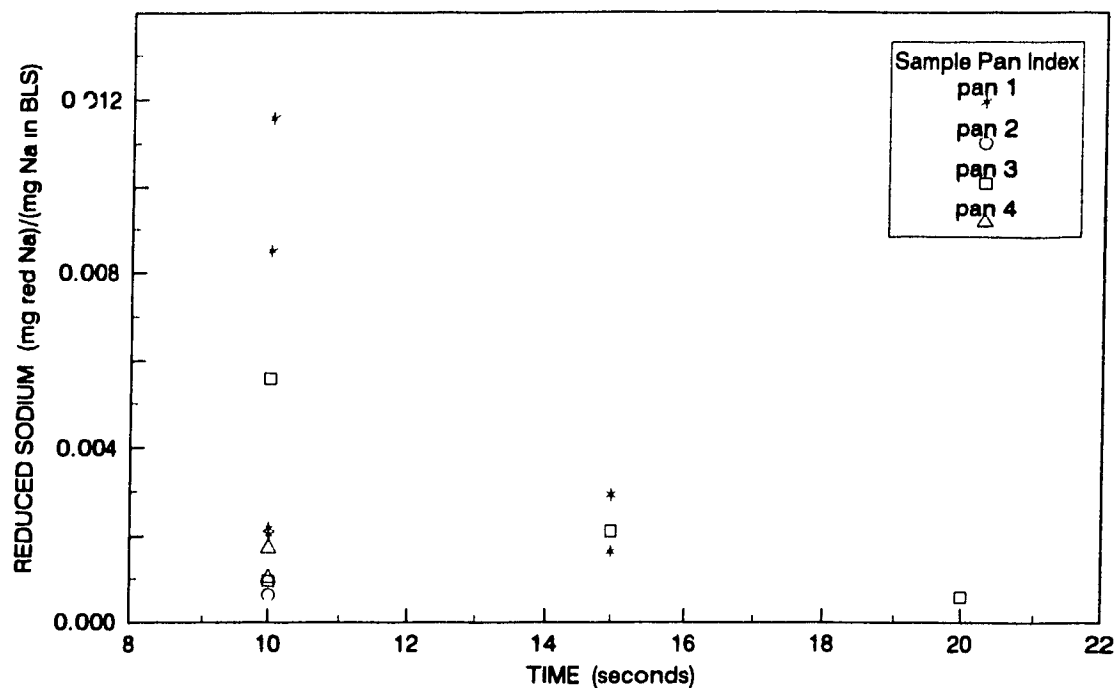


Figure 6.6 Reduced sodium as a function of pyrolysis time

An 800 TPD pulp mill, firing approximately 1.1 million kg of BLS per day (1) has a floor area of approximately 75 m². Assuming that the top 30 cm of the char bed is the so-called "active layer" with a char density of 375 kg/m³ (1), and is formed at a yield of 70% from BLS containing 20% sodium, it can be calculated that approximately 2400 kg of sodium will be present in this active layer. Assuming one percent of this sodium is in the reduced form, it follows that 24 kg of reduced sodium is present in the active char layer. Upon contact with water about 1.0 kg of hydrogen would be produced via [6.4]. At 900°C this quantity is equivalent to about 50 m³ of pure hydrogen. Assuming a mixture at the lower explosive limit of hydrogen in air of 4% (82), this is equivalent to a volume of about 1200 m³. Thus, a height of about 16 metres above the char bed could be filled with an explosive hydrogen-air mixture, which upon detonation could trigger a smelt water explosion.

Conclusions

The following conclusions can be drawn from the results and discussions presented in this chapter.

- i) The pyrophoric behaviour exhibited by some black liquor pyrolysis chars can be explained by the presence of reduced sodium in the char.
- ii) Oxidation of sulphide in reduced black liquor chars is not responsible for the pyrophoric nature of these chars.
- iii) The loss of sodium during combined pyrolysis and gasification of black liquor at 900°C is completely suppressed in an atmosphere containing 15% CO₂.
- iv) As in slow pyrolysis, sodium loss during fast pyrolysis of kraft black liquor in an inert atmosphere at 800°C and above is the result of decomposition of the complexes which Na₂CO₃ forms with the carbon matrix. At 800°C and below, the presence of 10% CO suppresses this decomposition during fast pyrolysis.
- v) Reduced sodium in chars reacts with water to produce hydrogen. The amount of reduced sodium present in a char bed might be sufficient to produce an explosive hydrogen-air mixture which upon detonation could trigger a smelt water explosion.
- vi) The quantity of reduced sodium present in black liquor chars is relatively constant with pyrolysis time once the process of sodium loss through reduced sodium desorption has begun.

CHAPTER 7 GENERAL CONCLUSIONS

The black liquor produced by the kraft pulping process is presently used to fuel chemical recovery boilers, Thomlinson furnaces, which, in addition to producing steam for electricity production and process use, effectively recover inorganic chemicals as molten salts for reuse in the pulping process. The processes which occur in these furnaces have only recently begun to be understood. The high cost of recovery boilers, the hazard created by the presence of molten salts, and the need for incremental capacity have fueled much fundamental research of black liquor thermal conversion processes with the objective of increased capacity, safer operation, and alternative, safer and less expensive, processes.

This thesis is concerned with pyrolysis, the first stage of black liquor thermal conversion processes and in particular in developing experimental methods to measure yields and rates of formation of pyrolysis products under well established gas atmospheres. A tube furnace with automated droplet introduction and retraction, coupled with a quadrupole mass spectrometer to perform continuous gas analysis, was the main experimental equipment used to study pyrolysis. Additional experiments investigating the presence of adsorbed elemental sodium in black liquor char were performed in a horizontal tube furnace, with a special apparatus and procedure used to detect the presence of elemental sodium. Unoxidized mill liquor in the "as fired" state at 70% solids was used. In addition to the use of mass spectrometry, gas chromatography and infrared gas analysis were used for gas analysis. Solids analysis utilized atomic adsorption spectrometry for alkali metals, ion chromatography for anions, and gasification for fixed carbon. Digital signal processing techniques were utilized to reduce noise in droplet temperature data and to correct the gas formation rate data for the time lag and dispersion of the apparatus.

Contributions to Knowledge

- 1) Thermodynamic calculations are reported for combined pyrolysis and gasification of kraft black liquor, in which the fluidizing gas is constituted of the pyrolysis products. Results are presented for dry solids and liquor. The thermodynamic effect of inert gas dilution is also determined.
- 2) Methods are developed to study single droplet black liquor pyrolysis using a quadrupole mass spectrometer coupled to a tube furnace. Also developed are procedures for establishing carbon and sulphur mass balances for this system.
- 3) Volatile production rate data are presented for black liquor droplet pyrolysis for all important sulphur gases and fixed gases, with the exception of H_2 . These data

- reveal an initial devolatilization phase which occurs during droplet drying.
- 4) Yields of important sulphur gases, fixed gases and hydrocarbons, condensable tars, and char are presented for black liquor droplet pyrolysis in pure helium over the range of 500 to 900°C. Sulphur in tar yields are also presented, as are sodium, fixed carbon, and carbonate yields in droplet pyrolysis char.
 - 5) Yields of important sulphur gases, important fixed gases, and chars are reported for droplet pyrolysis under 10% CO at 800°C and under 15% CO₂ at 900°C. These data indicate that CO and CO₂ may act as radical scavengers and account for the changes in yield of hydrocarbon species.
 - 6) Droplet measurements in pure helium at 800 and 900°C, in 10% CO at 800°C, and in 15% CO₂ at 900°C, show a temperature decrease after initial devolatilization due to the rapid endothermic reduction of sulphate to sulphide by carbon.
 - 7) Fast Fourier Transform (FFT) deconvolution of gas production data has been shown to be an effective method of correcting for the time lag and dispersion effects of a single droplet tube furnace reactor coupled to a mass spectrometer.
 - 8) Carbon disulphide, CS₂, has been identified as a production of black liquor droplet pyrolysis above 700°C and appears to be formed via reaction of H₂S with methane.
 - 9) Sodium is present in a fully reduced state, as adsorbed elemental sodium, in black liquor char produced by fast pyrolysis. This reduced sodium is responsible for the pyrophoric nature of some chars and is formed at 800°C and above under pure helium and at 900°C under partial CO atmospheres. Ten percent CO at 800°C prevents significant formation of fully reduced sodium. The amount of adsorbed elemental sodium present reaches an equilibrium surface concentration, and does not increase with time as sodium loss occurs.
 - 10) Fully reduced sodium in black liquor char reacts with water to produce hydrogen. Sufficient hydrogen could be generated in a recovery boiler to form an explosive mixture above the char bed. Detonation of such an explosive mixture could trigger a smelt-water explosion.
 - 11) Sodium loss from single droplets of kraft black liquor during pyrolysis at 900°C is completely suppressed by the presence of 15% CO₂.

Suggestions for Further Work

The following items are suggested as possible areas for future study in the fields of black liquor pyrolysis and combined pyrolysis and gasification.

- 1) Perform a rigorous kinetic analysis of data from black liquor droplet pyrolysis.
- 2) Develop new methods of determining droplet pyrolysis gas yields, such as GC analysis, and methods to determine hydrogen yields.
- 3) Perform black liquor droplet pyrolysis under nitrogen or argon so that kinetic hydrogen data can be obtained.
- 4) Perform black liquor droplet pyrolysis with the addition of CO; CO and CO₂; and CO, CO₂ and H₂O at furnace temperatures of 600 to 900°C, with the objective of evaluating the influence of reducing and gasification atmospheres on pyrolysis yields and kinetics.
- 5) Determine the influence of solids concentration and liquor type on yields for black liquor droplet pyrolysis.
- 6) Develop mathematical or empirical models for droplet pyrolysis based on the data gathered from 1), 2), 3), 4), and 5) above , using FFT deconvolution methods to correct experimental data for the system responses of each gas produced.
- 7) Perform fast pyrolysis experiments with the objective of establishing a sodium balance, so that the fate of sodium during pyrolysis can be determined.

References

- 1) T.N. Adams and J. Frederick, **Kraft Recovery Boiler Physical and Chemical Processes**, American Institute of Paper, New York, 1988.
- 2) P.E. Shick and T.M. Grace, **Review of Smelt-Water Explosions: A Special Report**, Project 3473-2, IPC, Appleton, 1982.
- 3) T.M. Grace, **Tappi**, Vol. 69 (1986) No. 6: 167-168.
- 4) T.M. Grace, **Proc. of 1992 Int. Chem. Rec. Conf.**, Tappi Press, Atlanta, 1992.
- 5) J.A. Fallavollita, M.M. Avedesjian, and A.S. Mujumdar, **Can. J. Chem. Eng.**, Vol. 65(1987): 812-817.
- 6) M.M. Avedesjian, G.J. Kubes, and A.R.P. van Heiningen, **IEA Proposal**, McGill University, Montreal, January 1990.
- 7) A.R.P. van Heiningen, J. Li, and J.A. Fallavollita, **Canadian Patent Application #583,409**, Nov. 17, 1988.
- 8) W.J. Frederick, R. Backman, and M. Hupa, **Proc. of 1992 Int. Chem. Rec. Conf.**, Tappi Press, Atlanta, 1992:617-625.
- 9) F.D. Harper, **Ph.D. Thesis**, IPC, Appleton, 1989.
- 10) J. Li, **M.Eng. Thesis**, McGill University, Montreal, 1986.
- 11) P.T. Miller, **Ph.D. Thesis**, The Institute of Paper Chemistry, Appleton, 1986.
- 12) E. Milanova, G.J. Kubes, and B.I. Fleming, **Proc. of 71st CPPA TS Annual Mtg.**, Montreal, January 1986:B67-71.
- 13) D. Strohbeen, **Ph.D. Thesis**, The Institute of Paper Chemistry, Appleton, 1982.
- 14) D.L. Feuerstein, J.F. Thomas, and D.L. Brink, **Tappi**, Vol. 50 (1967), No. 6: 258-262.
- 15) D.L. Brink, J.F. Thomas, and D.L. Feuerstein, **Tappi**, Vol. 50 (1967), No. 6: 276-285.
- 16) D.L. Brink, J.F. Thomas, and K.H. Jones, **Tappi**, Vol. 53 (1970), No. 5: 837-843.
- 17) P.K. Bhattacharya, V. Parthiban, and D. Kunzra, **Ind. Eng. Chem. Process Des. Dev.**, Vol. 25 (1986), No. 2: 420-426.
- 18) J. Li and A.R.P. van Heiningen, **Tappi**, Vol. 73 (1990), No. 12:213-219.
- 19) W.J. Frederick, P. Hyöty, M. Forssén, and M. Hupa, **Proc. of 1992 Int. Chem. Rec. Conf.**, Tappi Press, Atlanta, 1992:599-608.
- 20) M. Forssén, W.J. Frederick, M. Hupa, and P. Hyöty, **1991 AIChE Forest Prod. Sym. Proc.**, Tappi Press, Atlanta, 1992:11-22.
- 21) W.J. Frederick and M. Hupa, **Tappi**, Vol. 74 (1991), No. 11:192-194.
- 22) C.L. Verrill and K.M. Nichols, **1991 AIChE Forest Prod. Sym. Proc.**, Tappi Press, Atlanta, 1992:91-95.
- 23) C.L. Verrill and K.M. Nichols, **Proc. of 1992 Int. Chem. Rec. Conf.**, Tappi Press, Atlanta, 1992:609-615.
- 24) A. Björkman, **Proc. of 1981 Int. Conf. on Recovery of Pulping Chemicals**, Tappi Press, 1981:3-7.
- 25) W.J. Frederick, T. Noopila, and M. Hupa, **Journal of Pulp and Paper Science**, Vol. 17(1991), No. 5:164-170.
- 26) J. Li and A.R.P. van Heiningen, **Tappi**, Vol. 74(1991), No. 3:237-239.
- 27) C.L. Verrill, T.M. Grace, and K.M. Nichols, **IPST Technical Paper No. 486**, IPST, Atlanta, 1993.
- 28) P.J.J. Tromp and J. Moulijn, in **New Trends In Coal Science**, Y. Yurum (ed), Kluwer Academic Publishers, 1988: 305-338.

- 29) C.Y. Wen and S. Dutta, in **Coal Conversion Technology**, C.Y. Wen and E.S. Lee, Eds., Addison-Wesley, Reading, 1979.
- 30) E.M. Suuberg, W.A. Peters, and J.B. Howard, **Ind. Eng. Chem. Process Des. Dev.**, Vol. 17 (1978), No. 1: 37-46.
- 31) J.B. Howard, in **Chemistry of Coal Utilization**, 2nd Supp. Vol. (M.A. Elliott Ed.), John Wiley, New York, 1981:665-784.
- 32) S. Castillo, S. Bennini, G. Gas, and J.P. Traverse, **Fuel**, Vol. 68(1989), February:174-177.
- 33) D.W. McKee, in **Chemistry and Physics of Carbon**, P.L. Walker Jr. and P.A. Thrower, Eds., Vol.16, Marcel Dekker, New York, 1981:1-118.
- 34) J. Li, **Ph.D. Thesis**, McGill University, Montreal, 1989.
- 35) G.J. Kubes, "Course notes for 302-533, Pulp Production II", McGill Univ., Montreal, 1990.
- 36) A.R.P. van Heiningen, "Course notes for 302-532, Pulp Production I", McGill Univ., Montreal, 1991.
- 37) B. Blackwell and T. King, **Chemical Reactions in Kraft Recovery Boilers**, Sandwell and Company Ltd., Vancouver, 1985.
- 38) J. Li and A.R.P. van Heiningen, **Proc. of 1992 Int. Chem. Rec. Conf.**, Tappi Press, Atlanta, 1992:531-538.
- 39) J.G. Cantrell, D.T. Clay, and J.S. Hsieh, in **Chem. Eng. Tech. in Forest Prod. Proc.**, AIChE Forest Products Div., Vol. 2, Barbara Crowell (ed), 1988: 31-39.
- 40) M. Hupa, P. Solin, and P. Hyöty, **Proc. of TAPPI/CPPA Int. Rec. Conf.**, New Orleans, April 1985, Tappi Press, Atlanta, 1985:335-344.
- 41) A.R.P. van Heiningen, R. Alén, and V.T. Arpiainen, **Proc. of 1992 Int. Chem. Rec. Conf.**, Tappi Press, Atlanta, 1992:641-649.
- 42) Pejryd, L. and Hupa, M., **Proc. of TAPPI Pulping Conf. 1984**, TAPPI Press, Atlanta, GA, 1984:1.
- 43) T.W. Bauer and R.M. Dorland, **Can. J. Tech.**, Vol. 32(1954):91-101.
- 44) Zou, X., Kubes, G.J., van Heiningen, A.R.P., and Avedesian, M.M., **Proc. of TAPPI Pulping Conf. 1990**, TAPPI Press, Atlanta, 1990: 897-903.
- 45) Backman, R. and Hupa, M., Internal Report, Abo Akademi, Espoo, Finland, 1989.
- 46) Eriksson, G., **Chemica Scripta**, 8 (1975), 100-103.
- 47) Thompson, W.T., Pelton, A.D., and Bales, C.W., **F*A*C*T - Guide to Operation**, McGill University, Montreal, 1985.
- 48) Andersson, S., **Chemica Scripta**, 20 (1982), 164-170.
- 49) R. Backman, **Academic Dissertation Part VI**, Abo Akademi, Turku, Finland, 1989.
- 50) J.M. Prausnitz, **Molecular Thermodynamics of Fluid Phase Equilibria**, Prentice-Hall, Englewood Cliffs, 1968:388-394.
- 51) Barin, I. and Knacke, O., **Thermodynamic Properties of Inorganic Substances**, Springer, Berlin, 1973 (supplement, incl. Kubaschewski, O., 1977).
- 52) **Serial Publications from the Thermodynamics Research Center**, College Station, Texas, 77843.
- 53) Warnqvist, B., **Thermochemica Acta**, 37 (1980) 343-345.
- 54) **JANAF Thermochemical Tables with Supplements**, NBS, Washington, 1971-1978.
- 55) Rosen, R. and Sillen, L.G., **Acta Chem. Scand**, 14 (1960), No.3, 692-696.
- 56) M.B. Cerfontain, D. Agalianos, and J.A. Moulijn, **Carbon**, Vol. 25(1987), No. 3:351-359.
- 57) R.W. May, E.F. Pearson, and D. Scothern, **Pyrolysis-Gas Chromatography**, The Chemical Society, London, 1977:p27.

- 58) **Temperature Measurement Handbook and Encyclopedia**, Omega Engineering, Stamford, 1990.
- 59) J. Little and L. Shure, **Signal Processing Toolbox for use with MATLAB, User's Guide**, The Mathworks, South Natick, 1988.
- 60) T.W.G. Solomons, **Organic Chemistry**, 3rd. ed., John Wiley and Sons, New York, 1984.
- 61) **Micromass PC Manual Quasar**, Version 6, VG Instruments Limited, Chesire, England, 1990.
- 62) W.H. Press, B.P. Flannery, S.A. Teukolsky, and W.T. Vetterling, **Numerical Recipes, The Art of Scientific Computing**, Cambridge Univ. Press, Cambridge, 1986.
- 63) B. Iatridis and G.R. Gavalas, **Ind. Eng. Chem. Prod. Res. Dev.**, Vol. 18(1979), No. 2:127-130.
- 64) D.M. Himmelblau and K.B. Bischoff, **Process Analysis and Simulation, Deterministic Systems**, John Wiley, New York, 1968.
- 65) O. Levenspiel, **The Chemical Reactor Omnibook**, OSU Bookstores, Corvallis, 1989.
- 66) A.G. Sharpe, **Inorganic Chemistry**, Longman, London, 1981.
- 67) E.M. Suuberg, W.A. Peters, and J.B. Howard, **Ind. Eng. Chem. Process Des. Dev.**, Vol. 17(1978), No. 1:37-46.
- 68) V. Arpiainen and M. Lappi, **J. of Anal. and Applied Pyrolysis**, Vol. 16(1989):355-376.
- 69) **Physical and Thermodynamic Properties of Elements and Compounds**, AIChE Fuels and Petrochemicals Division.
- 70) D.A. Sams and F. Shadman, **AIChE J.**, Vol. 32(1986), No. 7:1132-1137.
- 71) M.B. Cerfontain and J.A. Moulijn, **Fuel**, Vol. 65 (1986), October:1349-1355.
- 72) C.A. Mims and J.K. Pabst, **Fuel**, Vol. 62 (1983), February:176-179.
- 73) J.A. Moulijn and F. Kapteijn, **Erdöl und Kohle - Erdgas - Petrochemie**, Bd. 40(1987), Heft 1:15-21.
- 74) P.J.J. Tromp and E.H.P. Cordfunke, **Thermochimica Acta**, Vol. 81(1984):113-123.
- 75) D.A. Sams, T. Talverdian, and F. Shadman, **Fuel**, Vol. 64(1983), September:1208-1214.
- 76) A. Volkov, O.D. Evseev, R.I. Ibatullina, and E.I. Dravolina, **Mezhvuz. Sb. Nauchn. Tr. Ser. Khim. Teknol. Tsellyul**, No. 7(1980):72-75.
- 77) G.W. Stewart, A. Chakrabarti, and W.R. Moore, **Proc. of High-Temp., High-Press. Particulate and Alkali Control in Coal Combustion Process Streams**, US DOE Contractor's Mtg., Morgantown, 1981.
- 78) A. Björkman and B. Warnqvist, **Pulp and Paper Can**, Vol. 89(1988), No. 11:T374-T380.
- 79) M. Matsukata, T. Fujikawa, E. Kikuchi, and Y. Morita, **Energy and Fuels**, Vol. 2(1988):750-756.
- 80) R.C. Reid, in **Advances in Chem. Eng. Vol. 12**, Academic Press, 1983: 105-208.
- 81) A Teder, **Svensk Papperstidning**, Vol 71(1968), No. 11:447.
- 82) J.G. Speight, in **Marks' Stand. Handbook for Mech. Eng.**, 9th ed , E.A. Avallone, T. Baumeister III editors, McGraw Hill, New York, 1987,p7-20.
- 83) R. Tegman and B. Warnqvist, **Acta Chem. Scand.**, 26 (1972) No. 1, 413-414.
- 84) R.C. Weast, ed., **CRC Handbook of Chemistry and Physics**, 57th Ed., CRC Press, Cleveland, 1976:D-179.
- 85) C.O. Franklin and A. Fitchett, **Pulp and Paper Can**, Vol. 83(1982), No. 10.

APPENDIX A Analysis For Back Dispersion In Shielding Tube

Conditions:

Q	=	1.0 slm (standard litres per minute at 1 at 273 K and 1 atm) minimum volumetric flow rate
P	=	1 atm absolute pressure
t	=	298 K temperature
d	=	0.016 m tube inside diameter
M _{O2}	=	32 molecular weight of oxygen
M _{Ar}	=	40 molecular weight of Argon
ΣV _{O2}	=	16.6 sum of structural volume increments for oxygen
ΣV _{Ar}	=	16.1 sum of structural volume increments for argon
μ	=	0.0218E-3 kg/m-s argon viscosity ¹ at 298 K, 1 atm
ρ	=	1.636 kg/m ³ argon ideal gas density at 298 K, 1 atm

The diffusivity of O₂ in Ar at 298 K using the method of Fuller *et al* as described by Geankoplis² is

$$\begin{aligned} \text{Diff}_{\text{O}_2\text{-Ar}} &= 1.0\text{E-}7 * T^{1.75} * (1/M_{\text{O}_2} + 1/M_{\text{Ar}})^{0.5} / \{[(\Sigma V_{\text{O}_2})^{1/3} + (\Sigma V_{\text{Ar}})^{1/3}]^2\} \\ &= 1.967\text{E-}5 \text{ m}^2/\text{s} \end{aligned}$$

The Schmidt number for oxygen diffusing in argon is

$$Sc = (\mu/\rho)/\text{Diff}_{\text{O}_2\text{-Ar}} = 0.677$$

The actual volumetric flow is

$$Q = (1.0 \text{ slm}/1000 \text{ l/m}^3)(1 \text{ min}/60\text{s})(298 \text{ K}/273 \text{ K}) = 1.819\text{E-}5 \text{ m}^3/\text{s}$$

The velocity U is

$$U = Q/\text{area} = Q/(\pi d^2/4) = 0.090 \text{ m/s}$$

Then the Reynolds number in the shielding tube is

$$Re = \rho * U * d / \mu = 109$$

and indicates laminar flow

In laminar flow, axial dispersion is due to both axial and radial diffusion³, but only axial diffusion leads to upstream dispersion. Thus for back dispersion, the axial dispersion coefficient D is equal to the diffusion coefficient Diff_{O₂-Ar} and

$$D/(U*d) = 0.014$$

Levenspiel⁴ shows that for an open-closed vessel, the appropriate flow model for the shielding tube, with the above value of D/(U*d) convective transport is more rapid than back diffusion, and thus oxygen diffusion backwards against the flow is not possible in the shielding tube of the present experimental apparatus.

1 C.J. Geankoplis, *Transport Processes and Unit Operations*, 2nd ed, Allyn and Bacon, Boston, 1983:p814.

2 *Ibid*, p 386.

3 O. Levenspiel, *Chemical Reactor Omnibook*, OSU Bookstores, Corvallis, 1989, p64-16.

4 *Ibid*, p64-8.